Theory of resonant multiphonon Raman scattering in graphene

D. M. Basko*
International School of Advanced Studies (SISSA), via Beirut 2-4, 34014 Trieste, Italy
(Received 2 May 2008; revised manuscript received 25 July 2008; published 23 September 2008)

We present a detailed calculation of intensities of two-phonon and four-phonon Raman peaks in graphene. Writing the low-energy Hamiltonian of the interaction of electrons with the crystal vibrations and the electromagnetic field from pure symmetry considerations, we describe the system in terms of just a few independent coupling constants, considered to be parameters of the theory. The electron-scattering rate is introduced phenomenologically as another parameter. The results of the calculation are used to extract information about these parameters from the experimentally measured Raman peak intensities. In particular, the Raman intensities are sensitive to the electron-scattering rate, which is not easy to measure by other techniques. Also, the Raman intensities depend on electron-phonon coupling constants; to reproduce the experimental results, one has to take into account renormalization of these coupling constants by electron-electron interaction.

DOI: 10.1103/PhysRevB.78.125418 PACS number(s): 73.23.−b, 73.20.Mf, 78.20.Bh, 78.30.−j

I. INTRODUCTION

In the past decades, Raman spectroscopy[1] techniques were successfully applied to carbon compounds, such as graphite (see Ref. 2, and references therein) and carbon nanotubes.[3,4] Upon the discovery of graphene,[5] Raman spectroscopy has proven to be a powerful tool to identify the number of layers, structure, doping, disorder, and to characterize the phonons and electron-phonon coupling (EPC).[6–12] So far, most of the attention was focused on the position and width of the Raman peaks.

Here we present a detailed calculation of the *intensities* of the multiphonon Raman peaks in graphene. Raman scattering involves an electron-hole pair as an intermediate state; we show that the multiphonon Raman peaks are strongly sensitive to the dynamics of this electron-hole pair. Thus, Raman scattering can be used as a tool to probe this dynamics. Writing the low-energy Hamiltonian of the interaction of electrons with the crystal vibrations and the electromagnetic field from pure symmetry considerations, we describe the system in terms of just a few independent coupling constants, considered to be parameters of the theory. The electron-scattering rate is introduced phenomenologically as another parameter. The results of the present calculation are used to extract information about these parameters from the Raman peak intensities measured experimentally.

As shown below, the Raman intensities strongly depend on the electron-scattering rate; moreover, the electron-phonon and electron-electron contributions to this rate can be separated. This is especially important as there are very few techniques giving experimental access to electron-scattering rates, which, in turn, determine the transport properties of graphene samples. Besides, the quasiclassical character of the process imposes a severe restriction on the electron and hole trajectories which can contribute to the two-phonon Raman scattering: upon the phonon emission the electron and the hole must be scattered backward. This restriction results in a significant polarization memory: it is almost three times more probable for the scattered photon to have the same polarization as the incident photon than to have the orthogonal polarization.

Also, the Raman intensities depend on electron-phonon coupling constants; to reproduce the experimental results, one has to take into account renormalization of these coupling constants by electron-electron interaction. This renormalization is missed by local or semilocal approximations to the density-functional theory, typically used for the *ab initio* calculation of the coupling constants.

A. Fully resonant processes

Since graphene is a nonpolar crystal, Raman scattering involves electronic excitations as intermediate states: the electromagnetic field of the incident laser beam interacts primarily with the electronic subsystem, and emission of phonons occurs due to electron-phonon interaction. The matrix element of the process can be schematically represented as

$$\mathcal{M} \sim \sum_{s_0,\ldots,s_n} \frac{\langle i|\hat{H}_{e\text{-}em}|s_0\rangle\langle s_0|\hat{H}_{e\text{-}ph}|s_1\rangle\cdots\langle s_{n-1}|\hat{H}_{e\text{-}ph}|s_n\rangle\langle s_n|\hat{H}_{e\text{-}em}|f\rangle}{(E_i - E_0 + 2i\gamma)(E_i - E_1 + 2i\gamma)\cdots(E_i - E_n + 2i\gamma)}. \tag{1}$$

Here $|i\rangle$ is the initial state of the process (the incident photon with a given frequency and polarization, and no excitations in the crystal), $|f\rangle$ is the final state (the emitted photon and n phonons left in the crystal), while s_k, $k=0,\ldots,n$, label the intermediate states where no photons are present, but an electron-hole pair is created in the crystal and k phonons have been emitted. E_i and E_k, $k=0,\ldots,n$, are the energies of these states and 2γ is the inverse lifetime of the electron

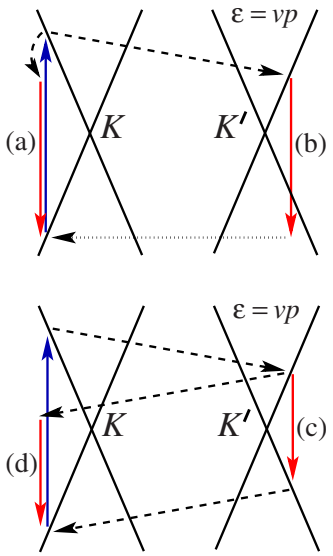

FIG. 1. (Color online) Schematic representation of the role of electron dispersion (Dirac cones, shown by solid lines) in the [(a) and (b)] one-phonon and [(c) and (d)] two-phonon Raman scatterings. Vertical solid arrows represent interband electronic transitions accompanied by photon absorption or emission (photon wave vector is neglected), dashed arrows represent phonon emission, and the horizontal dotted arrow represents the impurity scattering.

(hole) due to collisions. $\hat{H}_{e\text{-}em}$ and $\hat{H}_{e\text{-}ph}$ stand for the terms in the system Hamiltonian describing interaction of electrons with the electromagnetic field and with phonons, respectively.

In the calculations we do not include the phonon broadening, assuming the phonon states to have zero width. First, this approximation is consistent with the available experimental information: the phonon width is about $10-20\ \mathrm{cm}^{-1}$ $\approx 2-3$ meV at most,[9,10] while the electronic broadening is at least an order of magnitude higher (see the discussion below, Sec. II C). Second, this approximation is irrelevant provided that we calculate the integrated intensities of the Raman peaks, since they are determined by the total spectral weight of the phonon state which does not depend on the phonon broadening.

The photon wave vector is negligible, so momentum conservation requires that the sum of the wave vectors of emitted phonons must vanish (provided that the impurity scattering is neglected). For the same reason Raman scattering on one intervalley phonon must be impurity assisted [process (b) in Fig. 1, giving rise to the so-called D Raman peak]. D peak is absent in the experimental Raman spectrum of graphene,[6] showing that impurity scattering is indeed negligible in these samples.

Looking at the intermediate electronic states involved in the Raman scattering (Fig. 1), we notice that for one-phonon scattering [processes (a) and (b)] at least one intermediate state must be virtual, since energy and momentum conservation cannot be satisfied simultaneously in all processes. Thus, at least one of the factors in the denominator of Eq. (1) must be of the order of the phonon frequency ω_{ph} [for the impurity-assisted scattering one of the electron-phonon matrix elements in the numerator of Eq. (1) should be replaced by the electron-impurity matrix element]. For the two-phonon scattering [process (c)] all intermediate states can be real, so that all energy mismatches in the denominator of Eq. (1) can be nullified simultaneously and the result is determined by the electron-scattering rate 2γ. We emphasize the qualitative difference between the *fully resonant* process (c) and the double-resonant[13] process (b), where one intermediate state is still virtual. We also note the analogous difference between the two-phonon processes [(c) and (d)] in Fig. 1: only process (c) is fully resonant, the other one involves an energy mismatch of $2\omega_{ph}$. As a result, its amplitude will be smaller by a factor $\sim\gamma/\omega_{ph}$.

Obviously, these arguments can be extended to all multiphonon processes with odd and even numbers of phonons involved. In order to annihilate radiatively, the electron and the hole must have opposite momenta; if the total number of emitted phonons is odd, the electron and the hole must emit a different number of phonons, which is incompatible with energy conservation in all processes. Our main focus will thus be on even-phonon processes, as their intensities are determined by the electronic scattering.

The full resonance picture presented above assumes the mirror symmetry between the electron and the hole spectra. The electron-hole asymmetry can be included as a correction to the Dirac spectrum; the electron and the hole energies can be written as $vp \pm \alpha_0 p^2$, where p is the momentum counted from the Dirac point, v is the Dirac velocity, and α_0 is the asymmetry parameter. The energy scale Δ_{eh}, quantifying the role of the asymmetry in the Raman scattering, is defined as $\Delta_{eh}=\alpha_0(\omega_{in}^2-\omega_{out}^2)/(2v)^2$, where ω_{in} and ω_{out} are the frequencies of the incident and the scattered photons (the details are given in Secs. VI B and VII C). Namely, the arguments of the previous paragraph hold if $\Delta_{eh}\ll\gamma$. In the opposite case, it is Δ_{eh} that determines the smallest value of the denominators in Eq. (1). We will always assume that both $\gamma,\Delta_{eh}\ll\omega_{ph}$.

In the real space, the typical size of the region of space probed by the electron-hole pair in the fully resonant two-phonon Raman scattering is $\sim v/\max\{\gamma,\Delta_{eh}\}$. For the doubly resonant defect-induced one-phonon scattering, the inverse energy mismatch $1/\omega_{ph}$ determines the time duration of the process by virtue of the uncertainty principle, so the length scale of the process in the real space is v/ω_{ph}. Although this length scale is much shorter than v/γ, it is still much greater than the lattice constant or the electron wavelength v/ϵ. Most likely, it is this length scale that has been found in the spatial-resolved edge-assisted Raman scattering on a single intervalley phonon,[14] contrary to the interpretation of Cançado *et al.*[14]

B. Quasiclassical real-space picture

The fully resonant Raman scattering, where the energy is conserved in each of the elementary scattering processes, admits a simple quasiclassical description, described qualitatively in this section and justified rigorously in Secs. VI and VII. Let us denote by ϵ the energy of the electron and the hole in the photoexcited pair. Initially, it is given by the half of the excitation frequency ω_{in}, $\epsilon=\omega_{in}/2\sim 1$ eV. After the

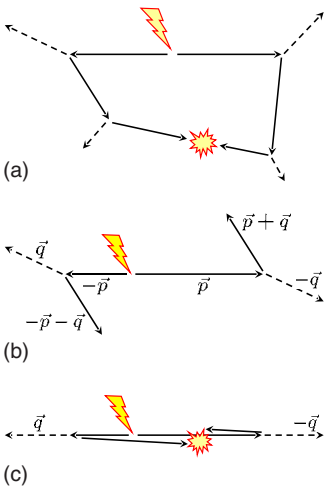

FIG. 2. (Color online) (a) An example of a quasiclassical electron-hole trajectory contributing to the four-phonon Raman scattering. [(b) and (c)] Trajectories with emission of two phonons (b) not contributing and (c) contributing to the two-phonon Raman scattering. In all pictures the lightning represents the incident photon which creates the pair. The solid lines denote the free propagation of the electron and the hole. The flash represents the radiative recombination of the electron-hole pair. The dashed lines denote the emitted phonons.

emission of n phonons it is decreased by $n\omega_{ph}$; assuming $\omega_{ph} \leqslant 0.2$ eV $\ll \epsilon$, we neglect this decrease in the qualitative considerations. Thus, during all the time taken by the Raman scattering, electron and hole can be viewed as wave packets of the size $\sim v/\epsilon$, propagating across the crystal along classical trajectories.

The electron and the hole are created in the same region of space of the size $\sim v/\epsilon$ around some point $\mathbf{r}_0$ at the moment of the arrival of the excitation photon. At this initial moment they have opposite momenta $\mathbf{p}, -\mathbf{p}$ and opposite velocities $\mathbf{v}, -\mathbf{v}$ (if the electron-hole asymmetry is taken into account, the two velocities will have slightly different magnitudes), so they move along the straight lines, their positions being $\mathbf{r}_e(t) = \mathbf{r}_0 + \mathbf{v}t$, $\mathbf{r}_h(t) = \mathbf{r}_0 - \mathbf{v}t$. After a typical time $t \sim 1/\gamma$ they undergo some scattering processes (e.g., phonon emission), where their momenta and (generally speaking) energies are changed. Each such elementary scattering process occurs during a short time $\sim 1/\epsilon \ll 1/\gamma$. Thus, the trajectories of the electron and the hole after their creation are represented by broken lines, with the typical segment length $\sim v/\gamma$ (the electron mean-free path). The crucial point is that in order to recombine radiatively and contribute to Raman signal, the electron and the hole should meet again within a spatial region of the size $\sim v/\epsilon$ and have opposite momenta. The latter condition automatically implies that the number of the phonons emitted by the electron and the hole is the same. These considerations are illustrated in Fig. 2.

In the presence of a significant electron-hole asymmetry, $\Delta_{eh} \gg \gamma$, the described picture is modified. Namely, one of the segments of either the electron or the hole trajectory has the length v/Δ_{eh} instead of v/γ, the corresponding time travelling being restricted by the phase mismatch rather than by collisions.

II. SUMMARY OF THE MAIN RESULTS

A. On the labeling of Raman peaks in graphene

For the single-phonon Raman peaks the commonly accepted notations are G for the peak at 1580 cm^{-1} corresponding to emission of an optical phonon with zero wave vector and D for the defect-induced peak at 1350 cm^{-1} corresponding to emission of an optical phonon with the wave vector near K or K' points of the Brillouin zone.[2] Sometimes one also distinguishes the so-called D' peak at 1620 cm^{-1}. This peak is also defect induced and corresponds to emission of an optical phonon with a small wave vector $q \sim \epsilon/v$. As mentioned above, in the present work we study only the clean graphene, hence D and D' peaks are of no interest to us.

Unfortunately, there is no single commonly accepted system for labeling of the multiphonon Raman peaks. The strong peak at 2700 cm^{-1}, corresponding to emission of two phonons with the opposite wave vectors near the K and K' points, was historically called G' (as it is not defect induced); sometimes it is denoted by $2D$ or by D^* to stress that it is the second overtone of the D peak. The peak at 3250 cm^{-1} corresponding to emission of two phonons with two opposite wave vectors near the Γ point is sometimes called G^*, $2G$, or $2D'$. The latter notation reflects the fact that the frequency of this peak is not exactly the double of that of the G peak but rather the double of the defect-induced D' peak.

In the following we use the notation $n\Gamma + mK$ to denote the peak corresponding to emission of n phonons with wave vectors within $\sim \epsilon/v$ from the Γ point and of m phonons with wave vectors within $\sim \epsilon/v$ from the K or K' points. For multiphonon peaks this nomenclature is unambiguous. Thus, the peaks at 2700 and at 3250 cm^{-1} will be called $2K$ and 2Γ, respectively.

B. One-phonon Raman processes

In the clean graphene the only one-phonon Raman process allowed by the momentum conservation corresponds to the emission of the E_2 optical phonon with zero wave vector and frequency at 1580 cm^{-1}. For this process the situation turns out to be drastically different from that described by the qualitative considerations of Sec. I A. As shown in Sec. V, if one approximates the electron spectrum by the Dirac cones, the numerator of Eq. (1) vanishes due to high symmetry of the low-energy electronic Dirac Hamiltonian (as compared to the microscopic symmetry of the crystal). Thus, the main contribution to the Raman amplitude comes from the regions of the electronic Brillouin zone far from the Dirac points. As a consequence, the typical energy mismatch in the denominator of Eq. (1) is of the order of the whole electronic bandwidth. Thus, the Raman process, responsible for the 1580 cm^{-1} peak, is completely off resonant and the picture shown in Fig. 1 for process (a) is wrong.

As a result, the intensity of the peak is expected to be insensitive to most external parameters: polarization, electron concentration, degree of disorder, etc. To characterize this intensity, one has to introduce an additional parameter into the theory which has no simple relation to the parameters of the low-energy effective Hamiltonian. The resulting

intensity of the peak is given by Eq. (55); it is proportional to the fourth power of the excitation frequency which is the standard result for Raman scattering when the difference between the frequencies of the incident and scattered photons is small. This dependence also agrees with the experimental results of Ref. 15.

Note that the results described above do not hold for the defect-induced peak at 1350 cm^{-1}. For this peak the double-resonance picture,[13] shown in Fig. 1, process (b), is fully adequate.

C. Two-phonon Raman processes

As the phonons are emitted by electrons with momentum $\omega_{in}/(2v)$, the largest possible phonon momentum is $q_{max}=(\omega_{in}+\omega_{out})/2v$, corresponding to the electron and hole backscattering (for the $2K$ peak at 2700 cm^{-1} we count the phonon momenta from the K and K' points). It would be natural to expect that any pair of phonons with opposite momenta $\mathbf{q}$, $-\mathbf{q}$ and $|\mathbf{q}|\leqslant q_{max}$ can be emitted, the only exception being $\mathbf{q}=0$ which is prohibited by symmetry[2] and the nearby ones which are suppressed due to the smallness of the matrix elements. These arguments would predict the width of the peak to be of the order of $(v_{ph}/v)\omega_{in}$, where v_{ph} is the K phonon group velocity. Besides, the shape of the peak would be strongly asymmetric: a sharp cutoff on the high-energy side at the frequency $2\omega_{ph}(q_{max})$ due to the resonance restriction and a smooth dropoff toward zero at $2\omega_{ph}(q=0)$ due to the matrix element suppression. The phonon dispersion can be deduced from the dependence of the frequency of the impurity-assisted one-phonon D peak in graphite on the excitation energy ω_{in}: $d\omega_{ph}/d\omega_{in}=v_{ph}/v\approx 50$ cm^{-1}/eV.[16–19] Thus, for $\omega_{in}=2$ eV these arguments give the width of the $2K$ peak to be about 200 cm^{-1}. However, the experimentally observed width is only about 30 cm^{-1} at $\omega_{in}=2.2$ eV, and its shape is quite symmetric.[6,9]

The observed small width of the peak is explained by the quasiclassical picture, presented in Sec. I B. If upon the emission of phonons the electron and the hole are scattered by an arbitrary angle, as shown in Fig. 2(b), they will not be able to meet at the same spatial point in order to recombine radiatively and contribute to the two-phonon Raman peak. Only if the scattering is backward, this event is possible, as illustrated in Fig. 2(c). This condition fixes the wave vectors of the emitted phonons to be $q=q_{max}=2\epsilon/v$. The small deviations of the scattering angle from π are restricted by the quantum diffraction, and the width of the two-phonon Raman peaks, instead of being $\sim(v_{ph}/v)\omega_{in}$, is determined by a much smaller energy scale (see the discussion below).

The dominance of the electron and hole backscattering manifests itself in the polariazion memory of the Raman signal. If the incident light is linearly polarized, the probability of excitation of the electron-hole pair with a given direction of momenta is proportional to $\sin^2\varphi$, where φ is the angle between the electric-field vector of the light and the momenta. Thus, upon backscattering and radiative recombination, the probability to detect a photon of the same polarization as the original one is $\propto\sin^4\varphi$ and that of the orthogonal polarization is $\propto\sin^2\varphi\cos^2\varphi$. Averaging over φ, we obtain the ratio of intensities for the detection of polarization parallel and perpendicular to that of the incident light to be $I_{\parallel}/I_{\perp}=3$. This ratio may be slightly decreased due to a finite aperture (see the discussion in Sec. IV B).

The calculation of the intensities of the two-phonon Raman peaks is performed in Sec. VI. The explicit expressions for the intensities of the $2K$ and 2Γ peaks, obtained under the assumption of Dirac spectrum for the electrons, are represented by Eqs. (66) and (69). Both are proportional to $1/\gamma^2$, where 2γ is the electron (hole) inelastic-scattering rate. If the latter is smaller than the electron-hole asymmetry Δ_{eh}, then, according to the arguments of Sec. I A, it is Δ_{eh} that restricts the energy denominators from below. Formally, this results in replacement (75) in both Eqs. (66) and (69).

Numerically, $\alpha_0(1\text{ eV})^2/v^2\sim 0.1$ eV (see, e.g., Ref. 20), so the relative correction to Eq. (66) for small Δ_{eh} can be estimated as $-[(1/2)\Delta_{eh}^2/(2\gamma)]^2/2\sim -10^{-4}(\omega_{in}/2\gamma)^2$. The total electronic broadenings 2γ were measured by time-resolved photoemission spectroscopy to be 20 meV in Ref. 21 and 25 meV in Ref. 22 (all values taken for $\epsilon=\omega_{in}/2=1$ eV). A recent angle-resolved photoemission spectroscopy (ARPES) measurement gives a significantly larger value for $2\gamma\sim 100$ meV.[23] Thus, the case $\gamma\gg\Delta_{eh}$ seems to be more relevant for the description of experiments than the opposite one.

The Raman matrix element corresponding to emission of two phonons with given wave vectors $\mathbf{q}$ and $-\mathbf{q}$ is given by Eq. (64) for $\gamma\gg\Delta_{eh}$. From this dependence one can deduce the line shape of the two-phonon peaks $2K$, 2Γ,

$$\frac{dI_{2\mu}}{d\omega}\propto\frac{1}{[(v/v_{ph,\mu})^2(\omega/2-\omega_\mu)^2+4\gamma^2]^{3/2}},\tag{2}$$

where $\mu=K$, Γ, $2\omega_\mu$ is the central frequency for each peak, and $v_{ph,\mu}$ is the group velocity of the corresponding phonon. Thus, the full width at half maximum (FWHM) of each peak is given by

$$\mathrm{FWHM}_{2\mu}=\sqrt{2^{2/3}-1}\frac{v_{ph,\mu}}{v}8\gamma\approx 0.77\frac{v_{ph,\mu}}{v}8\gamma.\tag{3}$$

For $\gamma\ll\Delta_{eh}$ the dependence of the Raman matrix element on q is described by Eq. (73). The line shape corresponds to *two* peaks separated by $(v_{ph,\mu}/v)4\Delta_{eh}$. Experimentally, one sees just one $2K$ peak with the FWHM about 30 cm^{-1} at the excitation frequency $\omega_{in}\approx 2$ eV.[6,9] This corresponds to an unrealistically large value of $2\gamma\sim 0.2$ eV. Most likely, this indicates that two-phonon peaks are broadened by other mechanisms, not taken into account in the present work. In particular, Eq. (2) neglects (i) the broadening of the phonon states and (ii) the anisotropy of the phonon dispersion (trigonal warping of the phonon spectrum). A detailed study of these effects would require introduction of additional parameters into the theory, so we prefer to postpone such study for the future work. It is worth emphasizing again that the *integrated* intensity of the peaks, which is the main focus of the present study, does not depend on these details.

In view of the results of the present paper it is worth mentioning the experimental measurements of the intensity I_{2K} as a function of doping. While in Ref. 9 no significant

dependence was observed, Ref. 12, where higher doping levels were reached, shows quite a strong dependence of I_{2K}/I_Γ on doping. The intensity I_Γ of the off-resonant single-phonon 1580 cm^{-1} peak should not depend on doping (although the phonon width does exhibit such a dependence, the total spectral weight of the phonon state, determining the integrated intensity of the peak, must be preserved). At the same time, the intensity I_{2K}, if determined by the electron inelastic lifetime, should be sensitive to the concentration of carriers. Indeed, in the intrinsic graphene at low temperatures the photoexcited carriers do not participate in electron-electron collisions, as the phase-space volume is restricted.[24] As the carriers are added to the system, the electron-electron collisions become possible, thus the total γ increases, and the intensity I_{2K} is decreased, in qualitative agreement with the observation in Ref. 12.

D. Four-phonon Raman processes

The motivation to study the four-phonon Raman process comes from the following picture for the fully resonant processes. The incident photon creates an electron and a hole—real quasiparticles which can participate in various scattering processes. If the electron emits a phonon with a momentum $\mathbf{q}$, the hole emits a phonon with the momentum $-\mathbf{q}$, and after that the electron and the hole recombine radiatively, the resulting photon will contribute to the two-phonon Raman peak. If they do not recombine at this stage, but each of them emits one more phonon, and they recombine afterward, the resulting photon will contribute to the four-phonon peak, etc. Three-phonon processes, not being fully resonant, are not interesting in this context.

Besides phonon emission and radiative recombination, electron and hole are subject to other inelastic-scattering processes, which can also be viewed as emission of some excitations of the system. In principle, Raman spectrum should also contain the contrubution from these excitations, which are left in the system after the radiative recombination of the electron and the hole. The key point is that for real quasiparticles, the probability to undergo a scattering process α is determined by the ratio of corresponding scattering rate $2\gamma_\alpha$ to the total scattering rate $2\gamma \equiv \Sigma_\alpha 2\gamma_\alpha$ not by the history. This probability determines the relative *frequency-integrated* intensity of the corresponding feature in the Raman spectrum. Thus, the ratio of integrated intensity $I_{(2n+2)K}$ of the Raman peak corresponding to $(2n+2)K$ phonons to that for $2nK$ phonons (I_{2nK}) must be proportional to $(\gamma_K/\gamma)^2$, where $2\gamma_K$ is the rate of emission of each of the two K phonons, and the square comes from the phonon emission by the electron and the hole. This conclusion depends weakly on the relation between γ and Δ_{eh} only through a logarithmic factor.

In the doped graphene, the most obvious competitor of the phonon emission is the electron-electron scattering; the optically excited electron can kick out another one from the Fermi sea, i.e., to emit another electron-hole pair. Thus, Raman spectrum should contain contribution from electron-hole pairs; however, their spectrum extends all the way to the energy of the photoexcited electron (optical energy) in a completely featureless way. Thus, it cannot be distinguished from the parasitic background which is always subtracted in the analysis of Raman spectra and cannot be seen in the Raman spectrum directly. However, assuming $\gamma = \gamma_K + \gamma_\Gamma + \gamma_{ee}$, where $2\gamma_\Gamma$ is the rate of emission of phonons from the vicinity of the Γ point of the first Brillouin zone and $2\gamma_{ee}$ is the electron-electron collision rate, one can extract the value of γ_{ee} relative to phonon emission rates from the experimental data. More precisely, in this way one obtains the rate of all inelastic-scattering processes where the electron loses energy far exceeding the phonon energy.

Note that arguments leading to $I_{(2n+2)K}/I_{2nK} \propto (\gamma_{ph}/\gamma)^2$ are not specific for graphene; in fact, this is nothing but Breit-Wigner formula, applied once for the electron and once for the hole. Multiphonon Raman scattering has been studied in wide-gap semiconductors both experimentally[25,26] (up to ten phonons were seen in the Raman spectra of CdS) and theoretically.[27,28] In a wide-gap semiconductor an optically excited electron does not have a sufficient energy to excite another electron across the gap, so the electron-electron channel is absent. In addition, interaction with only one-phonon mode is dominant, so the ratios of subsequent peaks are represented by a sequence of fixed numbers. The simple band structure (one valley for CdS in contrast to two valleys for graphene) allowed a calculation of the whole sequence. A more complicated electronic band structure in graphene makes it problematic to calculate the whole sequence, so we restrict ourselves to the calculation of I_{4K} for the most intense four-phonon peak.

This calculation is performed in Sec. VII. Its result depends, besides the relation between γ and Δ_{eh}, also on their relation to the energy scale $\omega_{in}(v_{ph}/v)$, characterizing the phonon dispersion. In Sec. II C we have already discussed this energy scale; for $\omega_{in}=2$ eV we have $\omega_{in}(v_{ph}/v) \approx 100\ cm^{-1} \approx 12$ meV. The meaning of this energy scale is the difference between the energies of the electron and the hole after each of them has emitted two phonons with almost arbitrary momenta (the only restriction is that the sum of all four phonon momenta must vanish). If $\omega_{in}(v_{ph}/v) \ll \gamma, \Delta_{eh}$, which seems to be the case (see the discussion in Sec. II C) then this difference can be neglected, and the intensity of the $4K$ peak is given by Eq. (101) for $\gamma \gg \Delta_{eh}$ (which is likely to be the case relevant for most experiments and which was reported in the short paper by Basko[29]) and by Eq. (104) for $\gamma \ll \Delta_{eh}$; the polarization memory is lost in both these cases, $I_\parallel \approx I_\perp$. In the case $\omega_{in}(v_{ph}/v) \gg \gamma, \Delta_{eh}$ the intensity I_{4K} is given by Eq. (118), and a significant polarization memory is expected, up to $I_\parallel/I_\perp \approx 3$.

A thorough experimental study of the intensity I_{4K} (in particular, its dependence on doping) is still lacking. Our prediction for the case $\gamma \gg \Delta_{ph}, \omega_{in}(v_{ph}/v)$, which we believe to be the experimentally relevant one, is[29,30]

$$\frac{I_{4K}}{I_{2K}} \approx 0.11\left(\frac{\gamma_K}{\gamma_K + \gamma_\Gamma + \gamma_{ee}}\right)^2. \tag{4}$$

E. Renormalization of the coupling constants

In the calculations of the Raman intensities, described above, electron-phonon coupling constants entered as param-

eters of the theory, without any assumptions about their values, except for the relations fixed by the symmetry of the crystal. In particular, the two-phonon peak intensities I_{2K} and $I_{2\Gamma}$ are determined by two independent dimensionless coupling constants which we denote λ_K and λ_Γ [see Eq. (24) for the definition]. A simple estimate of the coupling constants can be obtained from the tight-binding nearest-neighbor model of the graphene crystal. In this model the only parameter characterizing the electron spectrum is the nearest-neighbor electronic matrix element t_0, and the electron-phonon interaction is characterized by its change with the bond length, $\partial t_0/\partial a$. In this model we obtain λ_K/λ_Γ to be given by the inverse ratio of the corresponding phonon frequencies, about 1.2; the same result up to a few percent is obtained from the density-functional theory (DFT) calculations in Ref. 31. At the same time, by comparing the experimentally measured intensities of the different two-phonon peaks and using the result of our calculation performed in Sec. VI, we can independently extract the ratio of the coupling constants. According to the data of Ref. 6, $I_{2K}/I_{2\Gamma} \approx 20$, which gives $\lambda_K/\lambda_\Gamma \approx 3$.

To explain this discrepancy we first analyzed the effect of the electronic trigonal band warping, which affects I_{2K} and $I_{2\Gamma}$ differently. The corresponding calculation is done in Sec. VI B. For $\omega_{in}=2$ eV, we estimate the relative contributions of the warping term as 5×10^{-4} for I_{2K} and 5×10^{-2} for $I_{2\Gamma}$, which are far too little to account for the observed ratio $I_{2K}/I_{2\Gamma}$. We are thus led to the conclusion that the observed ratio $I_{2K}/I_{2\Gamma}$ must be due to the difference of the coupling constants not accounted for by the DFT calculation. A similar conclusion about the insufficiency of the DFT calculation of the electron-phonon coupling constants has been drawn in Ref. 32, where an attempt was made to explain the experimental data obtained by ARPES (Ref. 23) using the results of the DFT calculation.

At the same time, we should note that the dimensionless coupling constant λ_Γ for the phonons near the Γ point, as calculated by DFT (Ref. 31) ($\lambda_\Gamma \approx 0.028$), agrees reasonably well with the measured one: the measurements of the linear in the wave vector q term in the phonon dispersion (Kohn anomaly due to electron-phonon interaction), $\omega_{ph}(q) - \omega_{ph}(q=0) \approx (\lambda_\Gamma/8)vq$, give $\lambda_\Gamma \approx 0.024$ (see Ref. 33); the measurements of the dependence of the phonon frequency ω_{ph} on the electron Fermi energy ϵ_F, $\Delta\omega_{ph} \approx (\lambda_\Gamma/2\pi)|\epsilon_F|$, give $\lambda_\Gamma \approx 0.034$ (Ref. 9) and $\lambda_\Gamma \approx 0.027$.[10]

We show that the difference between the ratio $\lambda_K/\lambda_\Gamma \approx 3$ extracted from the Raman peak intensities and $\lambda_K/\lambda_\Gamma \approx 1.2$ obtained by the DFT calculation,[31] is due to the part of Coulomb interaction between electrons, not picked up by the DFT when local approximations are used for the exchange-correlation functional, such as the local-density approximation (LDA) or the generalized gradient approximation (GGA), namely, logarithmic renormalizations.[34] Coulomb interaction has been known to be a source of logarithmic renormalizations for Dirac fermions.[35–37] Coulomb renormalizations in graphene subject to a magnetic field have been considered in Ref. 38; Coulomb effect on static disorder has been studied in Refs. 39–41. Essentially, the idea of the renormalization of the coupling constants is that the matrix element of the electron-phonon interaction should be taken not between the noninteracting electronic states but between the states dressed by the Coulomb interaction. If the typical electronic energy in the problem is ϵ ($\sim$1 eV in the case of Raman scattering), the renormalization is determined by the Coulomb interaction at all length scales from the shortest ones (lattice constant) to the electron wavelength v/ϵ. It is this long-range part of the exchange and correlation that is missed by the local approximations in the DFT calculation, which take into account correctly only the short-range correlations (at the distances of the order of the lattice constant).

In Sec. VIII A we calculate the renormalization of the dimensionless electron-phonon coupling constants (a preliminary account of this work was given in the short paper[34]) and show that the coupling constant λ_Γ for the phonons near the Γ point is not renormalized (hence the agreement between the value of λ_Γ calculated by the DFT and measured in the experiments, as mentioned above), while the coupling constant λ_K for the phonons near the K point, which is responsible for the $2K$ Raman peak, is enhanced by the Coulomb interaction. This enhancement depends on the electronic energy, as shown in Fig. 22. For the electronic energy of 1 eV this enhancement is in quantitative agreement with the measured ratio $I_{2K}/I_{2\Gamma}$, provided that the screening of the Coulomb interaction by the substrate is weak. The dependence of the enhancement on the electronic energy translates into the dependence of $I_{2K}/I_{2\Gamma}$ on the excitation frequency, which can be checked experimentally. Similarly, as the Coulomb interaction is screened by the substrate with a dielectric constant ε_∞ (its high-frequency value), the dependence of $I_{2K}/I_{2\Gamma}$ on ε_∞ can also serve as an experimental check of the theory.

We also show in Sec. VIII B that the electron-phonon coupling itself is a source of logarithmic renormalizations. However, due to the smallness of the coupling constants this effect is much weaker than the effect of the Coulomb interaction.

F. Structure of the paper

In Sec. III the low-energy Hamiltonian of the interaction of electrons with the crystal vibrations and the electromagnetic field is written from pure symmetry considerations. In Sec. III A the symmetry of the graphene crystal is reviewed. In Sec. III B the symmetry considerations are used to write the electronic part of the Hamiltonian. Section III C is dedicated to the symmetry analysis of the Dirac part of the electron Hamiltonian, whose symmetry is significantly higher than the symmetry of the crystal. Section III D is dedicated to the symmetry analysis of the in-plane crystal vibrations. In Secs. III E and III F we write the Hamiltonian of interaction of electrons with the optical and acoustical vibrations, respectively. Section III G is dedicated to the symmetry analysis of the out-of-plane vibrations of the graphene crystal. In Sec. III H the Hamiltonian of the interaction of electrons with the electromagnetic field is written.

Section IV describes the general scheme of the calculation of Raman-peak intensities using the standard perturbation theory. In Sec. IV A Green's functions are introduced, and in Sec. IV B the general expression for the Raman-scattering

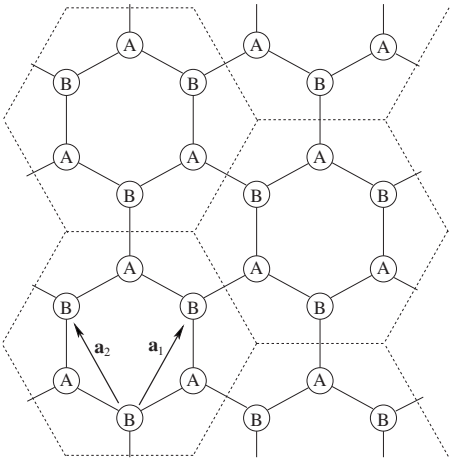

FIG. 3. The honeycomb lattice with two atoms (A and B) per unit cell. Tripled unit cells are shown by dashed hexagons.

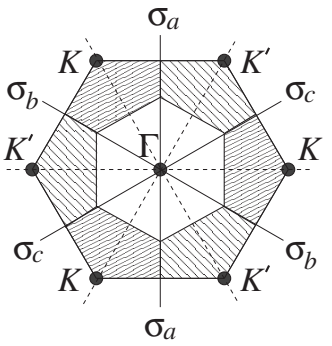

FIG. 4. The first Brillouin zone corresponding to the honeycomb lattice and its wrapping upon tripling of the unit cell. Regions with the same shading should be translated so that the K,K' points move to the Γ point to form the first Brillouin zone of the crystal with the tripled unit cell. Solid lines show the σ_a, σ_b, σ_c reflection axes. The σ_a', σ_b', σ_c' reflection axes are shown by dashed lines (not labeled).

probability is derived. In Sec. IV C we discuss the electron inelastic scattering and calculate the electronic self-energy due to the electron-phonon coupling.

In Sec. V one-phonon Raman scattering is discussed and it is shown that the calculation of the one-phonon peak intensity cannot be performed within the low-energy theory. In Sec. VI the two-phonon Raman-peak intensities are calculated, first, under the assumption of the Dirac electron spectrum (Sec. VI A) and then taking into account the trigonal band warping and electron-hole asymmetry (Sec. VI B). In Sec. VII the intensity I_{4K} of the most intense four-phonon peak is calculated. Sections VIII A and VIII B are dedicated to the renormalization of the electron-phonon coupling constants due to Coulomb interaction and due to the electron-phonon interaction, respectively.

III. SYMMETRIES AND HAMILTONIAN (REF. 42)

A. Symmetry of the crystal

Since the typical energy of the incident photon (about 2 eV) is much smaller than the π-electron bandwidth ($\sim$20 eV), one can expect the low-energy excitations to play the dominant role. In this section we employ standard symmetry analysis[43] to fix the form of the low-energy Hamiltonian. We prefer not to choose any specific basis and use algebraic properties.

The carbon atoms of graphene form a honeycomb lattice with two atoms per unit cell, labeled A and B (Fig. 3), the distance between nearest neighbors being $a=1.42$ Å. Three out of four electrons of the outer shell of each carbon atom form strong σ bonds with its three nearest neighbors and represent no interest to us. The remaining π orbitals (one per each carbon atom) give rise to the half-filled π band.

In this paper we will not consider the dimension, perpendicular to the crystal plane, so the point symmetry group of the graphene crystal is C_{6v}. It contains 12 elements: the identity, five rotations C_6^n, $n=1,\ldots,5$ (C_m denoting the rotation by $2\pi/m$), and six reflections in planes perpendicular to the crystal plane. The three reflections leaving the A and B sublattices invariant are denoted by σ_a, σ_b, σ_c, while those swapping the A and B sublattices points will be denoted by σ_a', σ_b', σ_c'. Table I lists the irreducible representations of the

TABLE I. Irreducible representations of the groups C_{6v} and C_{3v} and their characters.

C_{6v}	E	C_2	$2C_3$	$2C_6$	$\sigma_{a,b,c}$	$\sigma'_{a,b,c}$
A_1	1	1	1	1	1	1
A_2	1	1	1	1	−1	−1
B_2	1	−1	1	−1	1	−1
B_1	1	−1	1	−1	−1	1
E_1	2	−2	−1	1	0	0
E_2	2	2	−1	−1	0	0

C_{3v}	E	$2C_3$	$\sigma'_{a,b,c}$
A_1	1	1	1
A_2	1	1	−1
E	2	−1	0

group C_{6v} and their characters.

The first Brillouin zone of the crystal is a hexagon (Fig. 4). Out of the six corners of the hexagon only two are inequivalent. They are called K and K' points. The group of the wave vector at these points is C_{3v}. The states at these points are twice degenerate, transforming according to the two-dimensional irreducible representation (E) of C_{3v}. Transformations, swapping K and K', thus belonging to C_{6v} but not to C_{3v} (reflection σ_v in the plane, perpendicular to that of σ_v', and rotations C_2, C_6), fix the energies at K, K' to be equal. One can form real linear combinations of wave functions from K and K' points which transform according to E_1 and E_2 representations of C_{6v}. The degeneracy at K, K' points, in combination with the absence of any other states in the Brillouin zone with the same energy, fixes the Fermi level of a half-filled band to be at this energy, which is thus natural to choose as $\epsilon=0$.

Instead of dealing with degenerate states at two different points of the Brillouin zone (K, K'), one can triple the unit cell of the crystal. The new unit cell contains six atoms which form a hexagon (Fig. 3), while the new Brillouin zone is only $1/3$ of the original one (Fig. 4). The advantage of this approach is that now both K and K' are mapped onto the Γ point, so one does not have to consider the two of them separately.

Tripling of the unit cell means that two translations $t_{\mathbf{a}_1}$ and $t_{\mathbf{a}_2}$ are factorized out from the translation group of the crystal, so they should be added to the point group, which becomes $C_{6v}''=C_{6v}+(t_{\mathbf{a}_1}C_{6v})+(t_{\mathbf{a}_2}C_{6v})$. Irreducible representations of this group and their characters are shown in Table II. The states of the π electrons at the new Γ point form a six-dimensional representation which is reduced as A_1+B_2+G', where A_1 and B_2 states are the nondegenerate ones corresponding to the old Γ point, while the four-dimensional irreducible representation G' contains the zero-energy states inherited from the old K, K' points.

In order to write down the low-energy electronic Hamiltonian, we have to consider 4×4 Hermitian matrices acting in the four-dimensional space of the zero-energy electronic states. The basis in the 16-dimensional space of such matrices is provided by the generators of the SU(4) group forming a 16-dimensional reducible representation of C_{6v} or C_{6v}''. This representation is reduced as

$$(E_1+E_2)\times(E_1+E_2)=2(A_1+A_2+B_1+B_2+E_1+E_2) \tag{5}$$

within the group C_{6v} (the two sectors corresponding to matrices either diagonal or off diagonal in the KK' subspace) or as

$$G'\times G'=A_1+B_1+B_2+A_2+E_1+E_2+E_1'+E_2'+G' \tag{6}$$

within the group C_{6v}''. The correspondence between Eqs. (5) and (6) is given in Table III.

The most convenient way to identify the matrices is by specifying the irreducible representation, according to which they transform, rather by specifying their explicit form in some particular basis. So the matrix which transforms according to the A_2 representation of C_{6v}'' will be denoted by Σ_z and called the z component of the isospin (the only arbitrariness in this definition is the overall sign). The two matrices which transform according to the vector E_1 representation of C_{6v}'' will be denoted by $\{\Sigma_x,\Sigma_y\}\equiv\boldsymbol{\Sigma}$ [defined up to an arbitrary rotation, see Eq. (15a) below] and so on. The full list of definitions and notations is given in Table III.

Explicit expressions for the electronic matrices are not needed as long as their algebraic rules are specified. The simplest way to specify these rules is to express all the 16 matrices in terms of two sets, $\{\Sigma_x,\Sigma_y,\Sigma_z\}$ and $\{\Lambda_x,\Lambda_y,\Lambda_z\}$, and their products, where the matrices from the same set satisfy the Pauli-matrix algebra, while matrices from different sets just commute. In Appendix A we show how these rules can be established and give the explicit expressions for the matrices for some specific choices of the basis. We also note that $e^{(2\pi i/3)\Sigma_z}$ is the matrix of the C_3 rotation, $\Lambda_x\Sigma_z$ of the C_2 rotation, $\Lambda_z\Sigma_x$ of the σ_a' reflection, $\Lambda_y\Sigma_y$ of the σ_a reflection, and $e^{\pm(2\pi i/3)\Lambda_z}$ are the matrices of the two elementary translations.

B. Electronic wave functions and Hamiltonian

Since there are two π orbitals per unit cell, the eigenfunctions for each wave vector $\mathbf{k}$ in the Brillouin zone are given by $e^{i\mathbf{k}\mathbf{r}}\mathcal{U}_{\mathbf{k},\pm}(\mathbf{r},z)$, where the two Bloch functions $\mathcal{U}_{\mathbf{k},\pm}(\mathbf{r},z)$,

TABLE II. Irreducible representations of the group $C_{6v}''=C_{6v}+(t_{\mathbf{a}_1}C_{6v})+(t_{\mathbf{a}_2}C_{6v})$ and their characters.

C_{6v}''	E	$t_{\mathbf{a}_1}$, $t_{\mathbf{a}_2}$	C_2, $t_{\mathbf{a}_1}C_2$, $t_{\mathbf{a}_2}C_2$	C_3, C_3^2	$t_{\mathbf{a}_1}C_3$, $t_{\mathbf{a}_1}C_3^2$, $t_{\mathbf{a}_2}C_3$, $t_{\mathbf{a}_2}C_3^2$	C_6, C_6^5, $t_{\mathbf{a}_1}C_6$, $t_{\mathbf{a}_1}C_6^5$, $t_{\mathbf{a}_2}C_6$, $t_{\mathbf{a}_2}C_6^5$	$\sigma_{a,b,c}'$	$t_{\mathbf{a}_1}\sigma_{a,b,c}'$, $t_{\mathbf{a}_2}\sigma_{a,b,c}'$	$\sigma_{a,b,c}$, $t_{\mathbf{a}_1}\sigma_{a,b,c}$, $t_{\mathbf{a}_2}\sigma_{a,b,c}$
A_1	1	1	1	1	1	1	1	1	1
A_2	1	1	1	1	1	1	−1	−1	−1
B_2	1	1	−1	1	1	−1	−1	−1	1
B_1	1	1	−1	1	1	−1	1	1	−1
E_1	2	2	−2	−1	−1	1	0	0	0
E_2	2	2	2	−1	−1	−1	0	0	0
E_1'	2	−1	0	2	−1	0	2	−1	0
E_2'	2	−1	0	2	−1	0	−2	1	0
G'	4	−2	0	−2	1	0	0	0	0

TABLE III. Classification of 4×4 Hermitian matrices and their transformation properties under time reversal $\mathcal{T}$.

	KK'-diagonal matrices						KK'-off-diagonal matrices					
C''_{6v} irreps	A_1	B_1	A_2	B_2	E_1	E_2	E'_1		E'_2		G'	
C_{6v} irreps	A_1	B_1	A_2	B_2	E_1	E_2	A_1	B_1	A_2	B_2	E_1	E_2
Notation	$\mathbb{1}$	Λ_z	Σ_z	$\Lambda_z\Sigma_z$	Σ_x,Σ_y	$-\Lambda_z\Sigma_y,\Lambda_z\Sigma_x$	$\Lambda_x\Sigma_z$	$\Lambda_y\Sigma_z$	Λ_x	Λ_y	$\Lambda_x\Sigma_y,-\Lambda_x\Sigma_x$	$\Lambda_y\Sigma_x,\Lambda_y\Sigma_y$
$\mathcal{T}$	+	−	−	+	−	+	+	+	−	−	+	+

periodic in $\mathbf{r}=(x,y)$, are even and odd with respect to the reflection σ'_a and are normalized as

$$\int \mathcal{U}^*_{\mathbf{k},i}(\mathbf{r},z)\mathcal{U}_{\mathbf{k},j}(\mathbf{r},z)d^2\mathbf{r}dz = L_xL_y\delta_{ij}, \quad i,j=+,-, \tag{7}$$

where L_xL_y is the crystal area. It is more convenient to choose their linear combinations localized near each carbon atom: $\mathcal{U}_{\mathbf{k},A}=(\mathcal{U}_{\mathbf{k},+}+\mathcal{U}_{\mathbf{k},-})/\sqrt{2}$ and $\mathcal{U}_{\mathbf{k},B}=(\mathcal{U}_{\mathbf{k},+}-\mathcal{U}_{\mathbf{k},-})/\sqrt{2}$. In this basis an arbitrary wave function $\Psi(\mathbf{r},z)$ involving only low-energy states can be written in terms of a four-component smooth envelope function $\psi(\mathbf{r})$ or its Fourier transform $\psi(\mathbf{p})$, $pa\ll1$, as

$$\begin{aligned}\Psi(\mathbf{r},z) = \int \frac{d^2\mathbf{p}}{(2\pi)^2}[&\psi_{K,A}(\mathbf{p})e^{i(\mathbf{K}+\mathbf{p})\mathbf{r}}\mathcal{U}_{\mathbf{K},A}(\mathbf{r},z)\\ &+\psi_{K,B}(\mathbf{p})e^{i(\mathbf{K}+\mathbf{p})\mathbf{r}}\mathcal{U}_{\mathbf{K},B}(\mathbf{r},z)\\ &+\psi_{K',A}(\mathbf{p})e^{i(\mathbf{K}'+\mathbf{p})\mathbf{r}}\mathcal{U}_{\mathbf{K}',A}(\mathbf{r},z)\\ &+\psi_{K',B}(\mathbf{p})e^{i(\mathbf{K}'+\mathbf{p})\mathbf{r}}\mathcal{U}_{\mathbf{K}',B}(\mathbf{r},z)].\end{aligned} \tag{8}$$

The low-energy effective electronic Hamiltonian $H_{\mathrm{el}}(\mathbf{p})$ is defined as a 4×4 matrix whose matrix element between any two smooth envelope functions $\psi(\mathbf{r})$ and $\tilde{\psi}(\mathbf{r})$ coincides with the matrix element of the microscopic Hamiltonian $\mathcal{H}_{\mathrm{el}}(-i\nabla,-i\partial_z;\mathbf{r},z)$ including the periodic crystal potential between the corresponding full wave functions $\Psi(\mathbf{r},z)$ and $\tilde{\Psi}(\mathbf{r},z)$ (see Appendix B for details),

$$\begin{aligned}&\int \psi^\dagger(\mathbf{r})H_{\mathrm{el}}(-i\nabla)\tilde{\psi}(\mathbf{r})d^2\mathbf{r}\\ &\quad=\int \Psi^*(\mathbf{r},z)\mathcal{H}_{\mathrm{el}}(-i\nabla,-i\partial_z;\mathbf{r},z)\tilde{\Psi}(\mathbf{r},z)d^2\mathbf{r}dz.\end{aligned} \tag{9}$$

Strictly speaking, the spin index should also be attached to the enevlope function $\psi(\mathbf{r})$. However, it would make the formulas more cumbersome, and we prefer to omit it, as none of the calculations of the present paper will concern a nontrivial spin structure. The only role of the spin will be to provide an additional degeneracy, which will be accounted for and mentioned separately every time it will enter the calculations.

We expand the effective Hamiltonian in powers of $\mathbf{p}$: $H_{\mathrm{el}}(\mathbf{p})=H_1(\mathbf{p})+H_2(\mathbf{p})+\cdots$, where $H_n(\mathbf{p})=O(p^n)$. One can write down different terms from symmetry considerations, taking into account that momentum components p_x,p_y transform according to E_1 (vector) representation of C_{6v}. The leading term in the Hamiltonian, $H_1(\mathbf{p})$, must have the Dirac form,[44]

$$H_1(\mathbf{p}) = vp_x\Sigma_x + vp_y\Sigma_y \equiv v\mathbf{p}\boldsymbol{\Sigma}. \tag{10}$$

The coefficient v turns out to be equal to $v\approx10^8$ cm/s ≈7 eV A; it can be related to the nearest-neighbor coupling matrix element t of the tight-binding model as $v=3ta/2$. The four eigenstates of Hamiltonian (10) for each $\mathbf{p}$ can be classified by the value (±1) of projection of the isospin $\boldsymbol{\Sigma}$ on $\mathbf{p}$, corresponding to the energies $\pm v|\mathbf{p}|$. In other words, Hamiltonian (10) is diagonalized by a unitary transformation,

$$H_1(\mathbf{p}) = e^{-i\Sigma_z\varphi_{\mathbf{p}}/2}e^{-i\Sigma_y\pi/4}vp\Sigma_z e^{i\Sigma_y\pi/4}e^{i\Sigma_z\varphi_{\mathbf{p}}/2}, \tag{11}$$

where $\varphi_{\mathbf{p}}=\arctan(p_y/p_x)$ is the polar angle of the vector $\mathbf{p}$.

Various perturbations of the Dirac Hamiltonian (10) should also be classified according to Table III. Only those containing the matrix Σ_z will open a gap in the electron spectrum. Perturbations, not containing Σ_i, correspond to an energy shift of the whole spectrum (which may be accompanied by valley mixing if Λ_i matrices are involved). Perturbations, proportional to $\boldsymbol{\Sigma}$, correspond to a momentum shift of the Dirac points, which can be viewed as a gauge vector potential.

The next term in the Hamiltonian can be written by taking into account that the symmetric tensor p_ip_j can be decomposed into p^2, transforming according to A_1, and $2p_xp_y$, $p_x^2-p_y^2$, transforming according to E_2,

$$H_2(\mathbf{p}) = \alpha_0p^2\mathbb{1} + \alpha_3[-2p_xp_y\Sigma_y + (p_x^2-p_y^2)\Sigma_x]\Lambda_z. \tag{12}$$

The first term describes electron-hole asymmetry; it vanishes in the nearest-neighbor tight-binding model and appears only if coupling to the second-nearest neighbors is included. The second term, corresponding to E_2 representation, is responsible for the so-called trigonal band warping. In the nearest-neighbor tight-binding model its value is given by $-3ta^2/8$.

At this point it is convenient to introduce the time-reversal operation whose action on the microscopic spinless wave function is defined by $\Psi(\mathbf{r})\mapsto\Psi^*(\mathbf{r})$. For the four-component envelope function $\psi(\mathbf{r})$ this definition translates into

$$\psi(\mathbf{r})\underset{\mathcal{T}}{\mapsto}U_{\mathcal{T}}\psi^*(\mathbf{r}), \tag{13}$$

where $U_{\mathcal{T}}$ is a unitary 4×4 matrix, with an additional requirement $U_{\mathcal{T}}U^*_{\mathcal{T}}=\mathbb{1}$, whose explicit form depends on the

choice of the basis. The action of time reversal on the effective electronic Hamiltonian is defined by

$$H_{\mathrm{el}}(\mathbf{p},\mathbf{r}) \underset{\mathcal{T}}{\mapsto} U_{\mathcal{T}} H_{\mathrm{el}}^{*}(-\mathbf{p},\mathbf{r}) U_{\mathcal{T}}^{\dagger}. \tag{14}$$

Behavior of electronic matrices under the time reversal is listed in Table III.

Time-reversal symmetry of the Hamiltonian does not add any new symmetries to the spectrum, as compared to those imposed by the spatial symmetry C_{6v} (namely, C_{3v} symmetry of the spectrum around each of K,K' points and the mirror symmetry between the spectra at K and K' points), because the action of the time reversal on the wave vector is identical to that of the C_2 rotation, $\mathbf{K}+\mathbf{p} \mapsto \mathbf{K}'-\mathbf{p}$. However, some perturbations may lift the C_2 symmetry while still preserving the time-reversal one (see Secs. III E and III H).

C. Additional symmetries of the Dirac Hamiltonian

Dirac Hamiltonian (10) has a higher symmetry than the microscopic symmetry C_{6v}. The additional symmetries are (i) the full intravalley rotational symmetry $C_{\infty v}$,

$$\boldsymbol{\Sigma} \mapsto e^{-i\Sigma_z \varphi/2} \boldsymbol{\Sigma} e^{i\Sigma_z \varphi/2}, \tag{15a}$$

$$\begin{pmatrix} p_x \\ p_y \end{pmatrix} \mapsto \begin{pmatrix} \cos\varphi & -\sin\varphi \\ \sin\varphi & \cos\varphi \end{pmatrix} \begin{pmatrix} p_x \\ p_y \end{pmatrix}, \tag{15b}$$

which leaves $H_1(\mathbf{p})$ invariant and (ii) the chiral property,

$$U_{\mathcal{C}} H_1 U_{\mathcal{C}} = -H_1, \quad U_{\mathcal{C}} \equiv \Sigma_z, \tag{16}$$

which ensures the symmetry of the spectrum with respect to $\epsilon \to -\epsilon$ (i.e., particle-hole symmetry).

The intravalley "time-reversal" symmetry, mentioned in Ref. 45, can be represented as a combination of time reversal (13), intravalley rotation (15a) by π, and the C_2 rotation,

$$\psi \mapsto \Lambda_x \Sigma_z e^{-i\Sigma_z \pi/2} U_{\mathcal{T}} \psi^{*} = -i\Lambda_x U_{\mathcal{T}} \psi^{*}. \tag{17}$$

Applying this operation twice results in a minus sign, since the matrix Λ_x is odd under time reversal. If one wishes to include the second-order Hamiltonian (12), the A_1 term preserves only the rotational symmetry $C_{\infty v}$, while the E_2 term preserves only chiral property (16).

D. In-plane phonon modes

There is quite extensive literature dedicated to the phonon modes of graphene and graphite and their symmetry analysis (see, e.g., Ref. 2, and references therein). To make the presentation self-contained, we briefly repeat the facts which are necessary for the subsequent considerations.

The only phonons that can efficiently couple to the low-energy electronic states are those near the Γ point (coupling electronic states in the same valley) and near the K,K' points (coupling electronic states in different valleys; note that $\mathbf{K}-\mathbf{K}'$ is equivalent to $\mathbf{K}'$). As a result, each unit cell has 4 in-plane degrees of freedom (two per each carbon atom). At Γ point one has two acoustic and two optical modes. Coupling of the acoustical modes with a wave vector $\mathbf{q}$ to the electron motion must vanish as $q \to 0$ and thus be small in the parameter qa, but we consider them for the sake of completeness. For eight modes at K,K' points it is more convenient to consider their real linear combinations which transform according to $A_1+B_1+A_2+B_2+E_1+E_2$ representations of the group C_{6v}. All 12 modes are shown in Fig. 5. They are linearly polarized, in contrast to the basis with a definite wave vector, which would have a circular polarization.

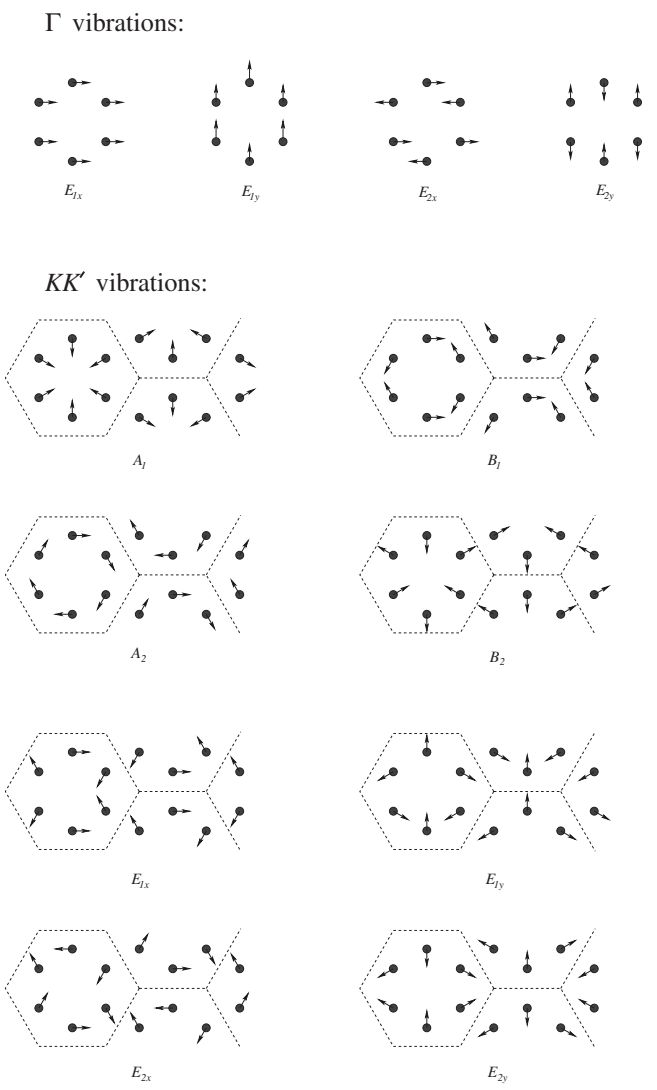

FIG. 5. In-plane phonon modes at Γ point and real linear combinations of the phonon modes at K,K' points corresponding to different irreducible representations of C_{6v}. The dashed lines show tripled unit cells.

After having mixed the K and K' modes, it is natural to switch to the tripled unit-cell representation. Analogous to Eq. (8) for electrons, an arbitrary lattice displacement pattern, involving phonon states with wave vectors close either to Γ, K, or K' points, can be expressed in terms of a smooth envelope function $u(\mathbf{r})$ or its Fourier transform $u(\mathbf{q})$. Since we have to specify two Cartesian components of displacements for each of the six atoms in the tripled unit cell, $\underline{\delta x} = (\delta x_1, \delta y_1, \ldots, \delta x_6, \delta y_6)^T$, the envelope of normal coordinates $u(\mathbf{q})$ is a 12-component vector,

$$\delta\underline{x}(\mathbf{R}) = \int \frac{d^2\mathbf{q}}{(2\pi)^2} \sum_{\mu=1}^{12} u_\mu(\mathbf{q}) e^{i\mathbf{q}\mathbf{R}} \underline{\mathcal{X}}_{\mathbf{q},\mu}, \tag{18}$$

where $\mathbf{R}$ spans a discrete set of points, labeling different unit cells, and $\underline{\mathcal{X}}_{\mathbf{q},\mu}$ is the pattern of displacements for the μth normal mode, normalized as

$$\underline{\mathcal{X}}^T_{-\mathbf{q},\mu} \underline{\mathcal{X}}_{\mathbf{q},\mu'} = 6\delta_{\mu\mu'}. \tag{19}$$

For $\mathbf{q}=0$ the 12 normal modes $\underline{\mathcal{X}}_{\mathbf{q}=0,\mu}$ are shown in Fig. 5. Introducing $\Pi_\mu(\mathbf{r})$, the canonically conjugate momentum to $u_\mu(\mathbf{r})$, we write the bare phonon Hamiltonian as

$$H_{ph} = \sum_{\mu=1}^{12} \int \frac{Nd^2\mathbf{r}}{L_x L_y} \left[\frac{\Pi^2_\mu(\mathbf{r})}{2M} + \frac{M}{2} u_\mu(\mathbf{r}) \omega^2_\mu(-i\nabla) u_\mu(\mathbf{r}) \right], \tag{20}$$

with $M=1.993\times10^{-23}$ g being the carbon atom mass, N the total number of the carbon atoms in the crystal, and $\omega_\mu(\mathbf{q})$ the frequency of the μth normal mode.

At $\mathbf{q}=0$ the modes belonging to the same irreducible representation of C''_{6v} are degenerate. Expansion of the phonon potential energy at small $\mathbf{q}$, describing the splitting, can be done analogously to that of the electronic Hamiltonian. It is convenient to preserve form (20) of the Hamiltonian, but instead of summing over normal modes μ one should sum over irreducible representations of C''_{6v}. For each irreducible representation $\omega^2(-i\nabla)$ becomes a matrix acting in the space of the degenerate modes belonging to this representation.

For two-dimensional representations (E_1 and E_2 at the Γ point and E'_1, E'_2 at K, K' points) we have to classify 2×2 Hermitian matrices according to irreducible representations in the corresponding decomposition,

$$E_1 \times E_1 = A_1 + A_2 + E_2, \tag{21a}$$

$$E_2 \times E_2 = A_1 + A_2 + E_2, \tag{21b}$$

$$E'_1 \times E'_1 = A_1 + A_2 + E'_1, \tag{21c}$$

$$E'_2 \times E'_2 = A_1 + A_2 + E'_2. \tag{21d}$$

The basis in the space of such matrices is provided by the unit matrix σ_0 transforming according to A_1, the Pauli matrix σ_z transforming according to A_2, and the Pauli matrices σ_x, σ_y transforming according to the third term in each decomposition. Since the components q_x, q_y transform according to E_1, the linear in $\mathbf{q}$ term is absent for all two-dimensional representations. For the four-dimensional representation G' we have to deal with 4×4 matrices, so everything is fully analogous to the electronic case, and these phonons also have Dirac spectrum. In the second order we have $q^2 \sim A_1$ and $q_x^2 - q_y^2, 2q_xq_y \sim E_2$, so we can write

$$\omega^2_{E_1}(\mathbf{q}) = \frac{v_L^2 + v_T^2}{2} q^2 + \frac{v_L^2 - v_T^2}{2} [(q_x^2 - q_y^2)\sigma_x - 2q_xq_y\sigma_y], \tag{22a}$$

$$\omega^2_{E_2}(\mathbf{q}) = \omega^2_{E_2} + \omega_{E_2}(J_L + J_T)q^2 + \omega_{E_2}(J_L - J_T)[(q_x^2 - q_y^2)\sigma_x - 2q_xq_y\sigma_y], \tag{22b}$$

$$\omega^2_{E'_1}(\mathbf{q}) = \omega^2_{E'_1} + 2\omega_{E'_1} J_{E'_1} q^2, \tag{22c}$$

$$\omega^2_{E'_2}(\mathbf{q}) = \omega^2_{E'_2} + 2\omega_{E'_2} J_{E'_2} q^2, \tag{22d}$$

$$\omega^2_{G'}(\mathbf{q}) = \omega^2_{G'} + 2\omega_{G'} v_{G'} \mathbf{q}\boldsymbol{\Sigma} + O(q^2). \tag{22e}$$

The 2×2 matrices appearing in Eqs. (22a) and (22b) can be diagonalized to yield the dispersion of the longitudinal and transverse phonons: $\omega_{E_1,L(T)}(\mathbf{q}) = v_{L(T)}q$ and $\omega_{E_2,L(T)}(\mathbf{q}) = \omega_{E_2} + J_{L(T)}q^2$.

E. Electronic coupling to in-plane optical phonons

In the electron-phonon interaction Hamiltonian the normal-mode displacements should be paired with the electronic matrices, corresponding to the same irreducible representation. For optical phonons it is sufficient to take the leading $\mathbf{q}=0$ term, so we have one independent coupling constant for each irreducible representation of the group C''_{6v},

$$H_{e\text{-opt}} = F_\Gamma [\mathbf{u}_{E_2} \times \Lambda_z \boldsymbol{\Sigma}]_z + F_K (u_{A_1} \Lambda_x \Sigma_z + u_{B_1} \Lambda_y \Sigma_z) + F'_K ([\mathbf{u}_{E_1} \times \Lambda_x \boldsymbol{\Sigma}]_z + \mathbf{u}_{E_2} \Lambda_y \boldsymbol{\Sigma}). \tag{23}$$

Note that E'_2 phonons cannot couple to the electron motion in this approximation since the corresponding matrices Λ_x, Λ_y change sign under the time reversal, while the electronic Hamiltonian must preserve time-reversal symmetry even in the crystal with displaced atoms. Electrons will couple to (i) momentum $\Pi_{E'_2}$, whose effect is small in the ratio of the phonon frequency $\omega_{E'_2}$ to the electron bandwidth, (ii) gradient $\nabla u_{E'_2}$, whose effect is small in the parameter qa, and (iii) the squares of displacements $u^2_{E'_2}$, whose effect is small in the parameter $1/(Ma^2\omega_{E'_2})$.

The three constants in Eq. (23) can be evaluated in the tight-binding approximation, where they are expressed in terms of $F \equiv \partial t/\partial a \approx 6$ eV/A—the change in the nearest-neighbor coupling matrix element with the distance between the atoms. We obtain $F_\Gamma = F_K = 3F$, while F'_K vanishes. This vanishing is an artifact of the nearest-neighbor bond-stretching approximation. If one takes into account the dependence of the electronic Hamiltonian on the angles between the bonds, F'_K becomes different from zero. Nevertheless, it is an order of magnitude smaller than F_K (e.g., density-functional theory calculations[31] give $F'_K/F_K \approx 0.13$), and we neglect the G' phonons for the rest of the paper. Thus, our attention will be focused on the two degenerate modes E_2 and E'_1, which will be referred to simply as Γ and K phonons, and their frequencies will be denoted by $\omega_{E_2,L}(\mathbf{q}) = \omega_{\Gamma,L}(\mathbf{q})$, $\omega_{E_2,T}(\mathbf{q}) = \omega_{\Gamma,T}(\mathbf{q})$, and $\omega_{E'_1}(\mathbf{q}) = \omega_K(\mathbf{q})$.

The strength of electron-phonon interaction can be conveniently characterized by the dimensionless coupling constants

$$\lambda_\Gamma = \frac{F_\Gamma^2}{M\omega_\Gamma(0)v^2}\frac{\sqrt{27}a^2}{4}, \quad \lambda_K = \frac{F_K^2}{M\omega_K(0)v^2}\frac{\sqrt{27}a^2}{4}, \quad (24)$$

where $\sqrt{27}a^2/4$ is the area per carbon atom. For $F_\Gamma = F_K = 3F$, $F = 6$ eV/Å, $M = 2.00 \times 10^{-23}$ g $= 2.88 \times 10^3$ (eV Å^2)$^{-1}$, $v = 10^6$ m/s $= 6.58$ eV Å, $\omega_\Gamma = 1580$ cm$^{-1} = 0.196$ eV, $\omega_K = 1370$ cm$^{-1} = 0.170$ eV, and $a = 1.42$ Å, we have

$$\frac{F_\Gamma^2}{M\omega_\Gamma v^2}\frac{\sqrt{27}a^2}{4} \approx 0.035, \quad \frac{F_K^2}{M\omega_K v^2}\frac{\sqrt{27}a^2}{4} \approx 0.040. \quad (25)$$

The easiest way to match the notations for the electron-phonon coupling constants, used in the present paper to those used in other works, is to compare observable quantities. For example, adding electrons to the system leads to a shift of the phonon frequencies. For the Γ phonons at $\mathbf{q}=0$ in the present notations this shift is expressed in terms of the Fermi energy ϵ_F as

$$\delta\omega_\Gamma = \frac{\lambda_\Gamma}{2\pi}\left(|\epsilon_F| + \frac{\omega_\Gamma}{4}\ln\frac{\omega_\Gamma - 2|\epsilon_F|}{\omega_\Gamma - 2|\epsilon_F|}\right). \quad (26)$$

Alternatively, one can look at the correction to the phonon dispersion as a function of the wave vector $\mathbf{q}$ (see Appendix E).

F. Electronic coupling to in-plane acoustical phonons

Since a uniform translation of the crystal cannot affect the electron motion, it can couple to acoustic phonons only through spatial and time derivatives of the corresponding displacements,

$$H_{e\text{-ac}} = \frac{\mathbf{\Pi}_{E_1}}{M}(\mathbf{p} + m_e v\mathbf{\Sigma}) + \Xi_0(\partial_x u_{E_1 x} + \partial_y u_{E_1 y})\mathbb{1} + \Xi_1(\partial_x u_{E_1 y} - \partial_y u_{E_1 x})\Sigma_z + \Xi_2[-(\partial_x u_{E_1 y} + \partial_y u_{E_1 x})\Sigma_y + (\partial_x u_{E_1 x} - \partial_y u_{E_1 y})\Sigma_x]\Lambda_z. \quad (27)$$

The general form of the coupling to $\mathbf{\Pi}_{E_1}$ in the first line follows from the symmetry considerations (the coefficient at $\mathbf{\Pi}_{E_1}$ should transform according to E_1 and change sign under time reversal). However, its exact form follows from the $\mathbf{k}\cdot\mathbf{p}$ perturbation theory (which identifies m_e with the free-electron mass) in combination with the requirement of Galilean invariance; if $\Psi(\mathbf{r},t)$ satisfied the Schrödinger equation for the stationary lattice, then for the lattice moving at a constant velocity $\dot{\mathbf{u}}_{E_1} = \mathbf{\Pi}_{E_1}/M$, the solution should be $\Psi(\mathbf{r} - \dot{\mathbf{u}}_{E_1}t, t)$ (we neglect the contribution of electrons to the total kinetic energy of the crystal). Coupling to the strain is written using the decomposition $E_1 \times E_1 = A_1 + A_2 + E_2$.

G. Out-of-plane phonons

The basis vectors for out-of-plane displacements coincide with those for the electronic wave-function amplitudes in the tight-binding picture (since in both cases single number is associated with each lattice site). At the Γ point the basis vectors represent A and B atoms shifting in the same direction or opposite directions, corresponding to A_1 and B_2 representations. For the K, K' phonons we have $E_1 + E_2$ representations of C_{6v} or the four-dimensional G' representation of C_{6v}'' in the tripled unit-cell picture. All six modes are shown in Fig. 6.

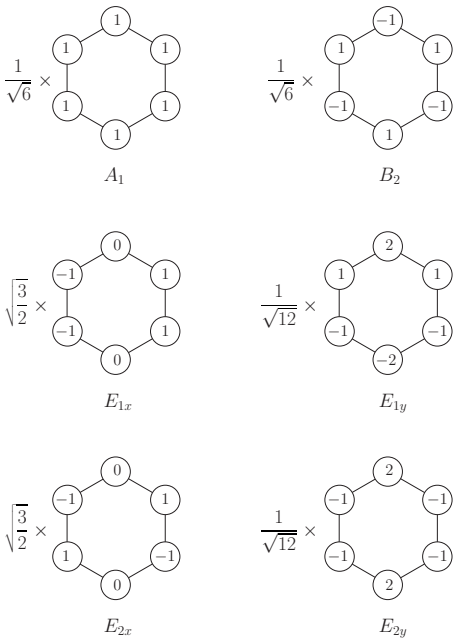

FIG. 6. Out-of-plane phonon modes at Γ point and real linear combinations of the phonon modes at K, K' points corresponding to different irreducible representations of C_{6v}.

For a suspended graphene sheet the A_1 mode has a frequency $\omega_{A_1}(\mathbf{q}) \propto q^2$ (see, e.g., Ref. 46). The frequencies of other modes are finite. All frequencies can be strongly affected by the interaction with the substrate (in particular, there will be no reason for the frequency of the A_1 mode to vanish at $\mathbf{q}=0$).

Out-of-plane displacements can couple to the electron motion only quadratically if the crystal is symmetric with respect to reflection in the crystal plane. While it is the case for a suspended graphene sheet, presence of a substrate may break this symmetry.[47]

H. Coupling to electromagnetic field

The Hamiltonian of interaction of electrons with the electromagnetic field, described by the long-wavelength scalar and vector potentials $\varphi(\mathbf{r})$ and $\mathbf{A}(\mathbf{r})$, can be obtained from the requirement of gauge invariance: $H_{\text{el}}(\mathbf{p}) \to H_{\text{el}}[\mathbf{p} - (e/c)\mathbf{A}] + e\varphi$. To the linear order in $\mathbf{A}$ we have

$$H_{e\text{-em}} = e\varphi - \frac{ev}{c}\mathbf{A}\mathbf{\Sigma}. \quad (28)$$

Besides coupling via gauge potentials, electrons can couple directly to electric and magnetic fields. Such terms are gauge invariant and cannot be deduced from the bare electronic Hamiltonian in the envelope function approxima-

tion, as they correspond to the effect of electromagnetic field on the microscopic Bloch functions. They should be introduced into the effective low-energy theory directly, and can be either calculated microscopically (see Appendix B for the calculation by $\mathbf{k}\cdot\mathbf{p}$ perturbation theory) or written from symmetry considerations.

The electric-field vector is invariant under time reversal, and its Cartesian components $\mathcal{E}_x$, $\mathcal{E}_y$, $\mathcal{E}_z$ transform according to $\mathcal{E}_z \sim A_1$, $(\mathcal{E}_x, \mathcal{E}_y) \sim E_1$ under C_{6v}. The magnetic-field vector changes sign under time reversal, and its components $\mathcal{B}_x$, $\mathcal{B}_y$, $\mathcal{B}_z$ transform as $\mathcal{B}_z \sim A_2$, $(-\mathcal{B}_y, \mathcal{B}_x) \sim E_1$ under C_{6v}. They can couple only to valley-diagonal matrices. Indeed, for uniform electric and magnetic fields the effective Hamiltonian must be invariant under translations, represented by the matrices $e^{\pm(2\pi i/3)\Lambda_z}$. This requirement is not satisfied by any matrix of the form $\Sigma_i\Lambda_x$, $\Sigma_i\Lambda_y$, $i=0,x,y,z$. In particular, the term proportional to $\mathcal{B}_x\Lambda_x\Sigma_x+\mathcal{B}_y\Lambda_x\Sigma_y$, considered in Ref. 48, must be absent (see Appendix B for a microscopic calculation).

These considerations enable us to write the Hamiltonian to the first order in the fields as

$$H'_{e\text{-}em} = -d_z\mathcal{E}_z\mathbb{1} + \mu_{xy}(\mathcal{B}_x\Sigma_y - \mathcal{B}_y\Sigma_x) - \mu_z\mathcal{B}_z\Sigma_z. \quad (29)$$

The first term in this Hamiltonian represents the coupling to the z component of electric-dipole moment of π electrons in each unit cell. The second term represents the coupling of the magnetic field to the in-plane component of the magnetic moment. These terms are forbidden for a suspended graphene sheet due to the symmetry with respect to reflection in the crystal plane but may be allowed if this symmetry is broken due to the presence of a substrate. On the contrary, the third term, corresponding to the z component of the magnetic moment of the unit cell, is allowed for a suspended graphene sheet as well (the z-component of the magnetic moment does not change sign under reflection in the crystal plane).

Terms quadratic in $\mathcal{E}$ and $\mathcal{B}$ correspond to polarizabilities of the unit cell. The corresponding Hamiltonian can be written following the same lines as above. This is, however, beyond the scope of our interest.

IV. RAMAN SCATTERING: GENERAL EXPRESSIONS

In this section we derive the general expressions for the Raman-scattering probability using the standard perturbation theory.

A. Green's functions

The second-quantized version of Dirac Hamiltonian (10) reads as

$$\hat{H}_1 = \int d^2\mathbf{r}\hat{\psi}^\dagger(\mathbf{r})(-iv\boldsymbol{\Sigma}\cdot\nabla)\hat{\psi}(\mathbf{r}). \quad (30)$$

Since all energies we are interested in ($\sim$1 eV) are much higher than temperature, we set the latter equal to zero. The zero-temperature electronic Green's function, corresponding to Hamiltonian (30), is given by

$$G(\mathbf{p},\epsilon) = -i\int \langle T\hat{\psi}(\mathbf{r},t)\hat{\psi}^\dagger(0,0)\rangle e^{-i\mathbf{p}\mathbf{r}+i\epsilon t}d^2\mathbf{r}dt$$

$$= \frac{\epsilon + v\mathbf{p}\cdot\boldsymbol{\Sigma}}{\epsilon^2 - (vp - io)^2}, \quad (31)$$

where io is the infinitesimal imaginary shift of the pole. T is the sign of the chronological ordering and the average is taken over the ground state of the system.

Upon quantization of the phonon field based on Hamiltonian (20), the normal-mode displacement operator and the bare phonon Hamiltonian become

$$\hat{u}_\mu(\mathbf{r}) = \sum_{\mathbf{q}} \frac{\hat{b}_{\mathbf{q},\mu}e^{i\mathbf{q}\mathbf{r}} + \hat{b}^\dagger_{\mathbf{q},\mu}e^{-i\mathbf{q}\mathbf{r}}}{\sqrt{2NM\omega_\mu(\mathbf{q})}}, \quad (32a)$$

$$\hat{H}_{ph} = \sum_{\mathbf{q},\mu} \omega_{\mathbf{q},\mu}\left(\hat{b}^\dagger_{\mathbf{q},\mu}\hat{b}_{\mathbf{q},\mu} + \frac{1}{2}\right), \quad (32b)$$

$$\sum_{\mathbf{q}} \equiv L_xL_y\int \frac{d^2\mathbf{q}}{(2\pi)^2}. \quad (32c)$$

The phonon Green's function is defined as

$$D_\mu(\mathbf{q},\omega) = -i\frac{2NM\omega_\mu(\mathbf{q})}{L_xL_y}\int \langle T\hat{u}_\mu(\mathbf{r},t)\hat{u}_\mu(0,0)\rangle e^{-i\mathbf{q}\mathbf{r}+i\omega t}d^2\mathbf{r}dt$$

$$= \frac{2\omega_\mu(\mathbf{q})}{\omega^2 - [\omega_\mu(\mathbf{q}) - io]^2}. \quad (33)$$

This definition implies that each electron-phonon vertex corresponding to the second-quantized version of the interaction Hamiltonian (23) contains, besides the coupling constant F_μ and the corresponding electronic matrix $\Lambda_i\Sigma_j=(\Lambda\Sigma)_\mu$, a factor $\sqrt{L_xL_y/[2NM\omega_\mu(\mathbf{q})]}$. Thus, the overall factor appearing in each vertex at small q is just $v\sqrt{\lambda_\mu/2}$, where λ_μ is the dimensionless coupling constant defined in Eq. (24). The factor $L_xL_y/N=\sqrt{27}a^2/4$ is the area per one carbon atom.

Upon quantization of the electromagnetic field the operator of the vector potential is expressed in terms of creation and annihilation operators $\hat{a}^\dagger_{\mathbf{Q},\ell}$, $\hat{a}_{\mathbf{Q},\ell}$ of three-dimensional photons in the quantization volume $V=L_xL_yL_z$ with the wave vector $\mathbf{Q}$ and two transverse polarizations $\ell=1,2$ with unit vectors $\mathbf{e}_{\mathbf{Q},\ell}$,

$$\hat{\mathbf{A}}(\mathbf{r}) = \sum_{\mathbf{Q},\ell}\sqrt{\frac{2\pi c}{VQ}}(\mathbf{e}_{\mathbf{Q},\ell}\hat{a}_{\mathbf{Q},\ell}e^{i\mathbf{Q}\mathbf{r}} + \mathbf{e}^*_{\mathbf{Q},\ell}\hat{a}^\dagger_{\mathbf{Q},\ell}e^{-i\mathbf{Q}\mathbf{r}}). \quad (34)$$

The photon propagator is defined analogously to the phonon one,

$$\Upsilon_\ell(\mathbf{Q},\Omega) = -i\frac{Q}{2\pi c}\int \langle T\hat{A}_\ell(\mathbf{r},t)\hat{A}_\ell(0,0)\rangle e^{-i\mathbf{Q}\mathbf{r}+i\Omega t}d^2\mathbf{r}dt$$

$$= \frac{2cQ}{\Omega^2 - [cQ - io]^2}, \quad (35)$$

so that each electron-photon vertex corresponding to the second-quantized version of the interaction Hamiltonian (28) contains the factor $e(v/c)$, playing the role of the coupling

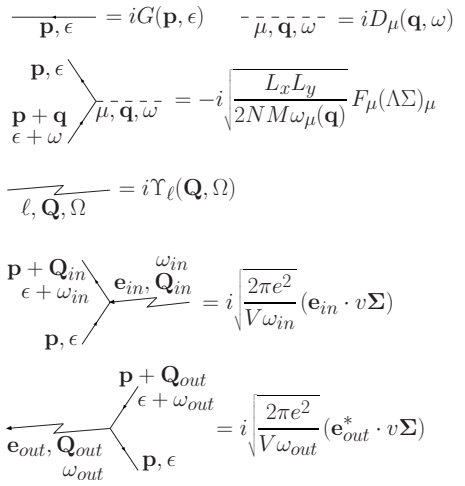

FIG. 7. Graphical representation of electron, phonon, and photon Green's functions and vertices.

constant, the electronic matrix $(\mathbf{e}_{\mathbf{Q},\ell}\cdot\boldsymbol{\Sigma})$, and a factor $\sqrt{2\pi c/Q}$.

Let us diagonalize each of the two electronic Green's functions, entering and leaving the electron-photon vertex, by transformation (11). Then, neglecting the change in the electronic momentum $\mathbf{p}$ upon emission of the photon, we transform the electronic matrix in the vertex as

$$e^{i\Sigma_z\varphi_\mathbf{p}i/2}e^{i\Sigma_y\pi/4}(\mathbf{e}_{\mathbf{Q},\ell}\cdot\boldsymbol{\Sigma})e^{-i\Sigma_z\varphi_\mathbf{p}/2}e^{-i\Sigma_y\pi/4} = \frac{(\mathbf{p}\cdot\mathbf{e}_{\mathbf{Q},\ell})}{|\mathbf{p}|}\Sigma_z + \frac{[\mathbf{p}\times\mathbf{e}_{\mathbf{Q},\ell}]_z}{|\mathbf{p}|}\Sigma_y, \tag{36}$$

where $\varphi_\mathbf{p}$ is the polar angle of the wave vector $\mathbf{p}$. Since we are interested in the interband transition, we need the Σ_y part of this expression, which tells us that the transition dipole moment is perpendicular to the electron momentum. The graphical representation of Green's functions and vertices, introduced in this section, is shown in Fig. 7.

B. Raman-scattering probability

Formally, n-phonon Raman scattering is a quantum-mechanical transition from the initial state with the crystal in the ground state and one incoming photon with the wave vector $\mathbf{Q}_{in}$, frequency $\omega_{in}=c|\mathbf{Q}_{in}|$, and polarization $\mathbf{e}_{in}$ into the final state with one outgoing photon with the wave vector $\mathbf{Q}_{out}$, frequency $\omega_{out}=c|\mathbf{Q}_{out}|$, polarization $\mathbf{e}_{out}$, and n phonons corresponding to normal modes $\mu_1,\ldots,\mu_n$ with wave vectors $\mathbf{q}_1,\ldots,\mathbf{q}_n$. Denoting the ground state of the system by $|\mathrm{vac}\rangle$, we represent these two states as $\hat{a}^\dagger_{in}|\mathrm{vac}\rangle$ and $\hat{a}^\dagger_{out}\hat{b}^\dagger_{\mu_1\mathbf{q}_1}\cdots\hat{b}^\dagger_{\mu_n\mathbf{q}_n}|\mathrm{vac}\rangle$. Let us introduce the S-matrix $\hat{S}(\infty)$ and define the amplitude of the n-phonon Raman scattering as

$$\mathcal{A}^{\mu_1\cdots\mu_n}_{\mathbf{q}_1\cdots\mathbf{q}_n}(\Omega;\{\omega_i\}_{i=1}^{i=n}) = \int\frac{\langle T\hat{a}_{out}(t)\hat{b}_{\mu_1\mathbf{q}_1}(t_1)\cdots\hat{b}_{\mu_n\mathbf{q}_n}(t_n)\hat{S}(\infty)\hat{a}^\dagger_{in}(0)\rangle}{\langle\hat{S}(\infty)\rangle} \times e^{i\Omega t}dt\prod_{i=1}^{n}e^{i\omega_it_i}dt_i. \tag{37}$$

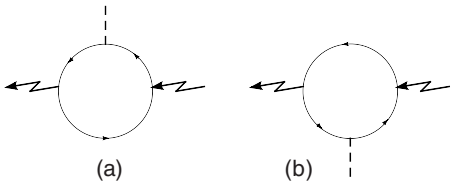

FIG. 8. Diagrams for the one-phonon Raman amplitude in the leading order.

Here the operators are taken in the interaction representation and T represents the chronological ordering.

The diagrammatic representation of amplitude (37) in the leading order in electron-photon and electron-phonon couplings is shown in Figs. 8 and 9 for $n=1$ and $n=2$, respectively. The incoming photon line corresponds to pairing of the operator $\hat{a}^\dagger_{in}$ and the outgoing lines to pairings of the operators $\hat{a}_{out}$, $\hat{b}_{\mu_i\mathbf{q}_i}$. The loop represents the intermediate states of the electron-hole pair; summation over the momentum circulating in the loop and integration over energy should be performed.

Let us separate Green's functions of the scattering particles [only the positive-frequency parts of Green's functions enter, as shown by the $(+)$ superscripts], the momentum-conserving δ function, and explicitly introduce the permutations $\mathcal{P}$ of the phonon indices,

$$\mathcal{A}^{\mu_1\cdots\mu_n}_{\mathbf{q}_1\cdots\mathbf{q}_n}(\Omega;\{\omega_i\}_{i=1}^{i=n}) = \frac{i}{\sqrt{V}}\Upsilon^{(+)}_{in}\left(\mathbf{Q}_{in},\Omega+\sum_{i=1}^{n}\omega_i\right)\frac{i}{\sqrt{V}}\Upsilon^{(+)}_{out}(\mathbf{Q}_{out},\Omega) \times\prod_{j=1}^{n}\frac{i}{\sqrt{L_xL_y}}D^{(+)}_{\mu_j}(\mathbf{q}_j,\omega_j)(2\pi)^2\delta\left(\sum_{i=1}^{n}\mathbf{q}_i+\mathbf{Q}_{out}-\mathbf{Q}_{in}\right) \times\sum_{\mathcal{P}}(-i)\mathcal{M}^{\mathcal{P}\{\mu_i\}}_{\mathcal{P}\{\mathbf{q}_i\}}(\Omega;\mathcal{P}\{\omega_i\}). \tag{38}$$

Then $-i\mathcal{M}$ is given by the sum of all topologically inequivalent diagrams with amputated external lines. Equivalently, in the leading order $\Sigma_\mathcal{P}(-i)\mathcal{M}_\mathcal{P}$ is given by the sum of all $(n+1)!$ connected pairings of electronic ψ operators while

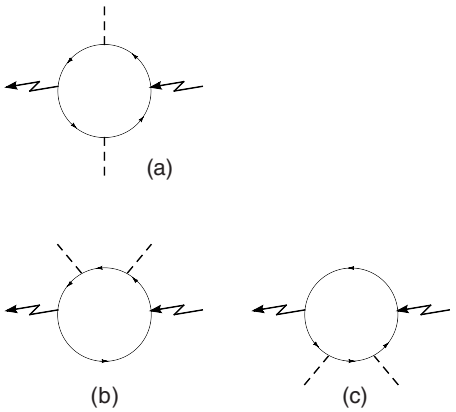

FIG. 9. Diagrams for the two-phonon Raman amplitude in the leading order.

electron-photon and electron-phonon vertices are held fixed.

The transition probability per unit time is given by

$$\lim_{t\to+\infty}\frac{1}{t}\left|\int \mathcal{A}^{\mu_1\cdots\mu_n}_{\mathbf{q}_1\cdots\mathbf{q}_n}(\Omega;\{\omega_i\}_{i=1}^{i=n})e^{-i\Omega t}\frac{d\Omega}{2\pi}\prod_{i=1}^{n}e^{-i\omega_i t}\frac{d\omega_i}{2\pi}\right|^2$$
$$=\frac{1}{V^2(L_xL_y)^n}2\pi\delta\left(\sum_{i=1}^{n}\omega_{\mathbf{q}_i}+\omega_{out}-\omega_{in}\right)$$
$$\times\left[(2\pi)^2\delta\left(\sum_{i=1}^{n}\mathbf{q}_i+\mathbf{Q}_{out}-\mathbf{Q}_{in}\right)\right]^2$$
$$\times\left|\sum_{\mathcal{P}}\mathcal{M}^{\mathcal{P}\{\mu_i\}}_{\mathcal{P}\{\mathbf{q}_i\}}(\omega_{out};\mathcal{P}\{\omega_{\mathbf{q}_i}\})\right|^2, \tag{39}$$

where we used the relation

$$\lim_{t\to+\infty}\frac{1}{t}\left|\frac{e^{izt}-1}{z}\right|^2=2\pi\delta(z). \tag{40}$$

The absolute dimensionless probability for the incoming photon to scatter with emission of n phonons of any kind is obtained by summing over all final states (here one should remember that a permutation of phonon arguments represents the same state) and multiplying by the photon attempt period L_z/c (at this point we also recall about the electron spin and multiply the matrix element by a factor of 2 which appears after tracing the Fermion loop with respect to spin indices),

$$I_n=\frac{1}{V^2}\frac{L_z}{c}\sum_{\mathbf{Q}_{out},\ell_{out}}\frac{1}{(L_xL_y)^n}\frac{1}{n!}$$
$$\times\sum_{\{\mu_i,\mathbf{q}_i\}}2\pi\delta\left(\sum_{i=1}^{n}\omega_{\mu_i}(\mathbf{q}_i)+c|\mathbf{Q}_{out}|-c|\mathbf{Q}_{in}|\right)$$
$$\times\left[(2\pi)^2\delta\left(\sum_{i=1}^{n}\mathbf{q}_i+\mathbf{Q}_{out}-\mathbf{Q}_{in}\right)\right]^2|2\mathcal{M}^{\{\mu_i\}}_{\{\mathbf{q}_i\}}|^2. \tag{41}$$

The square of the momentum δ function is taken care of by the relation $(2\pi)^2\delta(\mathbf{q}=0)=L_xL_y$, consistent with Eq. (32c). We can also pass to the spectrally resolved probability by inserting $1=\int d\omega_{out}\delta(\omega_{out}-c|\mathbf{Q}_{out}|)$,

$$\frac{dI_n}{d\omega_{out}}=\frac{1}{c}\sum_{\ell_{out}}\int\frac{d^3\mathbf{Q}_{out}}{(2\pi)^3}\delta(c|\mathbf{Q}_{out}|-\omega_{out})\frac{1}{(L_xL_y)^{n-1}}\frac{1}{n!}$$
$$\times\sum_{\{\mu_i\}}\sum_{\mathbf{q}_1+\cdots+\mathbf{q}_n=0}2\pi\delta\left(\sum_{i=1}^{n}\omega_{\mu_i}(\mathbf{q}_i)+\omega_{out}-\omega_{in}\right)$$
$$\times|2\mathcal{M}^{\{\mu_i\}}_{\{\mathbf{q}_i\}}|^2. \tag{42}$$

At first glance, the matrix element $\mathcal{M}^{\{\mu_i\}}_{\{\mathbf{q}_i\}}$ does not seem to depend on the outgoing photon wave vector $\mathbf{Q}_{out}$, since the latter is negligible in comparison with electron and phonon momenta contributing to $\mathcal{M}^{\{\mu_i\}}_{\{\mathbf{q}_i\}}$, so the integration over the photon wave vectors gives just $\omega^2_{out}/(2\pi^2c^3)$. However, $\mathcal{M}^{\{\mu_i\}}_{\{\mathbf{q}_i\}}$ depends on the orientation of the polarization vector $\mathbf{e}_{out}$, which, in turn, depends on the direction of $\mathbf{Q}_{out}$. Thus, we should consider the differential probability of emission into the elementary solid angle $do_{out}=\sin\Theta d\Theta d\Phi$, where the spherical angles $\Theta\in[0,\pi]$ and $\Phi\in[0,2\pi]$ parametrize the direction of $\mathbf{Q}_{out}$. For this differential probability we can write

$$4\pi\frac{dI_n}{do_{out}}=\frac{2\pi}{c}\frac{\omega^2_{out}}{2\pi^2c^3}\frac{1}{(L_xL_y)^{n-1}}\frac{1}{n!}\sum_{\{\mu_i\}}\sum_{\mathbf{q}_1+\cdots+\mathbf{q}_n=0}|2\mathcal{M}^{\{\mu_i\}}_{\{\mathbf{q}_i\}}|^2$$
$$=I_n^{\perp}(\mathbf{e}_{in}\cdot\mathbf{e}^*_{in})(\mathbf{e}_{out}\cdot\mathbf{e}^*_{out})+(I_n^{\parallel}-I_n^{\perp})$$
$$\times\frac{(\mathbf{e}_{in}\cdot\mathbf{e}_{out})(\mathbf{e}^*_{in}\cdot\mathbf{e}^*_{out})+(\mathbf{e}_{in}\cdot\mathbf{e}^*_{out})(\mathbf{e}^*_{in}\cdot\mathbf{e}_{out})}{2}. \tag{43}$$

We stress that only the *in-plane* components of the polarization vectors participate in these scalar products. In writing Eq. (43) we have assumed the crystal itself to be isotropic, which is true as long as the calculation is done for the Dirac spectrum. As soon as the trigonal warping term in Eq. (12) is taken into account, the orientation of the polarization vectors with respect to the crystal directions will enter. The corrections due to the trigonal warping will be analyzed in Sec. VI B and will be shown to be small.

For each direction of $\mathbf{Q}_{out}$ we can choose the basis of s and p polarizations,

$$\mathbf{e}_s=(-\sin\Phi,\cos\Phi,0),$$
$$\mathbf{e}_p=(-\cos\Theta\cos\Phi,-\cos\Theta\sin\Phi,\sin\Theta). \tag{44}$$

Suppose the light coming out from the sample is collected by a lens within a cone with the aperture $2\Theta_{det}$. Upon passing through the lens the polarization vectors change into

$$\mathbf{e}_s\to(-\sin\Phi,\cos\Phi,0),\quad \mathbf{e}_p\to(-\cos\Phi,-\sin\Phi,0), \tag{45}$$

so a linearly polarized detector oriented at an angle Φ_{det} will detect only those photons whose polarization before the lens was

$$\mathbf{e}_{\parallel}=\mathbf{e}_s\sin(\Phi-\Phi_{det})+\mathbf{e}_p\cos(\Phi-\Phi_{det}). \tag{46}$$

Averaging over the directions gives

$$I_n = \int_0^{\Theta_{det}} \frac{\sin\Theta d\Theta}{2} \int_0^{2\pi} \frac{d\Phi}{2\pi} e_\parallel^i e_\parallel^j \left[I_n^\perp (\mathbf{e}_{in}\cdot\mathbf{e}_{in}^*)\delta_{ij} + (I_n^\parallel - I_n^\perp)\frac{e_{in}^i (e_{in}^j)^* + (e_{in}^i)^* e_{in}^j}{2} \right]$$

$$= \int_0^{\Theta_{det}} \frac{\sin\Theta d\Theta}{16} [\delta_{ij}(1-\cos\Theta)^2 + 2e_{det}^i e_{det}^j (1+\cos\Theta)^2] \left[I_n^\perp (\mathbf{e}_{in}\cdot\mathbf{e}_{in}^*)\delta_{ij} + (I_n^\parallel - I_n^\perp)\frac{e_{in}^i (e_{in}^j)^* + (e_{in}^i)^* e_{in}^j}{2} \right]$$

$$= \frac{1}{48}\{(I_n^\parallel + I_n^\perp)(1-\cos\Theta_{det})^3 + 2I_n^\perp [8-(1+\cos\Theta_{det})^3]\}(\mathbf{e}_{in}\cdot\mathbf{e}_{in}^*) + \frac{1}{24}(I_n^\parallel - I_n^\perp)[8-(1+\cos\Theta_{det})^3]|(\mathbf{e}_{in}\cdot\mathbf{e}_{det})|^2, \quad (47)$$

where $\mathbf{e}_{det}=(\cos\Phi_{det},\sin\Phi_{det},0)$. Unpolarized detection corresponds to adding the contributions from two mutually perpendicular polarizations $\mathbf{e}_{det}$ and results in

$$I_n = \frac{4-3\cos\Theta_{det}-\cos^3\Theta_{det}}{12}(I_n^\parallel + I_n^\perp)(\mathbf{e}_{in}\cdot\mathbf{e}_{in}^*). \quad (48)$$

C. Inelastic broadening

As discussed in Sec. I A, when the number of emitted phonons is even, energy and momentum conservation can be satisfied in all elementary processes, represented by vertices on the diagrams for the Raman amplitude. As a consequence, the energy denominators of all electronic Green's functions forming the electron-hole loop can be nullified simultaneously, and the integral over the internal momentum and energy diverges. To cure this divergence it is essential to include broadening of the electronic states. In other words, the infinitesimal imaginary part $-io$ in the denominator of Green's function (31) should be replaced by the actual broadening $-i\gamma_{\mathbf{p}}=i\,\mathrm{Im}\,\Sigma(\mathbf{p},vp)$, where $\Sigma(\mathbf{p},\epsilon)$ is the electronic self-energy (the effect of $\mathrm{Re}\,\Sigma$ will be studied in Sec. VIII).

$\mathrm{Im}\,\Sigma(\mathbf{p},vp)$ corresponds to emission of some excitations by the electron (hole). One obvious candidate is the phonon itself; the corresponding contribution to $\Sigma(\mathbf{p},\epsilon)$ is represented by the first term in Fig. 10. Besides phonons, an electron can emit other kinds of excitations; the most important contribution can be expected to come from emission of electron-hole pairs. Emission of electron-hole pairs in the undoped graphene must be impurity assisted,[24] while in the doped case electrons can collide without impurities involved, so the electron-electron collision rate strongly depends on doping. The propagator of electron-hole pairs is represented in Fig. 10 by the wiggly line. We do not need the explicit form of the propagator, being interested only in the contribution to $\mathrm{Im}\,\Sigma$, introduced phenomenologically in the denominator of $G(\mathbf{p},\epsilon)$. The only property which is crucial for our consideration is that the spectrum of electron-hole pairs at each fixed wave vector is very broad as compared to Raman peak widths as well as to $\gamma_{\mathbf{p}}$.

The phonon contribution to $\Sigma(\mathbf{p},\epsilon)$ (the first term in Fig. 10) can be calculated explicitly.[49] Let us do it for the case of E_2 phonons,

$$-i\Sigma^\Gamma(\mathbf{p},\epsilon) = F_\Gamma^2 \int \frac{d\epsilon'}{2\pi}\frac{d^2\mathbf{p}'}{(2\pi)^2}\frac{\sqrt{27a^2}}{4}\frac{D_\Gamma(\mathbf{p}-\mathbf{p}',\epsilon-\epsilon')}{2M\omega_\Gamma(\mathbf{p}-\mathbf{p}')} \times [\Sigma_x\Lambda_z G(\mathbf{p}',\epsilon')\Sigma_x\Lambda_z + \Sigma_y\Lambda_z G(\mathbf{p}',\epsilon')\Sigma_y\Lambda_z]. \quad (49)$$

The two terms in the square brackets correspond to two-phonon polarizations. Integrating over ϵ' and neglecting the phonon dispersion, we obtain

$$\Sigma^\Gamma(\mathbf{p},\epsilon) = \frac{F_\Gamma^2}{M\omega_\Gamma v^2}\frac{\sqrt{27}a^2}{4}\frac{\epsilon}{2\pi}\int_0^{\xi_{max}}\frac{\xi' d\xi'}{\epsilon^2-(\xi'+\omega_\Gamma-io)^2} = \lambda_\Gamma\left[\frac{\omega_\Gamma-\epsilon}{4\pi}\ln\frac{\xi_{max}}{\omega_\Gamma-\epsilon} - (\epsilon\to-\epsilon)\right], \quad (50)$$

where ξ_{max} is an ultraviolet cutoff of the order of the electronic bandwidth. If we consider scattering on E_1' phonons (A_1 representation of C_{3v} in the K point), we obtain the same expression as Eq. (50) but with F_Γ and ω_Γ replaced by F_K and ω_K. The dimensionless coupling constants λ_Γ and λ_K are defined in Eq. (24).

To conclude this section, we note that Raman-scattering rate can be viewed as the imaginary part of the incoming photon self-energy; indeed, any diagram for the Raman matrix element, e.g., the first one in Fig. 9, can be obtained by cutting a photon self-energy diagram in to two, as shown in Fig. 11. Dressing electronic Green's function with self-energy corrections corresponds to going to higher orders of perturbation theory and taking into account diagrams of the

FIG. 10. Electron self-energy due to the interactions with phonons and with electron-hole pairs. The propagator of electron-hole pairs is shown by the wiggly line; its explicit form is not important for our calculation.

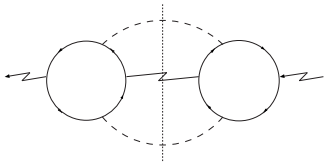

FIG. 11. Raman-scattering rate as the imaginary part of the photon self-energy: diagram (a) in Fig. 9 for the Raman matrix element is obtained by cutting the photon self-energy diagram in to two, as shown by the vertical short-dashed line.

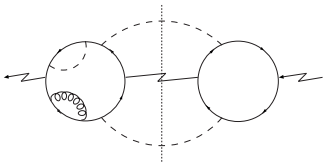

FIG. 12. A diagram corresponding to self-energy insertions in electronic Green's functions.

type shown in Fig. 12. One may ask what other diagrams may appear in the higher orders of perturbation theory and how important they are.

(i) Diagrams where the two electronic loops are connected with more phonon lines (Fig. 13) describe Raman scattering on the corresponding number of phonons. If the loops are connected with an electron-hole propagator, this corresponds to the contribution of electron-hole pairs to the Raman spectrum. As discussed in Sec. I A, the resulting spectrum is broad and featureless, so we are not interested in these processes. (ii) One can also insert phonon and electron-hole propagators as shown in Fig. 14. Such diagrams represent vertex corrections; their effect is analyzed in Sec. VIII. (iii) All diagrams involving more electron-photon vertices have an extra smallness in the parameter $e^2/c \approx 1/137$ and are neglected. (iv) Inserting electronic loops into phonon propagators describes the phonon frequency shift due to electron-electron interaction and phonon decay into the continuum of electron-hole pairs. They have been studied before, both theoretically[31,50–52] and experimentally.[9,10,33,53] However, shift and broadening of the phonon states are not important for our calculation, as we are interested in the frequency-integrated intensities of the Raman peaks. They are determined by the total phonon spectral weight, which is not changed by shift and broadening.

V. ONE-PHONON RAMAN SCATTERING (REF. 42)

Since the photon wave vector is negligibly small compared to all other scales in the problem, the in-plane momentum conservation requires the emitted phonon to belong to the Γ point. This fact explains the small width of the peak at 1580 cm^{-1}. The matrix element for the one-phonon process is given by two diagrams in Fig. 8,

$$\mathcal{M}^{x,y} = \frac{2\pi e^2 v^2}{i\sqrt{\omega_{in}\omega_{out}}} \sqrt{\frac{L_x L_y F_\Gamma^2}{2NM\omega_\Gamma(0)}} \int \frac{d\epsilon}{2\pi} \frac{d^2\mathbf{p}}{(2\pi)^2} \times \operatorname*{Tr}_{4\times 4} \{(\mathbf{e}_{in}\boldsymbol{\Sigma}) G(\mathbf{p},\epsilon_- - \omega_\Gamma) T_{x,y} G(\mathbf{p},\epsilon_-)(\mathbf{e}_{out}^*\boldsymbol{\Sigma}) G(\mathbf{p},\epsilon_+) + G(\mathbf{p},\epsilon_-)(\mathbf{e}_{out}^*\boldsymbol{\Sigma}) G(\mathbf{p},\epsilon_+) T_{x,y} G(\mathbf{p},\epsilon_+ + \omega_\Gamma)(\mathbf{e}_{in}\boldsymbol{\Sigma})\}, \tag{51}$$

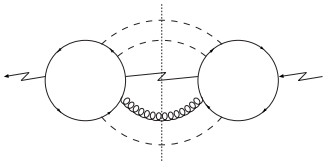

FIG. 13. A diagram describing emission of extra excitations.

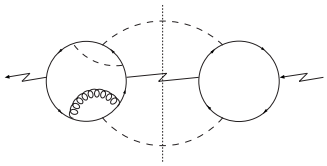

FIG. 14. A diagram representing vertex corrections.

where we denoted $T_x = \Lambda_z \Sigma_y$, $T_y = -\Lambda_z \Sigma_x$, $\epsilon_\pm \equiv \epsilon \pm \omega_{out}/2$, and $\omega_\Gamma \equiv \omega_\Gamma(\mathbf{q}=0)$.

At first glance, elementary power counting (we set $\epsilon \sim vp$ and note that each Green's function $G \sim 1/\epsilon$) tells us that the integral is logarithmically divergent at high energies. However, let us recall the continuous symmetry [Eqs. (15a) and (15b)] of Dirac Hamiltonian (10). Rotation (15b) of the dummy integration variable $\mathbf{p}$ by an arbitrary fixed angle φ cannot change the value of the integral. Thus, the integral must not change if each Green's function is replaced by $G \to e^{-i\Sigma_z\varphi/2} G e^{i\Sigma_z\varphi/2}$. Application of these $e^{\pm i\Sigma_z\varphi/2}$ to the vertices is equivalent to inverse rotation (15b) of the polarization vectors $\mathbf{e}_{in}, \mathbf{e}_{out}^*$ and of the matrices Σ_x, Σ_y. This gives us a *cubic* combination of $\sin\varphi, \cos\varphi$ which has no φ-independent terms. This may be viewed as conservation of the z component of the angular momentum: indeed, transformation properties under rotations $C_{\infty v}$ for both the photon polarization vectors $\mathbf{e}_{in}, \mathbf{e}_{out}$ and the E_2 phonon displacements $u_{E_{2x}}, u_{E_{2y}}$ correspond to the angular momentum $m = \pm 1$. As a result, for the Dirac spectrum the one-phonon matrix element (51) *must vanish*.

In fact, Eq. (51) gives zero even prior to the $\mathbf{p}$ integration. We just notice that

$$-i\Lambda_x G(\mathbf{p},\epsilon) i\Lambda_x = G(\mathbf{p},\epsilon), \tag{52a}$$

$$-i\Lambda_x \boldsymbol{\Sigma} i\Lambda_x = \boldsymbol{\Sigma}, \tag{52b}$$

$$-i\Lambda_x(\Lambda_z\boldsymbol{\Sigma}) i\Lambda_x = -\Lambda_z\boldsymbol{\Sigma}. \tag{52c}$$

The matrix $-i\Lambda_x$ is the combination of the matrix $\Lambda_x\Sigma_z$ (the full C_2 rotation) and $e^{-i\Sigma_z\pi/2}$ (rotation by π within each valley). This symmetry relates the spectra at the points $\mathbf{K}+\mathbf{p}$ and $\mathbf{K}'+\mathbf{p}$.

As a consequence, in order to describe the one-phonon Raman peak at 1580 cm^{-1}, one has to go beyond the leading order in the small-p expansion of the Hamiltonian [i.e., to take into account H_2 from Eq. (12)] and interaction vertices. Since Λ_x symmetry (52a) is broken by the second term of the Hamiltonian $H_2(\mathbf{p})$ [Eq. (12)], the result will be different from zero already at the next order in p. Then an additional power of p appears in the integrand of Eq. (51), so the divergence at the upper limit becomes linear rather than logarithmic. This means that the small-p expansion is inapplicable (i.e., all of its terms give the contribution of the same order), and the whole Brillouin zone is responsible for the 1580 cm^{-1} peak. We stress that this statement is valid in the clean limit when impurity scattering can be neglected. Impurity scattering can allow the one-phonon process in the leading order and make the integral convergent in the upper limit.[2] In the clean limit the proper tool for the calculation is

thus not the effective low-energy electronic theory but the *ab initio* band-structure methods, which are, of course, beyond the scope of the present work. For low photon energies we are interested in, we can simply add a term to the system Hamiltonian, corresponding to a direct photon-phonon interaction. The form of this Hamiltonian is fixed by the C_{6v} symmetry ($E_1 \times E_1 \times E_2$ contains only one A_1 representation),

$$H_{em\text{-}ph} = \frac{e^2}{v_R} \int d^2\mathbf{r}[(\mathcal{E}_x^2 - \mathcal{E}_y^2)u_{E_2x} + 2\mathcal{E}_x\mathcal{E}_y u_{E_2y}], \quad (53)$$

where $\mathcal{E}_x, \mathcal{E}_y$ are the in-plane Cartesian components of the electric-field vector $\mathcal{E} = -(1/c)\partial\mathbf{A}/\partial t$, e is the electron charge, and v_R is the unknown constant of the dimensionality of velocity. Since it originates from the electronic π band, its magnitude is roughly given by the product of the electronic bandwidth and the lattice constant, i.e., it should be of the same order as the electronic velocity v.

This Hamiltonian leads to the following expression for the one-phonon Raman matrix element:

$$\left.\begin{matrix}\mathcal{M}^x \\ \mathcal{M}^y\end{matrix}\right\} = \frac{2e^2}{v_R} \frac{2\pi\sqrt{\omega_{in}\omega_{out}}}{\sqrt{2NM\omega_\Gamma(0)/(L_xL_y)}} \left\{\begin{matrix} e_{in,x}e^*_{out,x} - e_{in,y}e^*_{out,y} \\ e_{in,x}e^*_{out,y} + e_{in,y}e^*_{out,x}\end{matrix}\right. . \quad (54)$$

The resulting intensity does not depend on the polarization of the detector. The sum over the two polarizations, calculated according to the prescription of Sec. IV B, is given by

$$I_\Gamma = 8\pi\left(\frac{e^2}{c}\right)^2 \frac{\omega_{in}\omega_{out}^3}{v_R^2c^2} \frac{\sqrt{27a^2}}{4M\omega_\Gamma(0)} \times \frac{4 - 3\cos\Theta_{det} - \cos^3\Theta_{det}}{6} (\mathbf{e}_{in}\cdot\mathbf{e}^*_{in}). \quad (55)$$

Furthermore, Eqs. (52a)–(52c) lead to vanishing of the Raman amplitude for any odd number of Γ phonons. This property resembles Furry's theorem in the spinor quantum electrodynamics.[54] There is, however, a difference: Furry's theorem holds for the sum of two diagrams containing an odd number of photon lines and differing by the direction of the electronic loop which cancel each other, while in Eq. (51) each of the two terms vanishes separately. We also note that K phonons can be emitted only in pairs; the excited electron-hole pair should switch valleys an even number of times in order to annihilate.[55] The difference from the one-phonon process is that the integral in the matrix element converges at large k even after the next term in the small-k expansion has been picked up. Thus, the three-phonon process can be described within the low-energy theory, but the corresponding amplitude will contain an additional smallness $\sim\omega_{in}a/c$.

VI. TWO-PHONON RAMAN SCATTERING

A. Calculation for the Dirac spectrum

First, let us focus on the $2K$ peak at 2700 cm^{-1}, which corresponds to emission of two scalar phonons (A_1 in terms of the C_{3v} symmetry or E_1' in terms of the C_{6v}'' symmetry) from the vicinity of the K and K' points. The integrated intensity of the $2K$ peak is given by

$$4\pi\frac{dI_{2K}}{do_{out}} = \frac{2\pi}{c^2}\frac{\omega_{out}^2}{2\pi^2c^2}\frac{1}{2}\cdot 2\int\frac{d^2\mathbf{q}}{(2\pi)^2}|2\mathcal{M}^K_\mathbf{q}|^2. \quad (56)$$

The factor $1/2$ in front of the sum eliminates double counting in the summation over the final states (phonon permutations), the factor of 2 comes from the sum over A_1 and B_1 modes (no cross terms arise, as they would yield a traceless combination $\Lambda_x\Lambda_y$), and the factor of 2 inside the square takes care of the spin degeneracy.

The diagrams for the two-phonon matrix element are shown in Fig. 9. Only the first diagram corresponds to the fully resonant process, described in Sec. I A; the other two give a contribution, smaller by a factor γ/ω_K. Thus, the matrix element is given by

$$\mathcal{M}^K_\mathbf{q} = \frac{2\pi e^2v^2}{\sqrt{\omega_{in}\omega_{out}}}\frac{L_xL_yF_K^2}{2NM\omega_K(\mathbf{q})}\int\frac{d\epsilon}{2\pi}\frac{d^2\mathbf{p}}{(2\pi)^2} \times \operatorname*{Tr}_{4\times4}\{(\mathbf{e}_{in}\cdot\Sigma)G(\mathbf{p},\epsilon_-)\Lambda_x\Sigma_zG(\mathbf{p}+\mathbf{q},\epsilon'_-) \times (\mathbf{e}^*_{out}\cdot\Sigma)G(\mathbf{p}+\mathbf{q},\epsilon'_+)\Lambda_x\Sigma_zG(\mathbf{p},\epsilon_+)\} + (\mathbf{q}\to-\mathbf{q}), \quad (57)$$

where $\epsilon_\pm = \epsilon \pm \omega_{in}/2$, $\epsilon'_\pm = \epsilon \pm \omega_{out}/2$. We diagonalize Green's functions by unitary transformation (11) and neglect the off-resonant contribution,

$$G(\mathbf{p},\epsilon_\pm) = U_\mathbf{p}^\dagger\frac{\epsilon_\pm + \Sigma_z\xi_\mathbf{p}}{\epsilon_\pm^2 - \xi_\mathbf{p}^2}U_\mathbf{p} \approx U_\mathbf{p}^\dagger\frac{(\mathbb{1}\pm\Sigma_z)/2}{\epsilon_\pm \mp \xi_\mathbf{p}}U_\mathbf{p}, \quad (58)$$

where $\xi_\mathbf{p} \equiv v|\mathbf{p}| - i\gamma_\mathbf{p}$, $U_\mathbf{p} = e^{i\Sigma_y\pi/4}e^{i\Sigma_z\varphi_\mathbf{p}/2}$, and $\varphi_\mathbf{p} = \arctan(p_y/p_x)$ is the polar angle of the vector $\mathbf{p}$. The unitary matrices rotate the vertices as

$$U_\mathbf{p}\Sigma_xU_{\mathbf{p}'}^\dagger = \Sigma_z\cos\frac{\varphi_\mathbf{p}+\varphi_{\mathbf{p}'}}{2} - \Sigma_y\sin\frac{\varphi_\mathbf{p}+\varphi_{\mathbf{p}'}}{2}, \quad (59a)$$

$$U_\mathbf{p}\Sigma_yU_{\mathbf{p}'}^\dagger = \Sigma_z\sin\frac{\varphi_\mathbf{p}+\varphi_{\mathbf{p}'}}{2} + \Sigma_y\cos\frac{\varphi_\mathbf{p}+\varphi_{\mathbf{p}'}}{2}, \quad (59b)$$

$$U_\mathbf{p}\Sigma_zU_{\mathbf{p}'}^\dagger = i\mathbb{1}\sin\frac{\varphi_\mathbf{p}-\varphi_{\mathbf{p}'}}{2} - \Sigma_x\cos\frac{\varphi_\mathbf{p}-\varphi_{\mathbf{p}'}}{2}, \quad (59c)$$

$$U_\mathbf{p}(\mathbf{e}_{in}\cdot\boldsymbol{\Sigma})U_\mathbf{p}^\dagger = (\mathbf{e}_\mathbf{p}\cdot\mathbf{e}_{in})\Sigma_z + [\mathbf{e}_\mathbf{p}\times\mathbf{e}_{in}]_z\Sigma_y, \quad (59d)$$

where $\mathbf{e}_\mathbf{p} = \mathbf{p}/|\mathbf{p}|$. We are interested in the Σ_y term in Eq. (59d), which corresponds to interband transitions and also tells us that the transition dipole moment is perpendicular to the electron momentum. In Eq. (59c), the rotated phonon vertex, we need the intraband term $\propto\mathbf{1}$. Evaluation of the trace gives

$$2\frac{[\mathbf{e}_\mathbf{p}\times\mathbf{e}_{in}]_z[\mathbf{e}_{\mathbf{p}+\mathbf{q}}\times\mathbf{e}^*_{out}]_z\sin^2(\varphi_{\mathbf{p}+\mathbf{q}}/2 - \varphi_\mathbf{p}/2)}{(\epsilon_- + \xi_\mathbf{p})(\epsilon'_- + \xi_{\mathbf{p}+\mathbf{q}})(\epsilon'_+ - \xi_{\mathbf{p}+\mathbf{q}})(\epsilon_+ - \xi_\mathbf{p})}. \quad (60)$$

We can rewrite each of the factors in the denominator of this expression as

$$\frac{1}{\epsilon-\omega_{in}/2+\xi_{\mathbf{p}}}=i\int_0^\infty d\bar{t}_0 e^{-i\epsilon\bar{t}_0+i(\omega_{in}/2-\xi_{\mathbf{p}})\bar{t}_0},$$

$$\frac{1}{\epsilon-\omega_{out}/2+\xi_{\mathbf{p}+\mathbf{q}}}=i\int_0^\infty d\bar{t}_1 e^{-i\epsilon\bar{t}_1+i(\omega_{out}/2-\xi_{\mathbf{p}+\mathbf{q}})\bar{t}_1},$$

$$\frac{1}{\epsilon+\omega_{in}/2-\xi_{\mathbf{p}}}=\frac{1}{i}\int_0^\infty dt_0 e^{i\epsilon t_0+i(\omega_{in}/2-\xi_{\mathbf{p}})t_0},$$

$$\frac{1}{\epsilon+\omega_{out}/2-\xi_{\mathbf{p}+\mathbf{q}}}=\frac{1}{i}\int_0^\infty dt_1 e^{i\epsilon t_1+i(\omega_{out}/2-\xi_{\mathbf{p}+\mathbf{q}})t_1}. \quad (61)$$

Integration over $d\epsilon/(2\pi)$ produces $\delta(t_0+t_1-\bar{t}_0-\bar{t}_1)$. Thus the times t_0,t_1 and $\bar{t}_0,\bar{t}_1$ can be interpreted as times spend in the corresponding intermediate states by the electron and the hole, respectively.

Let us denote $p_0=\omega_{in}/(2v)$, $p_1=\omega_{out}/(2v)$, and $\tilde{q}=q-p_0-p_1$, and let $\tilde{p}_\parallel,\tilde{p}_\perp$ be the components of the deviation $\tilde{\mathbf{p}}=\mathbf{p}+p_0\mathbf{e}_{\mathbf{q}}$ along $\mathbf{q}$ and perpendicular to $\mathbf{q}$, respectively. We expect the deviations to be small, so we approximate

$$\mathrm{Re}\,\xi_{\mathbf{p}}=v\sqrt{(-p_0+\tilde{p}_\parallel)^2+\tilde{p}_\perp^2}\approx vp_0-v\tilde{p}_\parallel+\frac{v\tilde{p}_\perp^2}{2p_0}, \quad (62a)$$

$$\mathrm{Re}\,\xi_{\mathbf{p}+\mathbf{q}}=v\sqrt{(p_1+\tilde{p}_\parallel+\tilde{q})^2+\tilde{p}_\perp^2}\approx vp_1+v\tilde{p}_\parallel+v\tilde{q}+\frac{v\tilde{p}_\perp^2}{2p_1}, \quad (62b)$$

and $\mathbf{e}_{\mathbf{p}}\approx-\mathbf{e}_{\mathbf{q}}$, $\mathbf{e}_{\mathbf{p}+\mathbf{q}}\approx\mathbf{e}_{\mathbf{q}}$, and $\varphi_{\mathbf{p}+\mathbf{q}}/2-\varphi_{\mathbf{p}}/2\approx\pi/2$. Integration over momentum deviation $\tilde{\mathbf{p}}$ is performed as (we denote $\gamma_{\mathbf{p}_0}+\gamma_{\mathbf{p}_0+\mathbf{q}}=2\gamma$ for brevity)

$$\begin{aligned}&\int_0^\infty dt_0dt_1d\bar{t}_0d\bar{t}_1\delta(t_0+t_1-\bar{t}_0-\bar{t}_1)e^{-iv\tilde{q}(t_1+\bar{t}_1)}\\&\times\int_{-\infty}^\infty\frac{d\tilde{p}_\parallel}{2\pi}e^{iv\tilde{p}_\parallel(t_0+\bar{t}_0-t_1-\bar{t}_1)}\int_{-\infty}^\infty\frac{d\tilde{p}_\perp}{2\pi}\\&\times e^{-[\gamma_{\mathbf{p}_0}+iv\tilde{p}_\perp^2/(2p_0)](t_0+\bar{t}_0)-[\gamma_{\mathbf{p}_0+\mathbf{q}}+iv\tilde{p}_\perp^2/(2p_1)](t_1+\bar{t}_1)}\\&=-\frac{1}{8v^2}\sqrt{\frac{\omega_{in}\omega_{out}}{\omega_{in}+\omega_{out}}}\frac{1}{(v\tilde{q}-2i\gamma)^{3/2}}, \quad (63)\end{aligned}$$

which gives the matrix element

$$\mathcal{M}_{\mathbf{q}}^K=\frac{2\pi e^2v^2}{\sqrt{\omega_{in}+\omega_{out}}}\frac{L_xL_yF_K^2}{2NM\omega_K(\mathbf{q})}\frac{1}{8v^2}\frac{2[\mathbf{e}_{\mathbf{q}}\times\mathbf{e}_{in}]_z[\mathbf{e}_{\mathbf{q}}\times\mathbf{e}_{out}^*]_z}{(v\tilde{q}-2i\gamma)^{3/2}}+(\mathbf{q}\to-\mathbf{q}). \quad (64)$$

This expression describes a strongly peaked q dependence of the matrix element $\mathcal{M}(\mathbf{q})$ around the value $q_{bs}=(\omega_{in}+\omega_{out})/(2v)$, corresponding to backscattering of the electron and the hole by the phonons. The width of the peak is determined by the *electron lifetime*: $\delta q\sim\gamma/v$. Such sharply peaked dependence cannot be derived from pure symmetry considerations, which just prescribe vanishing of the phonon matrix element for the forward scattering.[2] It is a consequence of the fully resonant character of the two-phonon Raman scattering, which should be contrasted to the double-resonant impurity-assisted single-phonon scattering. For the latter case, the scale determining the width of the peak is $\delta q\sim\omega_{in}/v$ [see Eq. (2) of Ref. 56].

The origin of such peaked dependence lies in the quasiclassical nature of the electron and hole motion. Namely, the incoming photon creates an electron with momentum $\mathbf{p}_0$, moving with the velocity $\mathbf{v}_0=\partial\,\mathrm{Re}\,\xi_{\mathbf{p}}/\partial\mathbf{p}|_{\mathbf{p}=\mathbf{p}_0}$, and a hole with momentum $-\mathbf{p}_0$, moving with the velocity $-\mathbf{v}_0$. After a time t_0 the electron emits a phonon of momentum $-\mathbf{q}$ and after a time $\bar{t}_0$ the hole emits a phonon of momentum $\mathbf{q}$. Afterward, at time $t_0+t_1=\bar{t}_0+\bar{t}_1$ they recombine and emit a photon. In order to recombine, they must meet at the same spatial point (as prescribed by the spatial δ function resulting from the integration over the deviations $\tilde{\mathbf{p}}$) with opposite momenta $\mathbf{p}_1=\mathbf{p}_0+\mathbf{q}$ and $-\mathbf{p}_1$ (as prescribed by the momentum conservation). It is possible only if the velocity $\mathbf{v}_1=\partial\,\mathrm{Re}\,\xi_{\mathbf{p}}/\partial\mathbf{p}|_{\mathbf{p}=\mathbf{p}_1}$ is directed oppositely to the initial velocity $\mathbf{v}_0$. The deviation of the typical scattering angle φ from π is $|\varphi-\pi|\sim\sqrt{\gamma/\omega_{in}}\ll1$, determined by the quantum diffraction [note that we had to expand the energy to the second order in $\tilde{p}_\perp$ in Eqs. (62a) and (62b)].

Proceeding with the calculation, we substitute Eq. (64) into Eq. (56). Angular averaging gives

$$\begin{aligned}&\int_0^{2\pi}\frac{d\varphi_{\mathbf{q}}}{2\pi}|[\mathbf{e}_{\mathbf{q}}\times\mathbf{e}_{in}]_z[\mathbf{e}_{\mathbf{q}}\times\mathbf{e}_{out}^*]_z|^2\\&=\frac{1}{8}[(\mathbf{e}_{in}\cdot\mathbf{e}_{out})(\mathbf{e}_{in}^*\cdot\mathbf{e}_{out}^*)+(\mathbf{e}_{in}\cdot\mathbf{e}_{out}^*)(\mathbf{e}_{in}^*\cdot\mathbf{e}_{out})\\&+(\mathbf{e}_{in}\cdot\mathbf{e}_{in}^*)(\mathbf{e}_{out}\cdot\mathbf{e}_{out}^*)], \quad (65)\end{aligned}$$

so that $I_{2K}^\parallel=3I_{2K}^\perp$, as seen from Eq. (43). We stress that only the in-plane components of the polarization vectors participate in these scalar products. Evaluating the q integral and using Eq. (47), we obtain the final result,

$$\begin{aligned}I_{2K}=&\left(\frac{e^2}{c}\right)^2\frac{v^2}{c^2}\frac{\omega_{out}^2}{8\gamma^2}\left(\frac{F_K^2}{Mv^2\omega_K(q_{bs})}\frac{\sqrt{27}a^2}{4}\right)^2\\&\times\frac{1}{8}\left[\frac{|\mathbf{e}_{in}|^2}{8}(1-\cos\Theta_{det})(3+\cos^2\Theta_{det})\right.\\&\left.+\frac{8-(1+\cos\Theta_{det})^3}{12}|(\mathbf{e}_{in}\cdot\mathbf{e}_{det})|^2\right], \quad (66)\end{aligned}$$

where $q_{bs}=(\omega_{in}+\omega_{out})/(2v)$ is the phonon wave vector corresponding to the backscattering and $\sqrt{27}a^2/4$ is the area per carbon atom. Equation (8) of Ref. 29 corresponds[30] to normal incidence ($|\mathbf{e}_{in}|=1$), collection in the full solid angle 4π, and summation over the two orthogonal directions of $\mathbf{e}_{det}$, which makes the second line of Eq. (66) equal to $1/3$.

Equation (66) shows how the dominant role of backscattering manifests itself in the polarization memory. Indeed, linearly polarized light preferentially excites electrons and holes with momenta perpendicular to the electric-field

vector. After the phonon emission these momenta change to the opposite, and the photon emitted after the annihilation has a preferred direction for the polarization, perpendicular to the electron and hole momenta. Quantitatively, Eq. (66) gives the ratio of intensities for $\mathbf{e}_{det}\|\mathbf{e}_{in}$ and $\mathbf{e}_{det}\perp\mathbf{e}_{in}$ to be 3 at $\Theta_{det}\to 0$ and 23/9 at $\Theta_{det}=\pi/2$ (collection into the solid angle 2π).

Let us now turn to the 2Γ phonon peak at 3250 cm^{-1}, corresponding to emission of two pseudovector E_2 phonons from the vicinity of the Γ point. Its integrated intensity can be calculated analogously,

$$4\pi\frac{dI_{2\Gamma}}{do_{out}}=\frac{2\pi}{c^2}\frac{\omega_{out}^2}{2\pi^2c^2}\frac{1}{2}\sum_{i,j=x,y}\int\frac{d^2\mathbf{q}}{(2\pi)^2}|2\mathcal{M}_{\mathbf{q}}^{ij}|^2. \tag{67}$$

As in Eq. (56), the factor 1/2 in front of the sum eliminates double counting in the summation over the final states(phonon permutations) and the factor of 2 inside the square takes care of the spin degeneracy. Here, however, the summation over the two-phonon modes is less simple. First, let us neglect the phonon dispersion, so that the longitudinal and transverse phonons are degenerate. The matrix element is given by

$$\begin{aligned}\mathcal{M}_{\mathbf{q}}^{ij}=&\frac{2\pi e^2v^2}{\sqrt{\omega_{in}\omega_{out}}}\frac{L_xL_yF_\Gamma^2}{2NM\omega_\Gamma}\int\frac{d\epsilon}{2\pi}\frac{d^2\mathbf{p}}{(2\pi)^2}\\&\times\operatorname*{Tr}_{4\times4}\{(\mathbf{e}_{in}\cdot\Sigma)G(\mathbf{p},\epsilon_-)T_iG(\mathbf{p}+\mathbf{q},\epsilon'_-)\\&\times(\mathbf{e}_{out}^*\cdot\Sigma)G(\mathbf{p}+\mathbf{q},\epsilon'_+)T_jG(\mathbf{p},\epsilon_+)\}+(\mathbf{q}\to-\mathbf{q}),\end{aligned} \tag{68}$$

where $T_x=\Lambda_z\Sigma_y$, $T_y=-\Lambda_z\Sigma_x$. Unitary transformation (11) rotates the isospin as given by Eqs. (59a) and (59b). Thus, the trace will be given by an expression, analogous to Eq. (60), but with the replacements,

$$\sin^2(\varphi_{\mathbf{p}+\mathbf{q}}/2-\varphi_{\mathbf{p}}/2)\to-\bar{e}^i\bar{e}^j,$$

$$\bar{e}^x=-\sin\frac{\varphi_{\mathbf{p}}+\varphi_{\mathbf{p}+\mathbf{q}}}{2},\quad \bar{e}^y=\cos\frac{\varphi_{\mathbf{p}}+\varphi_{\mathbf{p}+\mathbf{q}}}{2}.$$

All arguments leading to the dominance of backscattering remain valid, so we obtain $\bar{\mathbf{e}}=-\mathbf{e}_{\mathbf{q}}$ which means that only the longitudinal phonons are emitted. Summation of the probability over the two-phonon polarizations gives $(\bar{e}^x)^4+(\bar{e}^y)^4+2(\bar{e}^x)^2(\bar{e}^y)^2=1$, so the intensity of the 2Γ peak is given by one-half of expression (66) with replacements $F_K\to F_\Gamma$, $\omega_K\to\omega_{\Gamma,L}$,

$$\begin{aligned}I_{2\Gamma}=&\frac{1}{2}\left(\frac{e^2}{c}\right)^2\frac{v^2}{c^2}\frac{\omega_{out}^2}{8\gamma^2}\left(\frac{F_\Gamma^2}{Mv^2\omega_{\Gamma,L}(q_{bs})}\frac{\sqrt{27}a^2}{4}\right)^2\\&\times\frac{1}{8}\left[\frac{|\mathbf{e}_{in}|^2}{8}(1-\cos\Theta_{det})(3+\cos^2\Theta_{det})\right.\\&\left.+\frac{8-(1+\cos\Theta_{det})^3}{12}|(\mathbf{e}_{in}\cdot\mathbf{e}_{det})|^2\right].\end{aligned} \tag{69}$$

B. Effect of trigonal warping and electron-hole asymmetry

In Sec. VI A we have calculated the integrated intensities of $2K$ and 2Γ peaks at 2700 and 3250 cm^{-1}, respectively. According to the data of Ref. 6, $I_{2K}/I_{2\Gamma}\approx 20$. At the same time, for the corresponding electron-phonon coupling constants the nearest-neighbor bond-stretching approximation gives $F_K/F_\Gamma=1$, which agrees with DFT calculations of Ref. 31 with the precision of 1%. Then, what is the origin of such huge difference in the intensities of the two peaks. In this section we consider the effect of electron-hole asymmetry and trigonal band warping on the intensities of the two-phonon Raman peaks with the purpose to check whether the trigonal warping can explain the observed large difference of intensities I_{2K} and $I_{2\Gamma}$.

Typically, one neglects corrections to the Dirac spectrum $v|\mathbf{p}|$, arising from the quadratic term $H_2(\mathbf{p})$ in the electronic Hamiltonian, given by Eq. (12), as they are smaller than $v|\mathbf{p}|$ by a factor $pa\ll 1$. However, according to the results of Sec. VI A two-phonon scattering is sensitive to the directions of electronic velocities and momenta on the angular scale $\delta\varphi\sim\sqrt{\gamma/\omega_{in}}$. This means that effects of (i) phase mismatch between the electron and the hole, introduced by the first term in Eq. (12), and (ii) noncollinearity of velocity and momentum, introduced by the second term in Eq. (12), may become important already when $H_2(\mathbf{p})\sim\gamma$, which happens at a smaller energy scale than $H_2(\mathbf{p})\sim H_1(\mathbf{p})$. This means that, while including $H_2(\mathbf{p})$, we still can neglect higher-order terms of the expansion $(H_3,H_4,\cdots)$.

Thus, we repeat the calculations of Sec. VI A taking into account the $H_2(\mathbf{p})$ term only in the denominator of expression (60) (the numerator is a smooth function of $\mathbf{p}$, so corrections to it will be small as pa indeed). Quadratic term (12) in the Hamiltonian modifies the electron dispersion as

$$\mathrm{Re}\,\xi_{\mathbf{p}}=vp+\alpha_0p^2\pm\alpha_3\nu_\|(\mathbf{p})p^2, \tag{70a}$$

$$\mathrm{Re}\,\bar{\xi}_{\mathbf{p}}=vp-\alpha_0p^2\pm\alpha_3\nu_\|(\mathbf{p})p^2, \tag{70b}$$

$$\frac{\partial\,\mathrm{Re}\,\xi_{\mathbf{p}}}{\partial\mathbf{p}}=\left[\frac{v}{p}+2\alpha_0\pm2\alpha_3\nu_\|(\mathbf{p})\right]\mathbf{p}\pm2\alpha_3\nu_\perp(\mathbf{p})[\mathbf{e}_z\times\mathbf{p}], \tag{70c}$$

$$\nu_\|(\mathbf{p})=\frac{p_x^3-3p_xp_y^2}{p^3}=\cos3\varphi_{\mathbf{p}}, \tag{70d}$$

$$\nu_\perp(\mathbf{p})=\frac{3p_y^3-9p_x^2p_y}{p^3}=-3\sin3\varphi_{\mathbf{p}}, \tag{70e}$$

where the sign of the α_0 terms is "+" in $\xi_{\mathbf{p}}$ (electron dispersion) and "−" in $\bar{\xi}_{\mathbf{p}}$ (hole dispersion) and the signs of the α_3 terms are + and − for K and K' valleys, respectively.

For a given direction $\mathbf{e}_{\mathbf{q}}$ we choose $\mathbf{p}_0=-p_0\mathbf{e}_{\mathbf{q}}$, $\mathbf{p}_1=p_1\mathbf{e}_{\mathbf{q}}$, with p_0 and p_1 such that $\mathrm{Re}\,\xi_{\mathbf{p}_0}+\mathrm{Re}\,\bar{\xi}_{\mathbf{p}_0}=\omega_{in}$, $\mathrm{Re}\,\xi_{\mathbf{p}_1}+\mathrm{Re}\,\bar{\xi}_{\mathbf{p}_1}=\omega_{out}$ and denote $\tilde{q}=|\mathbf{q}|-p_0-p_1$, $\tilde{\mathbf{p}}=\mathbf{p}-\mathbf{p}_0$. The en-

ergies of the intermediate states to be substituted in Eq. (61) at the corresponding times can be approximated as

$$\mathrm{Re}\,\bar{\xi}_0 \approx \frac{\omega_{in}}{2} - \alpha_0 p_0^2 + \left[\frac{v}{p}_0 - 2\alpha_0 + 2\alpha_3 \nu_\parallel(\mathbf{p}_0)\right](\mathbf{p}_0\cdot\tilde{\mathbf{p}}) + 2\alpha_3\nu_\perp(\mathbf{p}_0)[\mathbf{p}_0\times\tilde{\mathbf{p}}]_z + \frac{v}{2p_0^3}[\mathbf{p}_0\times\tilde{\mathbf{p}}]_z^2, \tag{71a}$$

$$\mathrm{Re}\,\bar{\xi}_1 \approx \frac{\omega_{out}}{2} - \alpha_0 p_1^2 + \left[\frac{v}{p}_1 - 2\alpha_0 \mp 2\alpha_3 \nu_\parallel(\mathbf{p}_1)\right](\mathbf{p}_1\cdot\tilde{\mathbf{p}}) \mp 2\alpha_3\nu_\perp(\mathbf{p}_1)[\mathbf{p}_1\times\tilde{\mathbf{p}}]_z + \frac{v}{2p_1^3}[\mathbf{p}_1\times\tilde{\mathbf{p}}]_z^2 + v\tilde{q}, \tag{71b}$$

$$\mathrm{Re}\,\xi_0 \approx \frac{\omega_{in}}{2} + \alpha_0 p_0^2 + \left[\frac{v}{p}_0 + 2\alpha_0 + 2\alpha_3 \nu_\parallel(\mathbf{p}_0)\right](\mathbf{p}_0\cdot\tilde{\mathbf{p}}) + 2\alpha_3\nu_\perp(\mathbf{p}_0)[\mathbf{p}_0\times\tilde{\mathbf{p}}]_z + \frac{v}{2p_0^3}[\mathbf{p}_0\times\tilde{\mathbf{p}}]_z^2, \tag{71c}$$

$$\mathrm{Re}\,\xi_1 \approx \frac{\omega_{out}}{2} + \alpha_0 p_1^2 + \left[\frac{v}{p}_1 + 2\alpha_0 \mp 2\alpha_3 \nu_\parallel(\mathbf{p}_1)\right](\mathbf{p}_1\cdot\tilde{\mathbf{p}}) \mp 2\alpha_3\nu_\perp(\mathbf{p}_1)[\mathbf{p}_1\times\tilde{\mathbf{p}}]_z + \frac{v}{2p_1^3}[\mathbf{p}_1\times\tilde{\mathbf{p}}]_z^2 + v\tilde{q}. \tag{71d}$$

As before, the upper (lower) sign corresponds to emission of scalar E_1' (pseudovector E_2) phonons, accompanied by intervalley (intravalley) electron scattering. Then instead of Eq. (63) we have

$$\int_0^\infty dt_0 dt_1 d\bar{t}_0 d\bar{t}_1 \delta(t_0+t_1-\bar{t}_0-\bar{t}_1) e^{i\alpha_0(p_0^2-p_1^2)(t_1-\bar{t}_1)-\gamma_{\mathbf{p}_0}(t_0+\bar{t}_0)-\gamma_{\mathbf{p}_1}(t_1+\bar{t}_1)-iv\tilde{q}(t_1+\bar{t}_1)} \times \int \frac{dp_\parallel}{2\pi} e^{i\tilde{p}_\parallel v(t_0+\bar{t}_0-t_1-\bar{t}_1)+2i\tilde{p}_\parallel\alpha_0[p_0(t_0-\bar{t}_0)-p_1(t_1-\bar{t}_1)]-2i\tilde{p}_\parallel\alpha_3\nu_\parallel(\mathbf{q})[p_0(t_0+\bar{t}_0)\mp p_1(t_1+\bar{t}_1)]} \times \int \frac{dp_\perp}{2\pi} e^{-2i\tilde{p}_\perp\alpha_3\nu_\perp(\mathbf{q})[p_0(t_0+\bar{t}_0)\mp p_1(t_1+\bar{t}_1)]-i(v/2)\tilde{p}_\perp^2[(t_0+\bar{t}_0)/p_0+(t_1+\bar{t}_1)/p_1]}. \tag{72}$$

Let us denote $\gamma_{\mathbf{p}_0}+\gamma_{\mathbf{p}_1}=2\gamma$, introduce $T=t_0+\bar{t}_0=t_1+\bar{t}_1$ (the latter equality follows from the longitudinal spatial δ function in the leading order), $\tau=t_0-\bar{t}_0=-t_1+\bar{t}_1$, and rewrite the integral as

$$\int_{-\infty}^\infty d\tau \int_{|\tau|}^\infty \frac{dT}{4v} e^{i\alpha_0(p_0^2-p_1^2)\tau-(2\gamma+iv\tilde{q})T} \int_{-\infty}^\infty \frac{d\tilde{p}_\perp}{2\pi} e^{-2i\tilde{p}_\perp\alpha_3\nu_\perp(\mathbf{q})(p_0\mp p_1)T-i(v/p_0+v/p_1)\tilde{p}_\perp^2 T/2} = \frac{1}{8iv^2}\sqrt{\frac{\omega_{in}\omega_{out}}{\omega_{in}+\omega_{out}}}\frac{1}{\Delta_{eh}}\left(\frac{1}{\sqrt{\Delta_\perp+\Delta_{eh}+2i\gamma-v\tilde{q}}} - \frac{1}{\sqrt{\Delta_\perp-\Delta_{eh}+2i\gamma-v\tilde{q}}}\right), \tag{73}$$

where we also denoted

$$\Delta_\perp = 2[\alpha_3\nu_\perp(\mathbf{q})(p_0\mp p_1)]^2\frac{p_0p_1}{v(p_0+p_1)}, \tag{74a}$$

$$\Delta_{eh} = \alpha_0(p_0^2-p_1^2). \tag{74b}$$

Squaring the matrix element and performing the final integration, we obtain Eq. (66) with the replacement,

$$\frac{1}{\gamma^2} \to \frac{4}{\Delta_{eh}^2}\ln\frac{\gamma^2+\Delta_{eh}^2/4}{\gamma^2}. \tag{75}$$

The meaning of this replacement is that when the electron-hole asymmetry becomes greater than the level broadening, it starts to play the main role in restricting the energy denominators from below. Numerically, $\alpha_0(1\ \mathrm{eV})^2/v^2 \sim 0.1$ eV (see, e.g., Ref. 20), so the relative correction to Eq. (66) for small Δ_{eh} can be estimated as $-[(1/2)\Delta_{eh}^2/(2\gamma)]^2/2 \sim -10^{-4}(\omega_{in}/2\gamma)^2$. The total electronic broadenings 2γ were measured by time-resolved photoemission spectroscopy to be 20 meV in Ref. 21 and 25 meV in Ref. 22 (all values taken for $\epsilon=\omega_{in}/2=1$ eV). A recent ARPES measurement gives a significantly larger value for $2\gamma\sim 100$ meV, [23] which agrees better with Eqs. (25) and (50).

The effect of the trigonal warping term (the only one sensitive to the difference between intervalley and intravalley scatterings) turns out to be small in the parameter $\alpha_3\omega_{in}/v^2$ [in Eq. (73) warping enters through $\Delta_\perp$, which results only in a small shift of the integration variable $\tilde{q}$]. For $\omega_{in}=2$ eV, $\alpha_3=-va/4$ (tight-binding model), we estimate the relative contribution of the warping term as $\Delta_\perp/\omega_{in}\approx 5\times 10^{-4}$ and 5×10^{-2} for intervalley and intravalley scatterings, respectively. Thus, trigonal warping cannot account for the observed ratio $I_{2K}/I_{2\Gamma}$.

VII. FOUR-PHONON RAMAN SCATTERING

A. Resonant manifold

We will calculate only the intensity of the peak which we will call $4K$, the double of the $2K$ peak at 2700 cm^{-1}. The $4K$ peak corresponds to emission of four scalar phonons (A_1 in terms of the C_{3v} symmetry or E_1' in terms of the C_{6v}'' symmetry) from the vicinity of the K and K' points. We will not consider other four-phonon peaks as their intensity is smaller.

The integrated intensity of the $4K$ peak is given by

$$4\pi\frac{dI_{4K}}{do_{out}} = \frac{2\pi}{c^2}\frac{\omega_{out}^2}{2\pi^2c^2}\frac{1}{(L_xL_y)^3}\frac{8}{4!} \times \sum_{\mathbf{q}_1+\mathbf{q}_2=\bar{\mathbf{q}}_1+\bar{\mathbf{q}}_2} |2\mathcal{M}_{-\mathbf{q}_1,-\mathbf{q}_2,\bar{\mathbf{q}}_2,\bar{\mathbf{q}}_1}|^2. \tag{76}$$

The factor $1/4!$ in front of the sum ensures the proper summation over the final states (phonon permutations), the factor of 8 comes from the sum over A_1 and B_1 modes [one can have all four phonons A_1, all four B_1, or $4!/(2!\cdot 2!)=6$ combinations of two A_1 and two B_1 phonons, all other combinations yielding traceless products of Λ_x and Λ_y], and the factor of 2 inside the square takes care of the spin degeneracy. The only fully resonant diagram for the four-phonon matrix element is shown in Fig. 15. The matrix element is given by the sum of $4!=24$ permutations of the emitted phonon wave vectors $-\mathbf{q}_1$, $-\mathbf{q}_2$, $\bar{\mathbf{q}}_2$, $\bar{\mathbf{q}}_1$ [we denote $\omega_K(\mathbf{q})=\omega_{\mathbf{q}}$ for the sake of compactness],

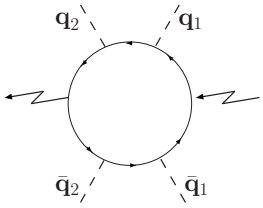

FIG. 15. The only fully resonant diagram for the four-phonon Raman amplitude in the leading order.

$$\mathcal{M}_{-\mathbf{q}_1,-\mathbf{q}_2,\bar{\mathbf{q}}_2,\bar{\mathbf{q}}_1} = \frac{2\pi e^2v^2}{\sqrt{\omega_{in}\omega_{out}}}\frac{[L_xL_yF_K^2/(2NM)]^2}{\sqrt{\omega_{\mathbf{q}_1}\omega_{\mathbf{q}_2}\omega_{\bar{\mathbf{q}}_1}\omega_{\bar{\mathbf{q}}_2}}}\int\frac{d\epsilon}{2\pi}\frac{d^2\mathbf{p}}{(2\pi)^2}\mathrm{Tr}_{4\times4}\{(\mathbf{e}_{in}\cdot\Sigma)G(\mathbf{p},\epsilon-\omega_{in}/2)\Sigma_zG(\mathbf{p}+\bar{\mathbf{q}}_1,\epsilon-\omega_{in}/2+\omega_{\bar{\mathbf{q}}_1})$$
$$\times\Sigma_zG(\mathbf{p}+\bar{\mathbf{q}}_1+\bar{\mathbf{q}}_2,\epsilon-\omega_{in}/2+\omega_{\bar{\mathbf{q}}_1}+\omega_{\bar{\mathbf{q}}_2})(\mathbf{e}_{out}^*\cdot\Sigma)G(\mathbf{p}+\mathbf{q}_1+\mathbf{q}_2,\epsilon+\omega_{in}/2-\omega_{\mathbf{q}_1}-\omega_{\mathbf{q}_2})$$
$$\times\Sigma_zG(\mathbf{p}+\mathbf{q}_1,\epsilon+\omega_{in}/2-\omega_{\mathbf{q}_1})\Sigma_zG(\mathbf{p},\epsilon+\omega_{in}/2)\}+(23\text{ other permutations of }\mathbf{q}\text{'s}). \tag{77}$$

Again, we switch to the basis of Dirac eigenstates according to Eqs. (58) and (59a)–(59d) and evaluate the trace,

$$\mathrm{Tr}_{4\times4}\{\cdots\} = 2\frac{[\mathbf{e}_{\mathbf{p}}\times\mathbf{e}_{in}]_z\sin(\varphi_{\mathbf{p}}/2-\varphi_{\mathbf{p}+\bar{\mathbf{q}}_1}/2)\sin(\varphi_{\mathbf{p}+\bar{\mathbf{q}}_1}/2-\varphi_{\mathbf{p}+\bar{\mathbf{q}}_1+\bar{\mathbf{q}}_2}/2)}{(\epsilon-\omega_{in}/2+\bar{\xi}_{\mathbf{p}})(\epsilon-\omega_{in}/2+\omega_{\bar{\mathbf{q}}_1}+\bar{\xi}_{\mathbf{p}+\bar{\mathbf{q}}_1})(\epsilon-\omega_{in}/2+\omega_{\bar{\mathbf{q}}_1}+\omega_{\bar{\mathbf{q}}_2}+\bar{\xi}_{\mathbf{p}+\bar{\mathbf{q}}_1+\bar{\mathbf{q}}_2})}$$
$$\times\frac{[\mathbf{e}_{\mathbf{p}+\mathbf{q}_1+\mathbf{q}_2}\times\mathbf{e}_{out}^*]_z\sin(\varphi_{\mathbf{p}+\mathbf{q}_1+\mathbf{q}_2}/2-\varphi_{\mathbf{p}+\mathbf{q}_1}/2)\sin(\varphi_{\mathbf{p}+\mathbf{q}_1}/2-\varphi_{\mathbf{p}}/2)}{(\epsilon+\omega_{in}/2-\omega_{\mathbf{q}_1}-\omega_{\mathbf{q}_2}-\xi_{\mathbf{p}+\mathbf{q}_1+\mathbf{q}_2})(\epsilon+\omega_{in}/2-\omega_{\mathbf{q}_1}-\xi_{\mathbf{p}+\mathbf{q}_1})(\epsilon+\omega_{in}/2-\xi_{\mathbf{p}})}. \tag{78}$$

Just like for the two-phonon scattering, the dominant contribution to the integrals will come from those momenta which make small all the factors in the denominators of the above expression. The real parts of the electron and hole dispersion, $\mathrm{Re}\,\xi_{\mathbf{p}}$, $\mathrm{Re}\,\bar{\xi}_{\mathbf{p}}$, are given by Eqs. (70a) and (70b), and $\mathrm{Im}\,\xi_{\mathbf{p}}=\mathrm{Im}\,\bar{\xi}_{\mathbf{p}}=-\gamma_{\mathbf{p}}$.

Four-phonon wave vectors $-\mathbf{q}_1$, $-\mathbf{q}_2$, $\bar{\mathbf{q}}_2$, $\bar{\mathbf{q}}_1$, such that $\mathbf{q}_1+\mathbf{q}_2=\bar{\mathbf{q}}_2+\bar{\mathbf{q}}_1$, will be said to satisfy resonance conditions if exists a vector $\mathbf{p}_0$ such that the following equalities hold:

$$\mathrm{Re}\,\xi_{\mathbf{p}_0} = \frac{\omega_{in}}{2}, \tag{79a}$$

$$\mathrm{Re}\,\xi_{\mathbf{p}_0+\mathbf{q}_1} = \frac{\omega_{in}}{2}-\omega_{\mathbf{q}_1}, \tag{79b}$$

$$\mathrm{Re}\,\xi_{\mathbf{p}_0+\bar{\mathbf{q}}_1} = \frac{\omega_{in}}{2}-\omega_{\bar{\mathbf{q}}_1}, \tag{79c}$$

$$\mathrm{Re}\,\xi_{\mathbf{p}_0+\mathbf{q}_1+\mathbf{q}_2} = \frac{\omega_{in}}{2}-\omega_{\mathbf{q}_1}-\omega_{\mathbf{q}_2}, \tag{79d}$$

$$\mathrm{Re}\,\xi_{\mathbf{p}_0+\bar{\mathbf{q}}_1+\bar{\mathbf{q}}_2} = \frac{\omega_{in}}{2}-\omega_{\bar{\mathbf{q}}_1}-\omega_{\bar{\mathbf{q}}_2}. \tag{79e}$$

The structure of the manifold defined by these conditions essentially depends on (i) whether we take into account the electron-hole asymmetry or just set $\mathrm{Re}\,\xi_{\mathbf{p}}=\mathrm{Re}\,\bar{\xi}_{\mathbf{p}}=v|\mathbf{p}|$ and (ii) whether we take into account the phonon dispersion or just set $\omega_{\mathbf{q}}=\omega_0$. Indeed, subtracting Eq. (70e) from Eq. (79d), we obtain

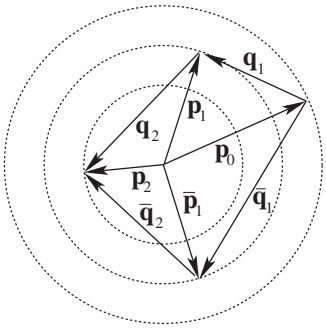

FIG. 16. Structure of the resonant manifold of electron and phonon momenta for four-phonon Raman scattering in the approximation $\mathrm{Re}\,\xi_{\mathbf{p}}=\mathrm{Re}\,\bar{\xi}_{\mathbf{p}}=v|\mathbf{p}|$, $\omega_{\mathbf{q}}=\omega_0$.

$$\omega_{\mathbf{q}_1}+\omega_{\mathbf{q}_2}+\mathrm{Re}\,\xi_{\mathbf{p}_0+\mathbf{q}_1+\mathbf{q}_2}=\omega_{\bar{\mathbf{q}}_1}+\omega_{\bar{\mathbf{q}}_2}+\mathrm{Re}\,\bar{\xi}_{\mathbf{p}_0+\mathbf{q}_1+\mathbf{q}_2}, \tag{80}$$

which in the phonon-dispersionless case represents either an identity if $\xi_{\mathbf{p}}=\bar{\xi}_{\mathbf{p}}$ or can never be satisfied if $\xi_{\mathbf{p}}\neq\bar{\xi}_{\mathbf{p}}$, thus leading to a finite-energy mismatch; only in the phonon-dispersive case it represents a nontrivial equation. As will be seen in Sec. VII F, the quantitative condition for the phonon dispersion to matter is that the phonon group velocity $v_{ph}>v\,\max\{\gamma,\Delta_{eh}\}/\omega_{in}$, where γ is the typical value of the electron broadening and Δ_{eh} is the typical value of the electron-hole asymmetry, defined analogously to Eq. (74b).

First, let us focus on the electron-hole symmetric and dispersionless case, $\mathrm{Re}\,\xi_{\mathbf{p}}=\mathrm{Re}\,\bar{\xi}_{\mathbf{p}}=v|\mathbf{p}|$, $\omega_{\mathbf{q}}=\omega_0$ when the structure of the resonant manifold [Eqs. (79a)–(79e)] is the simplest. The resonant manifold can be parametrized by four polar angles φ_0, φ_1, $\bar{\varphi}_1$, φ_2, which determine the positions of the four momenta $\mathbf{p}_0$, $\mathbf{p}_1\equiv\mathbf{p}_0+\mathbf{q}_1$, $\bar{\mathbf{p}}_1\equiv\mathbf{p}_0+\bar{\mathbf{q}}_1$, and $\mathbf{p}_2\equiv\mathbf{p}_0+\mathbf{q}_1+\mathbf{q}_2=\mathbf{p}_0+\bar{\mathbf{q}}_1+\bar{\mathbf{q}}_2$ on the three circles $v|\mathbf{p}_0|=\omega_{in}/2$, $v|\mathbf{p}_1|=v|\bar{\mathbf{p}}_1|=\omega_{in}/2-\omega_0$, and $v|\mathbf{p}_2|=\omega_{in}/2-2\omega_0$ (Fig. 16). Since the total number of independent phonon variables is six, there are two more variables besides the four angles, which correspond to deviations of the phonon momenta from the resonant manifold. There is a freedom of choice for them, and we choose them to correspond to stretching of the vectors $\mathbf{p}_1,\bar{\mathbf{p}}_1$ (denoted by $w,\bar{w}$, respectively),

$$\delta\mathbf{q}_1=-[\mathbf{e}_z\times\mathbf{p}_0]\delta\varphi_0+[\mathbf{e}_z\times\mathbf{p}_1]\delta\varphi_1+\mathbf{p}_1\delta w, \tag{81a}$$

$$\delta\mathbf{q}_2=[\mathbf{e}_z\times\mathbf{p}_2]\delta\varphi_2-[\mathbf{e}_z\times\mathbf{p}_1]\delta\varphi_1-\mathbf{p}_1\delta w, \tag{81b}$$

$$\delta\bar{\mathbf{q}}_1=-[\mathbf{e}_z\times\mathbf{p}_0]\delta\varphi_0+[\mathbf{e}_z\times\bar{\mathbf{p}}_1]\delta\bar{\varphi}_1+\bar{\mathbf{p}}_1\delta\bar{w}, \tag{81c}$$

$$\delta\bar{\mathbf{q}}_2=[\mathbf{e}_z\times\mathbf{p}_2]\delta\varphi_2-[\mathbf{e}_z\times\bar{\mathbf{p}}_1]\delta\bar{\varphi}_1-\bar{\mathbf{p}}_1\delta\bar{w}. \tag{81d}$$

The $\mathbf{q}$ integration measure is transformed as

$$d^2\mathbf{q}_1d^2\mathbf{q}_2d^2\bar{\mathbf{q}}_1=|\mathbf{p}_1|^2|\bar{\mathbf{p}}_1|^2|[\mathbf{p}_0\times\mathbf{p}_2]_z|\times d\varphi_0d\varphi_2d\varphi_1d\bar{\varphi}_1dwd\bar{w}. \tag{82}$$

Thus, six independent integration variables, parametrizing the final state, have been separated into two groups: four angles, determining the position of the phonon momenta on the resonant manifold, and two deviations $w,\bar{w}$ from the manifold. The dependence of the integrand on the first group of variables is smooth, and we will call them slow variables. The deviations from the manifold, on the contrary, suppress the integrand dramatically, so we will call them fast variables.

Let us now consider the other 23 permutations of the phonon wave vectors $-\mathbf{q}_1$, $-\mathbf{q}_2$, $\bar{\mathbf{q}}_2$, $\bar{\mathbf{q}}_1$, which have to be added in order to obtain the correct value of the matrix element $\mathcal{M}$. We need to check whether contributions to $\mathcal{M}$ from different permutations can be large at the same time (i.e., for the same values of the integration variables $-\mathbf{q}_1$, $-\mathbf{q}_2$, $\bar{\mathbf{q}}_2$, $\bar{\mathbf{q}}_1$). If this is not the case for all 23 permutations, then the summation over all permutations in $\mathcal{M}$ would just cancel the factor $1/4!$ in Eq. (76).

First, we note that if three momenta $\mathbf{p}_0$, $\mathbf{p}_0+\mathbf{q}_1$, and $\mathbf{p}_0+\mathbf{q}_1+\mathbf{q}_2$ satisfy the resonance conditions (79a)–(79e) (i.e., they lie on the corresponding circles) for some $\mathbf{p}_0$, then the momenta $\mathbf{p}_0'$, $\mathbf{p}_0'+\mathbf{q}_2$, and $\mathbf{p}_0'+\mathbf{q}_1+\mathbf{q}_2$ do not satisfy these conditions for any $\mathbf{p}_0'$. Indeed, the vector $\mathbf{q}_1+\mathbf{q}_2$ can be placed on the circles only in two ways, which leaves only two choices for the momentum $\mathbf{p}_0'$: $\mathbf{p}_0'=\mathbf{p}_0$ or the symmetric one. For none of them does $\mathbf{p}_0'+\mathbf{q}_2$ lie on the circle, unless the configuration of momenta has special symmetries. This means that the corresponding contribution to the matrix element is small, so the permutation $\mathbf{q}_1\leftrightarrow\mathbf{q}_2$ should be discarded. By analogous argument we can discard all 14 permutations which leave at least one of the $\mathbf{q}$'s in place (this immediately leaves only two choices for $\mathbf{p}_0'$ which can be inspected). Four cyclic permutations are eliminated because the circles have different radii. The permutation $\mathbf{q}_1\leftrightarrow\mathbf{q}_2,\bar{\mathbf{q}}_1\leftrightarrow\bar{\mathbf{q}}_2$ is eliminated by the very first argument. Thus, we are left with four permutations. One is $-\mathbf{q}_1,-\mathbf{q}_2,\bar{\mathbf{q}}_2,\bar{\mathbf{q}}_1\rightarrow\bar{\mathbf{q}}_1,\bar{\mathbf{q}}_2,-\mathbf{q}_2,-\mathbf{q}_1$, and it *does* satisfy resonance conditions (79a)–(79e) if one chooses $\mathbf{p}_0'=-\mathbf{p}_0$. The other three are obtained from it by swapping the first two momenta, the last two, or both, and thus do not satisfy the resonance conditions. The permutation $-\mathbf{q}_1,-\mathbf{q}_2,\bar{\mathbf{q}}_2,\bar{\mathbf{q}}_1\rightarrow\bar{\mathbf{q}}_1,\bar{\mathbf{q}}_2,-\mathbf{q}_2,-\mathbf{q}_1$ is nothing else but the result of reversal of the electronic line direction in the loop in Fig. 15. As seen from Eq. (78), this permutation gives exactly the same contribution as the original one. Thus, their interference results in an additional factor of 2 besides cancellation of $1/4!$ in Eq. (76).

B. Quasiclassical representation

Now let us pass to time representation for the matrix element $\mathcal{M}$ by rewriting each factor in the denominator of expression (78) analogously to Eq. (61). We introduce three time variables for the electron and three for the hole, denoted by t_0, t_1, t_2 and $\bar{t}_0$, $\bar{t}_1$, $\bar{t}_2$, respectively. Next, we introduce the deviation $\tilde{\mathbf{p}}=\mathbf{p}-\mathbf{p}_0$ from the point $\mathbf{p}_0$ fixed by the resonance conditions and expand each factor in the denominator of expression (78) as

$$-\frac{\omega_{in}}{2}+\bar{\xi}_{\mathbf{p}}\approx\bar{\mathbf{v}}_0\tilde{\mathbf{p}}-i\bar{\gamma}_0-\alpha_0p_0^2, \tag{83a}$$

$$-\frac{\omega_{in}}{2}+\omega_{\bar{\mathbf{q}}_1}+\bar{\xi}_{\mathbf{p}+\bar{\mathbf{q}}_1}\approx\bar{\mathbf{v}}_1\tilde{\mathbf{p}}-i\bar{\gamma}_1+\bar{w}v\bar{p}_1+\delta\omega_{\bar{\mathbf{q}}_1}-\alpha_0p_1^2, \tag{83b}$$

$$-\frac{\omega_{in}}{2}+\omega_{\bar{\mathbf{q}}_1}+\omega_{\bar{\mathbf{q}}_2}+\bar{\xi}_{\mathbf{p}+\bar{\mathbf{q}}_1+\bar{\mathbf{q}}_2}\approx\bar{\mathbf{v}}_2\tilde{\mathbf{p}}-i\bar{\gamma}_2+\delta\omega_{\bar{\mathbf{q}}_1}+\delta\omega_{\bar{\mathbf{q}}_2}-\alpha_0p_2^2, \tag{83c}$$

$$\frac{\omega_{in}}{2}-\xi_{\mathbf{p}}\approx-\mathbf{v}_0\tilde{\mathbf{p}}+i\gamma_0-\alpha_0p_0^2, \tag{83d}$$

$$\frac{\omega_{in}}{2}-\omega_{\mathbf{q}_1}-\xi_{\mathbf{p}+\mathbf{q}_1}\approx-\mathbf{v}_1\tilde{\mathbf{p}}+i\gamma_1-wvp_1-\delta\omega_{\mathbf{q}_1}-\alpha_0p_1^2, \tag{83e}$$

$$\frac{\omega_{in}}{2}-\omega_{\mathbf{q}_1}-\omega_{\mathbf{q}_2}-\xi_{\mathbf{p}+\mathbf{q}_1+\mathbf{q}_2}\approx-\mathbf{v}_2\tilde{\mathbf{p}}+i\gamma_2-\delta\omega_{\mathbf{q}_1}-\delta\omega_{\mathbf{q}_2}-\alpha_0p_2^2, \tag{83f}$$

where $\mathbf{v}_i,-\bar{\mathbf{v}}_i$ and $\gamma_i,\bar{\gamma}_i$ are the velocities and the damping rates of the electron and the hole, respectively, in the ith intermediate state. In Eqs. (83a)–(83f) we have also taken into account the electron-hole asymmetry and the phonon dispersion $\delta\omega_{\mathbf{q}}=\omega_{\mathbf{q}}-\omega_0$, both assumed to be weak: $\alpha_0p_{0,1,2}^2\ll\omega_0$, $|\delta\omega_{\mathbf{q}}|\ll\omega_0$. Within this approximation we can take $\mathbf{v}_0=\bar{\mathbf{v}}_0$ and $\mathbf{v}_2=\bar{\mathbf{v}}_2$.

The numerator of Eq. (78) is a smooth function of momenta on the scale γ/v, so it can be taken at $\tilde{\mathbf{p}}=0$, i.e., on the resonant manifold. Then the integration over $d^2\tilde{\mathbf{p}}/(2\pi)^2$ gives a spatial δ function,

$$\int\frac{d^2\tilde{\mathbf{p}}}{(2\pi)^2}e^{-i\tilde{\mathbf{p}}(\bar{\mathbf{v}}_0\bar{t}_0+\bar{\mathbf{v}}_1\bar{t}_1+\bar{\mathbf{v}}_2\bar{t}_2+\mathbf{v}_0t_0+\mathbf{v}_1t_1+\mathbf{v}_2t_2)}=\delta(\bar{\mathbf{v}}_0\bar{t}_0+\bar{\mathbf{v}}_1\bar{t}_1+\bar{\mathbf{v}}_2\bar{t}_2+\mathbf{v}_0t_0+\mathbf{v}_1t_1+\mathbf{v}_2t_2),$$

so in order to recombine, the electron and the hole should meet at the same spatial point. As a result, the denominator of Eq. (78), integrated over $d\epsilon/(2\pi)$ and $d^2\tilde{\mathbf{p}}/(2\pi)^2$, is rewritten as

$$\int_0^\infty e^{-\eta}\delta(t_0+t_1+t_2-\bar{t}_0-\bar{t}_1-\bar{t}_2)\times\delta(\bar{\mathbf{v}}_0\bar{t}_0+\bar{\mathbf{v}}_1\bar{t}_1+\bar{\mathbf{v}}_2\bar{t}_2+\mathbf{v}_0t_0+\mathbf{v}_1t_1+\mathbf{v}_2t_2)\times dt_0dt_1dt_2d\bar{t}_0d\bar{t}_1d\bar{t}_2, \tag{84a}$$

$$\eta=i[wvp_1t_1+\bar{w}v\bar{p}_1\bar{t}_1+\delta\omega_{\mathbf{q}_1}(t_1+t_2)+\delta\omega_{\mathbf{q}_2}t_2+\delta\omega_{\bar{\mathbf{q}}_1}(\bar{t}_1+\bar{t}_2)+\delta\omega_{\bar{\mathbf{q}}_2}\bar{t}_2]+i\alpha_0\sum_{i=0}^{2}p_i^2(t_i-\bar{t}_i)+\sum_{i=0}^{2}(\gamma_it_i+\bar{\gamma}_i\bar{t}_i). \tag{84b}$$

C. Integration over deviations

The part of the summation over final phonon states in Eq. (76), corresponding to the integration over the deviations $w,\bar{w}$, can be performed explicitly. Let us open the δ functions in Eq. (84a) choosing t_0, t_1, $\bar{t}_1$ as independent variables,

$$t_0+\bar{t}_0=\frac{[\mathbf{v}_2\times(\mathbf{v}_1t_1+\bar{\mathbf{v}}_1\bar{t}_1)]_z}{[\mathbf{v}_0\times\mathbf{v}_2]_z}, \tag{85a}$$

$$t_2+\bar{t}_2=\frac{[\mathbf{v}_0\times(\mathbf{v}_1t_1+\bar{\mathbf{v}}_1\bar{t}_1)]_z}{[\mathbf{v}_2\times\mathbf{v}_0]_z}, \tag{85b}$$

$$t_2,\bar{t}_2=\mp\left(t_0+\frac{t_1-\bar{t}_1}{2}\right)+\frac{[(\mathbf{v}_0\mp\mathbf{v}_2)\times(\mathbf{v}_1t_1+\bar{\mathbf{v}}_1\bar{t}_1)]_z}{2[\mathbf{v}_2\times\mathbf{v}_0]_z}. \tag{85c}$$

The Jacobian of this transformation is given by

$$\int d\bar{t}_0dt_2d\bar{t}_2\delta(t_0+t_1+t_2-\bar{t}_0-\bar{t}_1-\bar{t}_2)\times\delta[\mathbf{v}_0(t_0+\bar{t}_0)+\mathbf{v}_2(t_2+\bar{t}_2)+\mathbf{v}_1t_1+\bar{\mathbf{v}}_1\bar{t}_1]=\frac{1}{2|[\mathbf{v}_0\times\mathbf{v}_2]_z|}. \tag{85d}$$

The detuning phase from Eq. (84b) can be written as

$$\mathrm{Im}\,\eta=wvp_1t_1+\bar{w}v\bar{p}_1\bar{t}_1+\Delta t_0, \tag{86a}$$

$$\Delta\equiv\delta\omega_{\bar{\mathbf{q}}_1}+\delta\omega_{\bar{\mathbf{q}}_2}-\delta\omega_{\mathbf{q}_1}-\delta\omega_{\mathbf{q}_2}+2\Delta_{eh}, \tag{86b}$$

where all detunings at $t_1,\bar{t}_1$ have been absorbed into a shift of $w,\bar{w}$. The energy mismatch due to electron-hole asymmetry, $\Delta_{eh}=\alpha_0(p_{in}^2-p_{out}^2)$, is analogous to that defined in Eq. (74b). The damping factor is (we use the fact that $\gamma_0=\bar{\gamma}_0$, $\gamma_2=\bar{\gamma}_2$)

$$\begin{aligned}\mathrm{Re}\,\eta&=\gamma_0(t_0+\bar{t}_0)+\gamma_1t_1+\bar{\gamma}_1\bar{t}_1+\gamma_2(t_2+\bar{t}_2)\\&=\left(\frac{[\mathbf{v}_2\times\mathbf{v}_1]_z}{[\mathbf{v}_0\times\mathbf{v}_2]_z}\gamma_0+\gamma_1+\frac{[\mathbf{v}_0\times\mathbf{v}_1]_z}{[\mathbf{v}_2\times\mathbf{v}_0]_z}\gamma_2\right)t_1\\&\quad+\left(\frac{[\mathbf{v}_2\times\bar{\mathbf{v}}_1]_z}{[\mathbf{v}_0\times\mathbf{v}_2]_z}\gamma_0+\bar{\gamma}_1+\frac{[\mathbf{v}_0\times\bar{\mathbf{v}}_1]_z}{[\mathbf{v}_2\times\mathbf{v}_0]_z}\gamma_2\right)\bar{t}_1\\&\equiv\gamma_xt_1+\gamma_y\bar{t}_1.\end{aligned} \tag{87}$$

The two times $t_1,\bar{t}_1$ can be taken to vary independently from 0 to ∞. The integration domain for t_0, which we denote by $\mathcal{O}$, besides the condition $t_0>0$, is determined by the inequalities

$$t_0<\frac{[\mathbf{v}_2\times(\mathbf{v}_1t_1+\bar{\mathbf{v}}_1\bar{t}_1)]_z}{[\mathbf{v}_0\times\mathbf{v}_2]_z}, \tag{88a}$$

$$t_0<\frac{\bar{t}_1-t_1}{2}+\frac{[(\mathbf{v}_2-\mathbf{v}_0)\times(\mathbf{v}_1t_1+\bar{\mathbf{v}}_1\bar{t}_1)]_z}{2[\mathbf{v}_0\times\mathbf{v}_2]_z}, \tag{88b}$$

$$t_0>\frac{\bar{t}_1-t_1}{2}+\frac{[(\mathbf{v}_2+\mathbf{v}_0)\times(\mathbf{v}_1t_1+\bar{\mathbf{v}}_1\bar{t}_1)]_z}{2[\mathbf{v}_0\times\mathbf{v}_2]_z}. \tag{88c}$$

Consider integral (84a). Squaring its modulus and integrating over $w,\bar{w}$, we obtain

$$\mathcal{I} \equiv \int |\text{Eq. (84a)}|^2 dw d\bar{w}$$

$$= \frac{\pi^2}{v^2 p_1 \bar{p}_1 [\mathbf{v}_0 \times \mathbf{v}_2]_z^2} \int_0^\infty dt_1 d\bar{t}_1 e^{-2\gamma_x t_1 - 2\gamma_y \bar{t}_1}$$

$$\times \int_{\mathcal{O}} dt_0 dt_0' e^{i\Delta(t_0 - t_0')}. \tag{89}$$

We pass to the polar coordinates in the $(t_1, \bar{t}_1)$ plane,

$$t_1 = t \cos\phi, \quad \bar{t}_1 = t \sin\phi, \tag{90}$$

and parametrize the region $\mathcal{O}$ as

$$\mathcal{O} = \{t_0 : t\zeta_{min}(\phi) < t_0 < t\zeta_{max}(\phi)\}, \tag{91}$$

where $\zeta_{min}(\phi)$ and $\zeta_{max}(\phi)$ are piecewise functions of the form $\alpha \cos\phi + \beta \sin\phi$, corresponding to various conditions (88a)–(88c). Performing the integration, we obtain

$$\mathcal{I} = \frac{\pi^2}{v^2 p_1 \bar{p}_1 [\mathbf{v}_0 \times \mathbf{v}_2]_z^2} \frac{2}{\Delta^4} \int_0^{\pi/2} d\phi$$

$$\times \mathcal{F}\left(\zeta_{max}(\phi) - \zeta_{min}(\phi), \frac{2\gamma_x \cos\phi + 2\gamma_y \sin\phi}{\Delta}\right), \tag{92a}$$

$$\mathcal{F}(x,y) \equiv \int_0^\infty (1 - \cos xt) e^{-yt} t dt = \frac{x^2(x^2 + 3y^2)}{y^2(x^2 + y^2)^2}. \tag{92b}$$

D. Angular integration and polarization dependence

Let us collect all the factors in the expression for I_{2D*} [we denote $\mathbf{e}_{0,2} = (\cos\varphi_{0,2}, \sin\varphi_{0,2})$]

$$4\pi \frac{dI_{4K}}{do_{out}} = 2\pi \left(\frac{e^2}{c}\right)^2 \frac{v^2}{c^2} \left(\frac{\lambda_K}{2\pi}\right)^4 \frac{\omega_{out}^2 (\omega_{in} + \omega_{out})^2}{4}$$

$$\times \int \frac{d\varphi_0 d\varphi_2 d\varphi_1 d\bar{\varphi}_1}{|\sin(\varphi_0 - \varphi_2)|} |[\mathbf{e}_0 \times \mathbf{e}_{in}]_z|^2 |[\mathbf{e}_2 \times \mathbf{e}_{out}]_z|^2$$

$$\times \sin^2 \frac{\varphi_0 - \varphi_1}{2} \sin^2 \frac{\varphi_1 - \varphi_2}{2} \sin^2 \frac{\varphi_0 - \bar{\varphi}_1}{2}$$

$$\times \sin^2 \frac{\bar{\varphi}_1 - \varphi_2}{2} \int_0^{\pi/2} \frac{d\phi}{\Delta^4}$$

$$\times \mathcal{F}\left(\zeta_{max}(\phi) - \zeta_{min}(\phi), \frac{2\gamma_x \cos\phi + 2\gamma_y \sin\phi}{\Delta}\right). \tag{93}$$

A system of two linear equations,

$$\mathbf{v}_0 t_{in} + \mathbf{v}_1 t_1 + \mathbf{v}_2 t_{out} + \bar{\mathbf{v}}_1 \bar{t}_1 = 0, \tag{94}$$

has solutions with $t_{in}, t_{out}, t_1, \bar{t}_1 > 0$ if and only if the four vectors $\mathbf{v}_0$, $\mathbf{v}_1$, $\mathbf{v}_2$, $\bar{\mathbf{v}}_1$ do not lie in one half-plane. Having found t_{in}, t_{out}, t_1, $\bar{t}_1$, we can always split $t_{in} = t_0 + \bar{t}_0$, $t_{out} = t_2 + \bar{t}_2$ in such a way that $t_0 + t_1 + t_2 = \bar{t}_0 + \bar{t}_2 + \bar{t}_2$ (since any side of a quadrangle is shorter than the sum of the other three sides). This condition on the vectors $\mathbf{v}_0$, $\mathbf{v}_1$, $\mathbf{v}_2$, $\bar{\mathbf{v}}_1$ translates into the following condition on the angles (since all conditions are on $\varphi_2 - \varphi_0$, $\varphi_1 - \varphi_0$, and $\bar{\varphi}_1 - \varphi_0$, we set $\varphi_0 = 0$ for brevity):

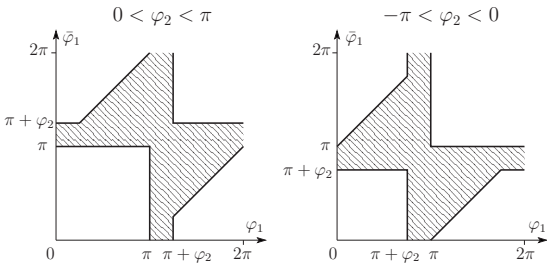

FIG. 17. Region of integration over $\varphi_1, \bar{\varphi}_1$ as determined by inequalities (95) for $0 < \varphi_2 < \pi$ and $\pi < \varphi_2 < 2\pi$.

$$0 \leqslant \varphi_2 < \pi,$$

$$\varphi_1: \quad [0;\varphi_2] \quad [\varphi_2;\pi) \quad (\pi;\varphi_2+\pi) \quad (\varphi_2+\pi;2\pi],$$

$$\bar{\varphi}_1: \quad (\pi;\varphi_2+\pi) \quad (\pi;\varphi_1+\pi) \quad (0;2\pi) \quad (\varphi_1-\pi;\varphi_2+\pi),$$

$$-\pi < \varphi_2 \leqslant 0,$$

$$\varphi_1: \quad [0;\varphi_2+\pi) \quad (\varphi_2+\pi;\pi] \quad (\pi;\varphi_2+2\pi] \quad [\varphi_2+2\pi;2\pi],$$

$$\bar{\varphi}_1: \quad (\varphi_2+\pi;\varphi_1+\pi) \quad (0;2\pi) \quad (\varphi_1-\pi;\pi) \quad (\varphi_2+\pi;\pi),$$

$$\varphi_2 = \pi,$$

$$\varphi_1: \quad (0;\pi) \quad (\pi;2\pi),$$

$$\bar{\varphi}_1: \quad (\pi;2\pi) \quad (0;\pi), \tag{95}$$

which define the domain of the angular integration. We also show it schematically in Fig. 17.

Upon integration over $\varphi_1, \bar{\varphi}_1$ Eq. (93) can be written in the form

$$4\pi \frac{dI_{4K}}{do_{out}} = \int_0^{2\pi} d\varphi_0 d\varphi_2 \mathcal{J}(\varphi_0 - \varphi_2) |[\mathbf{e}_0 \times \mathbf{e}_{in}]_z|^2 |[\mathbf{e}_2 \times \mathbf{e}_{out}]_z|^2. \tag{96}$$

The function $\mathcal{J}(\varphi)$ is real and even, $\mathcal{J}(\varphi) = \mathcal{J}(-\varphi)$, as can be seen from Eq. (78), so its Fourier series reads as

$$\mathcal{J}(\varphi) = \frac{\mathcal{J}_0}{2\pi} + \sum_{n=1}^{\infty} \frac{\mathcal{J}_n}{\pi} \cos n\varphi, \quad \mathcal{J}_n = \int_0^{2\pi} d\varphi \mathcal{J}(\varphi) \cos n\varphi. \tag{97}$$

Then the angular integration gives

$$4\pi\frac{I_{4K}}{do_{out}} = 2\pi|\mathbf{e}_{in}|^2|\mathbf{e}_{out}|^2 \times\left\{\frac{\mathcal{J}_0}{4}+\frac{\mathcal{J}_2}{8}[\cos^2(\varphi_{in}-\varphi_{out})-\sin^2(\varphi_{in}-\varphi_{out})]\right\} = 2\pi\left(\frac{\mathcal{J}_0}{4}-\frac{\mathcal{J}_2}{8}\right)|\mathbf{e}_{in}|^2|\mathbf{e}_{out}|^2 + 2\pi\frac{\mathcal{J}_2}{8}[|\mathbf{e}_{in}\cdot\mathbf{e}^*_{out}|^2+|\mathbf{e}_{in}\cdot\mathbf{e}_{out}|^2]. \quad (98)$$

Comparing this with Eq. (43), we obtain $I^{\perp,\parallel}_{4K} = 2\pi(\mathcal{J}_0/4 \mp \mathcal{J}_2/8)$.

E. Dispersionless phonons

For $\Delta=0$ (electron-hole symmetric case) the last integral in Eq. (93) can be written as

$$\int_0^{\pi/2} d\phi \frac{3[\zeta_{max}(\phi)-\zeta_{min}(\phi)]^2}{16[\gamma_x\cos\phi+\gamma_y\sin\phi]^4}. \quad (99)$$

Numerical evaluation of the angular integral (for simplicity we set all $\gamma_0=\gamma_1=\bar{\gamma}_1=\gamma_2=\gamma$) gives the following expression for $\mathcal{J}_0,\mathcal{J}_2$ to be substituted in Eq. (98):

$$\left.\begin{matrix}\mathcal{J}_0\\ \mathcal{J}_2\end{matrix}\right\} = \left(\frac{e^2}{c}\right)^2\frac{v^2}{c^2}\left(\frac{\lambda_K}{2\pi}\right)^4\frac{\omega^2_{out}(\omega_{in}+\omega_{out})^2}{4}\frac{3\pi}{8\gamma^4}\left\{\begin{matrix}0.0440\\ -0.0017.\end{matrix}\right. \quad (100)$$

This results in $I^{\perp}_{4K}\approx I^{\parallel}_{4K}$, so the polarization memory is almost completely lost. Adding the contributions from two mutually perpendicular detection polarizations [Eq. (48)], we obtain

$$I_{4K} = 0.0440\left(\frac{e^2}{c}\right)^2\frac{v^2}{c^2}\left(\frac{\lambda_K}{2\pi}\right)^4\frac{\omega^2_{out}(\omega_{in}+\omega_{out})^2}{4} \times\frac{\pi^2}{8\gamma^4}\frac{4-3\cos\Theta_{det}-\cos^3\Theta_{det}}{4}|\mathbf{e}_{in}|^2. \quad (101)$$

For $|\mathbf{e}_{in}|=1$, $\Theta_{det}=\pi$, and $\omega_{in}\approx\omega_{out}$ this expression corresponds[30] to Eq. (9) of Ref. 29.

For $|\Delta_{eh}|\gg\gamma_x,\gamma_y$ (strong electron-hole asymmetry) the last integral in Eq. (93) can be written as

$$\int_0^{\pi/2}\frac{d\phi}{4\Delta^2[\gamma_x\cos\phi+\gamma_y\sin\phi]^2}. \quad (102)$$

Numerical evaluation of the angular integral gives

$$\left.\begin{matrix}\mathcal{J}_0\\ \mathcal{J}_2\end{matrix}\right\} = \left(\frac{e^2}{c}\right)^2\frac{v^2}{c^2}\left(\frac{\lambda_K}{2\pi}\right)^4\frac{\omega^2_{out}(\omega_{in}+\omega_{out})^2}{4}\frac{\pi}{8\gamma^2\Delta^2_{eh}}\left\{\begin{matrix}2.60\\ 0.06.\end{matrix}\right. \quad (103)$$

To obtain the expression for I_{4K} one should replace $0.0440 \to 2.60$, $\pi^2/(8\gamma^4)\to\pi^2/(24\gamma^2\Delta^2_{eh})$ in Eq. (101),

$$I_{4K} = 2.60\left(\frac{e^2}{c}\right)^2\frac{v^2}{c^2}\left(\frac{\lambda_K}{2\pi}\right)^4\frac{\omega^2_{out}(\omega_{in}+\omega_{out})^2}{4} \times\frac{\pi^2}{24\gamma^2\Delta^2_{eh}}\frac{4-3\cos\Theta_{det}-\cos^3\Theta_{det}}{4}|\mathbf{e}_{in}|^2. \quad (104)$$

F. Dispersive phonons

In the case when Δ varies strongly compared to γ but vanishes on a certain submanifold of the resonant manifold, the appropriate way to approximate the last integral in Eq. (93) is

$$2\pi\delta(\Delta)\int_0^{\pi/2} d\phi\frac{\zeta_{max}(\phi)-\zeta_{min}(\phi)}{8[\gamma_x\cos\phi+\gamma_y\sin\phi]^3}. \quad (105)$$

This expression corresponds to complete suppression of interference between trajectories of different shapes by the phase mismatch coming from the difference of the phonon frequencies. In this case the electron-hole dynamics can be described by a kinetic equation, analyzed in Appendix C (up to an overall interference factor, see the discussion in the end of Appendix C).

First, let us focus on the apparent singularity at $\sin|\varphi_2-\varphi_0|\to 0$ in the angular integral in Eq. (93). For *generic* $\varphi_1,\bar{\varphi}_1$, we see from Eq. (87) that $\gamma_{x,y}\propto 1/\sin(\varphi_2-\varphi_0)$ and from Eqs. (88a)–(88c) that $\zeta_{max}(\phi)$ either stays finite (at $\varphi_2\approx\varphi_0$) or also diverges as $1/\sin(\varphi_2-\varphi_0)$ (at $\varphi_2\approx\varphi_0+\pi$). Thus, the power of $\sin(\varphi_2-\varphi_0)$ in the numerator of expression (105) is sufficient to suppress the singularity.

The real danger in the angular integral comes from singularities of the Jacobian corresponding to the resolution of $\delta(\Delta)$, i.e., values of $\varphi_1,\bar{\varphi}_1$ such that

$$\frac{\partial(\omega_{\mathbf{p}_1-\mathbf{p}_0}+\omega_{\mathbf{p}_2-\mathbf{p}_1})}{\partial\varphi_1}=0, \quad \frac{\partial(\omega_{\bar{\mathbf{p}}_1-\mathbf{p}_0}+\omega_{\mathbf{p}_2-\bar{\mathbf{p}}_1})}{\partial\bar{\varphi}_1}=0. \quad (106)$$

Looking at the integrals,

$$\int_{-1}^{1}dxdy\,\delta(x-y^2)=\int_{-1}^{1}\frac{dx}{2\sqrt{|x|}}=2, \quad (107a)$$

$$\int_{-1}^{1}dxdy\,\delta(x^2+y^2)=\int_0^1 2\pi r dr\frac{\delta(r)}{2r}=\frac{\pi}{2}, \quad (107b)$$

$$\int_{-1}^{1}dxdy\,\delta(x^2-y^2)=2\int_{-1}^{1}\frac{dx}{2|x|}=2\ln\frac{1}{0}, \quad (107c)$$

we notice that the logarithmic divergence appears when both φ_1 and $\bar{\varphi}_1$ lie near one of these special points. Note that both φ_1 and $\bar{\varphi}_1$ should lie near the same solution for the energy δ function itself to be satisfied.

At this point we have to assume a particular form of the phonon dispersion $\omega_{\mathbf{q}}$. We take the conical dispersion $\omega_{\mathbf{q}}=\omega_0+v_{ph}|\mathbf{q}|$ valid for $\omega_0/v\ll q\ll 1/a$.[57] Then the singular points are determined from the equation

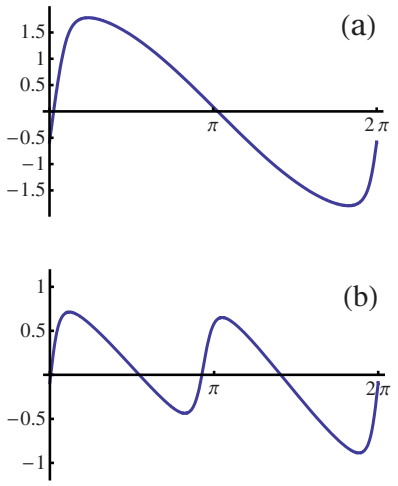

FIG. 18. (Color online) Plot of the left-hand side of Eq. (108a) as a function of φ_1 for (a) $\varphi_0=0$, $\varphi_2=0.2$ and (b) $\varphi_2=\pi-0.2$. The incident laser frequency $\omega_{in}=2$ eV, $\omega_0=0.17$ eV.

$$\frac{p_0}{q_1}\sin(\varphi_1-\varphi_0)+\frac{p_2}{q_2}\sin(\varphi_1-\varphi_2)=0, \tag{108a}$$

$$q_1=\sqrt{p_0^2+p_1^2-2p_0p_1\cos(\varphi_1-\varphi_0)}, \tag{108b}$$

$$q_2=\sqrt{p_1^2+p_2^2-2p_1p_2\cos(\varphi_2-\varphi_1)}, \tag{108c}$$

which is the same for φ_1 and $\bar{\varphi}_1$, since $p_1=\bar{p}_1$. Let us denote the singular points by φ_1^s, labeled by the index s. Around each singular point we can expand

$$\omega_{\mathbf{q}_1}+\omega_{\mathbf{q}_2}\approx\omega_s+\frac{\omega_s''}{2}\tilde{\varphi}_1^2,\quad \tilde{\varphi}_1=\varphi_1-\varphi_1^s, \tag{109a}$$

$$\omega_{\bar{\mathbf{q}}_1}+\omega_{\bar{\mathbf{q}}_2}\approx\omega_s+\frac{\omega_s''}{2}\tilde{\bar{\varphi}}_1^2,\quad \tilde{\bar{\varphi}}_1=\bar{\varphi}_1-\varphi_1^s. \tag{109b}$$

The second derivative in each singular point is given by

$$\frac{v_{ph}}{2q_1}p_1p_0\cos(\varphi_1^s-\varphi_0)+\frac{v_{ph}}{2q_2}p_1p_2\cos(\varphi_1^s-\varphi_2)$$
$$-\frac{v_{ph}}{4q_1^3}p_1^2p_0^2\sin^2(\varphi_1^s-\varphi_0)-\frac{v_{ph}}{4q_2^3}p_1^2p_2^2\sin^2(\varphi_1^s-\varphi_2)$$
$$\equiv\omega_s''(\varphi_0,\varphi_2). \tag{110}$$

To get an idea of the location of singular points, we plot the left-hand side of Eq. (108a) as a function of φ_1 for φ_2 close to φ_0 and to $\varphi_0+\pi$ (Fig. 18). We see that in the first case Eq. (108a) has two solutions, while in the second case four. This means that there is a special value of φ_2 between 0 and π (together with the symmetric one), such that Eq. (108a) has three solutions and at the third solution the derivative ω_s'', defined in Eq. (110), vanishes. This situation will take place as long as $\omega_0/\omega_{in}<(3-\sqrt{5})/4=0.191\cdots$, i.e., $\omega_{in}>0.9$ eV, as can be established by setting $\varphi_0=0$, $\varphi_1=\varphi_2=\pi$ [so that Eq. (108a) is satisfied] and equating $\omega_s''=0$. However, when these conditions are fulfilled and when φ_2 takes this special value, the third solution for φ_1 always lies in the smaller sector between φ_0 and φ_2 and does not belong to the integration region. As a result, there is always just one solution of Eq. (108a), which satisfies $\pi<\varphi_1-\varphi_0<\pi+\varphi_2-\varphi_0$ for $0<\varphi_2-\varphi_0<\pi$ and $\varphi_2-\varphi_0-\pi<\varphi_1-\varphi_0<\pi$ for $\pi<\varphi_2-\varphi_0<2\pi$ [i.e., inequalities (95)] and thus contributes to the intensity integral. We denote this solution by φ_1^0.

Integration over the deviations $\tilde{\varphi}_1=\varphi_1-\varphi_1^0$, $\tilde{\bar{\varphi}}_1=\bar{\varphi}_1-\varphi_1^0$ gives

$$\tilde{\varphi}_1d\tilde{\bar{\varphi}}_1 2\pi\delta(\Delta)=\frac{4\pi}{|\omega''|}\int d\tilde{\varphi}_1d\tilde{\bar{\varphi}}_1\delta(\tilde{\varphi}_1^2-\tilde{\bar{\varphi}}_1^2-4\Delta_{eh}/\omega'')$$
$$=\int\frac{|2\pi/\omega''|d\tilde{\varphi}_1d\tilde{\bar{\varphi}}_1}{\sqrt{\tilde{\bar{\varphi}}_1^2+4\Delta_{eh}/\omega''}}\sum_{\pm}\delta\left(\tilde{\varphi}_1\pm\sqrt{\tilde{\bar{\varphi}}_1^2+\frac{4\Delta_{eh}}{\omega''}}\right)$$
$$\approx\frac{4\pi}{|\omega''|}\ln\left|\frac{\omega''}{\max\{\gamma,\Delta_{eh}\}}\right|. \tag{111}$$

Generally, the upper and lower integration limits here are of the order of ±1; more precise knowledge is not needed for the calculation of the leading logarithmic term. It is important that the energy δ function has a finite width $\sim\gamma$, which may cut off the divergency first, if it is greater than Δ_{eh}. The innermost integral over ϕ, assumed to be a nonsingular function of $\varphi_1,\bar{\varphi}_1$, can be taken at $\varphi_1=\bar{\varphi}_1=\varphi_1^0$. To check the validity of this assumption, we have to study in more detail the behavior of the integral at $\varphi_2-\varphi_0\to0,\pi$.

To make the formulas more compact, in the following we set $\varphi_0=0$ as all angles can be counted from φ_0. For simplicity we also perform the calculations in the limit $\omega_0\ll\omega_{in}$. Then, assuming $-\pi<\varphi_2<\pi$, we simply obtain $\varphi_1^0=\pi+\varphi_2/2$.

Let us start from the simpler case of φ_2 close to $\pm\pi$, denoting $\tilde{\varphi}_2=\varphi_2+\pi$ if $-\pi<\varphi_2<0$ and $\tilde{\varphi}_2=\varphi_2-\pi$ if $0<\varphi_2<\pi$. Then for $\varphi_1=\bar{\varphi}_1=\varphi_0$ we have

$$\zeta_{max}(\phi)=-\frac{\cos\phi+\sin\phi}{2\sin|\tilde{\varphi}_2/2|}+\frac{1}{2}\min\{-\cos\phi+\sin\phi,0\}, \tag{112a}$$

$$\zeta_{min}(\phi)=\frac{1}{2}\max\{-\cos\phi+\sin\phi,0\}. \tag{112b}$$

For $|\tilde{\varphi}_2|\ll1$ the condition $\zeta_{max}(\phi)>\zeta_{min}(\phi)$ severely restricts the integration domain in ϕ, so $\varphi_2\approx\pm\pi$ does not introduce any extra singularities.

For $|\varphi_2|\ll1$ we have

$$\zeta_{max}(\phi)=\min\left\{\frac{\cos\phi+\sin\phi}{2}-f_1(\phi),\sin\phi\right\}, \tag{113a}$$

$$\zeta_{min}(\phi)=\max\left\{\frac{\sin\phi-\cos\phi}{2}-f_1(\phi),0\right\}, \tag{113b}$$

$$f_1(\phi) = \frac{\tilde{\varphi}_1 \cos\phi + \tilde{\bar{\varphi}}_1 \sin\phi}{\varphi_2}. \tag{113c}$$

Again setting all $\gamma_0=\gamma_1=\bar{\gamma}_1=\gamma_2=\gamma$, we obtain simply $\gamma_x=\gamma_y=2\gamma$. The requirement $\zeta_{min}(\phi)<\zeta_{max}(\phi)$ translates into

$$|f_1(\phi)| < \frac{\cos\phi+\sin\phi}{2}. \tag{114}$$

If $|\varphi_1|,|\tilde{\bar{\varphi}}_1| \gg |\varphi_2|$, then only $\tilde{\varphi}_1 \approx -\tilde{\bar{\varphi}}_1$ contribute to integral (111) (for $\tilde{\varphi}_1 \approx \tilde{\bar{\varphi}}_1$ the domain of integration is restricted by $|\tilde{\varphi}_1|<\varphi_2/2$). Then constraint (114) allows only small deviations of ϕ from $\pi/4$, thus we can approximate $f_1(\phi) \approx -\sqrt{2}(\tilde{\varphi}_1/\varphi_2)(\phi-\pi/4)$. In the opposite limiting case, $|\varphi_1|,|\tilde{\bar{\varphi}}_1| \ll |\varphi_2|$, range of ϕ is almost unrestricted, and both $\tilde{\varphi}_1 \approx \pm\tilde{\bar{\varphi}}_1$ will contribute. The ϕ integral in Eq. (105) in these two limiting cases is calculated to be

$$\int_0^{\pi/2} d\phi \frac{\zeta_{max}(\phi)-\zeta_{min}(\phi)}{8[\gamma_x\cos\phi+\gamma_y\sin\phi]^3} \approx \frac{1}{256\gamma^3}\min\left\{1,\left|\frac{\varphi_2}{2\tilde{\varphi}_1}\right|\right\}. \tag{115}$$

Thus, we conclude that for $|\varphi_2| \ll 1$ the upper cutoff in logarithmic integral (111) is $|\varphi_2|$ and not of the order of 1. Thus, upon integration over φ_2 we obtain the second logarithmic divergence, which should be cut off at $|\varphi_2| \sim 1$ above and $|\varphi_2| \sim \max\{\gamma,\Delta_{eh}\}/\omega''$ below.

We restrict ourselves to the calculation of the leading logarithmic asymptotics, so second derivative (110) can be taken at $\varphi_2=\varphi_0=0$ and is simply $\omega''=-\omega_{in}v_{ph}/(4v)$. The function $\mathcal{J}(\varphi)$, defined in Eq. (96), can be taken to be

$$\mathcal{J}(\varphi) = \frac{\pi^2}{8}\left(\frac{e^2}{c}\right)^2\frac{v^2}{c^2}\left(\frac{\lambda_K}{2\pi}\right)^4\frac{\omega_{in}^3}{\gamma^3}\frac{v}{v_{ph}}\frac{1}{|\varphi|}\ln\frac{|\varphi|\omega_{in}v_{ph}/v}{\max\{\gamma,\Delta_{eh}\}}. \tag{116}$$

The final integration leads to the following expression for $\mathcal{J}_0,\mathcal{J}_2$ to be substituted in Eq. (98):

$$\mathcal{J}_0 = \mathcal{J}_2 = \frac{\pi^2}{8}\left(\frac{e^2}{c}\right)^2\frac{v^2}{c^2}\left(\frac{\lambda_K}{2\pi}\right)^4\frac{\omega_{in}^3}{\gamma^3}\frac{v}{v_{ph}}\ln^2\frac{\omega_{in}v_{ph}/v}{\max\{\gamma,\Delta_{eh}\}}, \tag{117}$$

so that $I_{4K}^{\parallel}=3I_{4K}^{\perp}$, as for two-phonon scattering. Thus, the polarization dependence is the same as that described in Sec. VI A. Using Eq. (47), we obtain the final result,

$$I_{4K} = \left(\frac{e^2}{c}\right)^2\frac{v^2}{c^2}\left(\frac{\lambda_K}{2\pi}\right)^4\frac{\omega_{in}^3}{\gamma^3}\frac{v}{v_{ph}}\ln^2\frac{\omega_{in}v_{ph}/v}{\max\{\gamma,\Delta_{eh}\}} \times \frac{\pi^3}{32}\left[\frac{|\mathbf{e}_{in}|^2}{8}(1-\cos\Theta_{det})(3+\cos^2\Theta_{det}) + \frac{8-(1+\cos\Theta_{det})^3}{12}|(\mathbf{e}_{in}\cdot\mathbf{e}_{det})|^2\right]. \tag{118}$$

To conclude this section, we note that the leading logarithmic term, calculated here, is not sensitive to the assumption of the conical phonon dispersion $\omega_{\mathbf{q}}$. The same result will be obtained for dispersion of any shape; the phonon group velocity should be taken at the wave vector $q=\omega_{in}/v$, corresponding to electron backscattering.

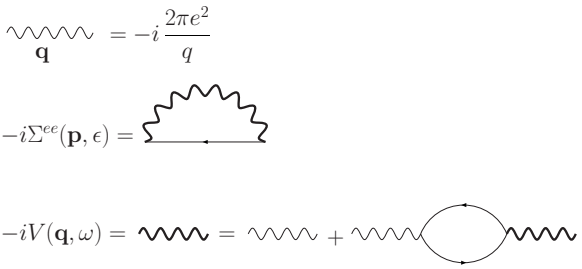

FIG. 19. Electronic self-energy from the RPA-screened Coulomb interaction.

VIII. RENORMALIZATION OF THE COUPLING CONSTANTS

A. Coulomb renormalization

As discussed in the beginning of Sec. VI B, the measured ratio of the integrated intensities of $2K$ and 2Γ peaks at 2700 and 3250 cm^{-1}, $I_{2K}/I_{2\Gamma}\approx 20$,[6] is in noticeable disagreement with the calculated values of electron-phonon coupling constants.[31] In this section we investigate how the electron-phonon coupling constants are renormalized by the Coulomb interaction between electrons. A brief account of this part has been reported in the short publication.[34]

We are going to consider only the long-range part of the Coulomb interaction (i.e., smooth on the length scale of the lattice constant). Such interaction does not mix the states in different valleys, so the interaction Hamiltonian can be written as

$$\hat{H}_{ee} = \frac{e^2}{2}\int d^2\mathbf{r}d^2\mathbf{r}'\frac{\hat{\rho}(\mathbf{r})\hat{\rho}(\mathbf{r}')}{|\mathbf{r}-\mathbf{r}'|}, \quad \hat{\rho}(\mathbf{r}) = \hat{\psi}^\dagger(\mathbf{r})\hat{\psi}(\mathbf{r}). \tag{119}$$

In this equation we have not included explicitly the screening by the background dielectric constant of the substrate ε_∞ (the high-frequency value), which can be taken into account by incorporating it into e^2.

The electronic self-energy due to the Coulomb interaction (the Fock term) $\Sigma^{ee}(\mathbf{p},\epsilon)$ is shown in Fig. 19. Its leading logarithmic asymptotics is given by[37]

$$\Sigma^{ee}(\mathbf{p},\epsilon) = i\int\frac{d\omega}{2\pi}\frac{d^2\mathbf{q}}{(2\pi)^2}V(\mathbf{q},\omega)G(\mathbf{p}-\mathbf{q},\epsilon-\omega) \approx \frac{8}{\pi^2\mathcal{N}}[f(g)(2\epsilon-v\mathbf{p}\boldsymbol{\Sigma})-\tilde{f}(g)(\epsilon-v\mathbf{p}\boldsymbol{\Sigma})]\ln\frac{\xi_{max}}{\xi_{min}}, \tag{120}$$

$$f(g) = 1-\frac{\pi}{2g}+\frac{\arccos g}{g\sqrt{1-g^2}}, \quad \tilde{f}(g) = \frac{g\arccos g}{\sqrt{1-g^2}}, \tag{121}$$

$$V(\mathbf{q},\omega)=\frac{16g}{\mathcal{N}}\frac{v}{q}\frac{\sqrt{(vq)^2-\omega^2}}{gvq+\sqrt{(vq)^2-\omega^2}}. \tag{122}$$

Here we have introduced the total number of the Dirac species, $\mathcal{N}=4$, which takes into account the valley and the spin degeneracy (the latter enters as factor of 2 multiplying the electron polarization operator). The lower cutoff $\xi_{min}\sim max\{vp,\epsilon\}$, the upper cutoff $\xi_{max}\sim v/a$ is of the order of the electronic bandwidth, and the dimensionless Coulomb coupling constant is defined as

$$g=\frac{\pi\mathcal{N}e^2}{8v}. \tag{123}$$

The derivation of Eq. (120) is given in Appendix D. The logarithmic divergence in the Fock self-energy Σ^{ee} is due to the long-distance nature of the Coulomb interaction and thus is not picked up by local approximations such as LDA or GGA.

The random-phase approximation (RPA) for $V(\mathbf{q},\omega)$, shown in Fig. 19, corresponds to expansion of the coefficient in front of the logarithm to the leading order in the parameter $1/\mathcal{N}=0.25$, assumed to be small. This assumption is better justified than the expansion in g, which would be obtained if we used the bare coupling $2\pi e^2/q$ instead of the RPA-dressed one $V(\mathbf{q},\omega)$. Indeed, for $\mathcal{N}=4$ we have $g=(\pi/2)(e^2/v)\approx 3.4$; taking into account the background dielectric screening reduces it to $g\sim 1$.

The presence of the large logarithm invalidates the simple first-order expansion in $1/\mathcal{N}$ and makes it necessary to sum all leading logaritmic terms $\sim(1/\mathcal{N})^n\ln^n(\xi_{max}/\xi_{min})$ of the perturbation theory. This summation is performed using the standard renormalization-group (RG) procedure. Let us introduce the running cutoff $\xi_{max}e^{-\ell}$. One RG step consists of reducing the cutoff, $\ell\to\ell+\delta\ell$, so that $e^{\delta\ell}\gg 1$, while $(1/\mathcal{N})\delta\ell\ll 1$. Inverse Green's function transforms as

$$\epsilon-v\mathbf{p}\cdot\mathbf{\Sigma}-\Sigma(\mathbf{p},\epsilon)=\frac{\epsilon-(v+\delta v)\mathbf{p}\cdot\mathbf{\Sigma}}{1+\delta Z}, \tag{124}$$

where Z is chosen to preserve the coefficient at ϵ upon rescaling of the electronic fields, $\psi\to(1+\delta Z/2)\psi$,

$$\frac{1}{1+\delta Z}=1-\frac{\partial\Sigma}{\partial\epsilon}. \tag{125}$$

The renormalization of the velocity is then given by

$$\frac{\delta v}{v}=\frac{\partial\Sigma}{\partial\epsilon}+\frac{\partial\Sigma}{\partial(v\mathbf{p}\cdot\mathbf{\Sigma})}. \tag{126}$$

Next, we need to determine renormalization of the coupling constants. The electron charge is not renormalized, as guaranteed by the gauge invariance, so the renormalization of the Coulomb coupling constant g is determined by renormalization of the velocity v. The correction to the electron-phonon coupling constants is determined by the diagram in Fig. 20 and is evaluated in Appendix D. The results are

$$\frac{\delta F_\Gamma}{F_\Gamma}=\delta Z+\frac{8}{\pi^2\mathcal{N}}[\tilde{f}(g)-f(g)]\ln\frac{\xi_{max}}{\xi_{min}}, \tag{127a}$$

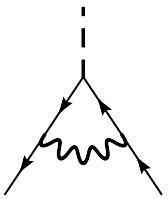

FIG. 20. Diagram describing the logarithmic correction to the electron-phonon vertex due to the Coulomb interaction in the order $O(1/\mathcal{N})$.

$$\frac{\delta F_K}{F_K}=\delta Z+\frac{8}{\pi^2\mathcal{N}}\tilde{f}(g)\ln\frac{\xi_{max}}{\xi_{min}}. \tag{127b}$$

Let us pass to dimensionless electron-phonon coupling constants λ_Γ, λ_K, introduced in Eq. (24). Then the equations for the RG flow are the following:

$$\frac{d\ln g}{d\ell}=-\frac{8}{\pi^2\mathcal{N}}f(g), \tag{128a}$$

$$\frac{d\ln\lambda_\Gamma}{d\ell}=0, \tag{128b}$$

$$\frac{d\ln\lambda_K}{d\ell}=\frac{16}{\pi^2\mathcal{N}}f(g). \tag{128c}$$

As $f(g)$ is positive and monotonous (see Fig. 21), g flows to weak coupling;[35] if the initial value of g is large,

$$f(g)=1-\frac{\pi}{2g}+O(g^{-2})\Rightarrow g(\ell)=g(0)e^{-8\ell/(\pi^2\mathcal{N})}, \tag{129}$$

while at small g we have

$$f(g)=\frac{\pi g}{4}+O(g^2)\Rightarrow g(\ell)=\frac{g(0)}{1+2\ell g(0)/(\pi\mathcal{N})}. \tag{130}$$

Integration of Eqs. (128a)–(128c) yields the following relation:

$$\frac{\lambda_K(\ell)}{\lambda_K(0)}=\left[\frac{g(0)}{g(\ell)}\right]^2=\left[\frac{v(\ell)}{v(0)}\right]^2, \tag{131}$$

which, in principle, can be checked experimentally. Thus, λ_K is enhanced, which is in qualitative agreement with the Raman data; according to the results of Sec. VI A, the ratio of the intensities of the two-phonon peaks is $I_{2K}/I_{2\Gamma}=2(\lambda_{A_1}/\lambda_\Gamma)^2$.

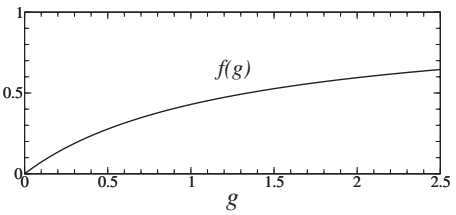

FIG. 21. Plot of the function $f(g)$ defined in Eq. (121).

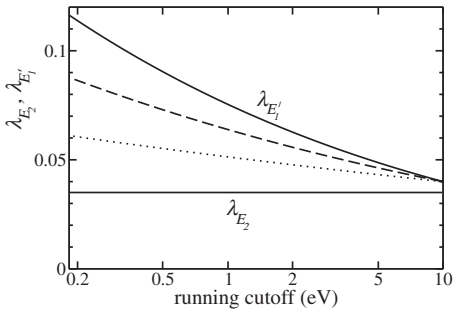

FIG. 22. Dependence of the dimensionless coupling constant λ_K on the running cutoff $\xi_{max}e^{-\ell}$ (to be identified with the electronic energy), represented by three upper curves starting from the bare value 0.04 at 10 eV, for three values of the bare Coulomb coupling $g(0)=3.4, 1.5, 0.5$ (solid, dashed, and dotted curves, corresponding to the substrate dielectric constant $\varepsilon_\infty=1, 2.3, 6.8$, respectively) as determined by Eqs. (128a)–(128c). The constant $\lambda_\Gamma=0.035$ is unchanged.

To study the behavior of the coupling constants quantitatively, we solve Eqs. (128a)–(128c) numerically. The largest value of ℓ is determined by the lower cutoff $\xi_{min}\sim\omega_\mu \sim 0.2$ eV. In Fig. 22, we show the flow of λ_K for three values of the bare Coulomb coupling constant: $g(0)=3.4$ (corresponding to no dielectric screening at all), $g(0)=1.5$, and $g(0)=0.5$. The bare values of the the electron-phonon coupling constants $\lambda_\Gamma(0)=0.035$, $\lambda_K(0)=0.040$ were chosen (i) to satisfy the relation $\lambda_\Gamma(0)/\lambda_K(0)=\omega_K/\omega_\Gamma$, valid in the tight-binding approximation, and (ii) to reproduce the experimental value $\lambda_\Gamma\approx 0.035$. Note that the RPA calculation without the RG collection of all leading logarithmic terms would give all dependencies in Fig. 22 to be straight lines with slopes fixed at 10 eV. A comparable error would be produced by the *GW* approximation, which neglects vertex corrections and thus picks up correctly only the first term of the logarithmic series.

To estimate the EPC strength relevant for Raman scattering, we identify the running cutoff with the typical electronic energy, involved in the process, thus stopping the RG flow at electronic energies $\epsilon\sim 1$ eV (half of the incident laser frequency). In the unscreened case, $g(0)=3.4$, it gives $\lambda_{A_1}/\lambda_\Gamma \approx 3.2$, in agreement with the observed ratio $I_{2K}/I_{2\Gamma}\approx 20$.

Finally, we wish to note that the cancellation of the self-energy and vertex corrections, leading to $d\lambda_\Gamma/d\ell=0$ in Eq. (128b), is not occasional. Indeed, comparing Eqs. (23) and (28), we can see that coupling to the E_2 phonon displacement $\mathbf{u}_{E_2}$ has the same form as the coupling to the vector potential $\mathbf{A}$ with the correspondence $u_{E_{2x}}\leftrightarrow A_y$, $-u_{E_{2y}}\leftrightarrow A_x$ (up to the sign, different for the K,K' valleys). This means that a uniform phonon displacement $\mathbf{u}_{E_2}$ can be gauged out of the electronic Hamiltonian, which should hold for both intial and renormalized Hamiltonians. Thus, gauge invariance requires that F_Γ is renormalized in the same way as the velocity v. Since $\lambda_\Gamma\propto F_\Gamma^2/v^2$, it must remain constant.

B. Renormalization due to the electron-phonon coupling

It turns out that the Coulomb interaction is not the only source of renormalizations. Since the electron-phonon self-energy $\Sigma^{ph}(\mathbf{p},\epsilon)$, calculated in Sec. IV C, also has a logarithmic divergence, renormalizations due to electron-phonon interaction should be taken into account as well. However, in practice, the electron-phonon coupling is so weak ($\lambda_\mu\ll 1$, see Sec. VIII A), that its effect is negligible, so that Sec. VIII A contains all the practical information. Still, for the sake of completeness, in this section we describe the theory of renormalizations due to electron-phonon coupling.

Let us return to the electron-phonon self-energy $\Sigma^{ph}(\mathbf{p},\epsilon)=\Sigma^\Gamma(\mathbf{p},\epsilon)+\Sigma^K(\mathbf{p},\epsilon)$, calculated in Sec. IV C. The leading logarithmic asymptotics of Σ^{ph} is given by (see also Appendix D)

$$\Sigma^{ph}(\mathbf{p},\epsilon)=i\int\frac{d\omega}{2\pi}\frac{d^2\mathbf{q}}{(2\pi)^2}\sum_\mu\frac{F_\mu^2}{2M\omega_\mu}\frac{\sqrt{27}a^2}{4}D_\mu(\omega)$$
$$\times(\Lambda\Sigma)_\mu G(\mathbf{p}-\mathbf{q},\epsilon-\omega)(\Lambda\Sigma)_\mu$$
$$\approx\frac{\lambda_\Gamma+\lambda_K}{2\pi}\epsilon\ln\frac{\xi_{max}}{\xi_{min}}. \qquad (132)$$

Here the phonon mode index μ runs over the two modes belonging to the E_2 representation and the two modes belonging to the E_1' representation, the corresponding matrices $(\Lambda\Sigma)_\mu$ being $-\Lambda_z\Sigma_y$, $\Lambda_z\Sigma_x$, $\Lambda_x\Sigma_z$, and $\Lambda_y\Sigma_z$. The upper and lower cutoffs are given by $\xi_{max}\sim v/a$, $\xi_{min}\sim max\{\epsilon,\omega_\mu\}$. The dimensionless constants λ_Γ, λ_K, defined in Eq. (24), will be treated as small parameters.

The latter statement deserves some discussion. In principle, one could proceed analogously to the Coulomb case; instead of doing the perturbative expansion in λ_μ, one could dress the bare phonon propagators by the appropriate polarization operators $\Pi(\mathbf{q},\omega)$, corresponding to $1/\mathcal{N}$ expansion (the polarization operators for different matrix vertices are calculated in Appendix E). Since $\Pi(\mathbf{q},\omega)\propto q$ at large q, the dressed phonon frequency would grow as $\sqrt{q}$ and Σ^{ph} would no longer diverge logarithmically. However, the inelastic x-ray scattering data for the phonon dispersion[33] show that the phonon dispersion is smaller than the phonon frequency itself. Thus, the renormalization of the phonon frequency remains small even at $q\sim 1/a$, so the perturbative expansion in λ_μ is more justified, and we neglect the phonon dispersion.

The logarithmically divergent integrals in Eqs. (120) and (132) have different structure due to different forms of the screened interaction $V(\mathbf{q},\omega)$ and the phonon propagator $D_\mu(\omega)$. In Eq. (120) the integral is dominated by the frequencies $|\omega|\sim vq$, while in Eq. (132) it is $|\omega|\sim\omega_\mu$, since $D_\mu(\omega)\propto 1/\omega^2$ at $|\omega|\gg\omega_\mu$. Thus, in the calculation of the leading logarithmic asymptotics it is sufficient to approximate $D_\mu(\omega)\approx -2\pi i\delta(\omega)$ (see Appendix D). This substitution makes the phonon propagator (combined with electron-phonon vertices) formally analogous to the correlator of a static disorder potential (in other words, from the point of view of electrons with $\epsilon\gg\omega_\mu$ the lattice is effectively frozen). Thus, renormalizations due to electron-phonon interaction at $\epsilon\gg\omega_\mu$ are equivalent to those due to static disorder.[39,40,58] This equivalence holds only in the leading order in electron-phonon coupling, since in higher orders the phonon propagator is dressed by polarization loops and the static disorder correlator is not.

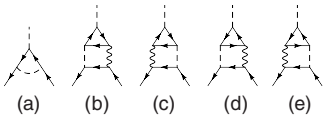

FIG. 23. Diagrams describing the logarithmic correction to the electron-phonon vertex due to the electron-phonon interaction in the order $O(1/\mathcal{N},\lambda_\mu^2)$. Diagrams (b)–(e) vanish.

Logarithmic corrections to the electron-phonon vertex in the order $O(1/\mathcal{N},\lambda_\mu^2)$ are shown in Fig. 23. All diagrams vanish, except the first one, which gives a nonzero correction to λ_K,

$$\frac{\delta F_\Gamma}{F_\Gamma} = \delta Z + 0, \tag{133a}$$

$$\frac{\delta F_K}{F_K} = \delta Z - \frac{\lambda_\Gamma}{2\pi} \ln \frac{\xi_{max}}{\xi_{min}}. \tag{133b}$$

The diagrams of Fig. 23, however, do not exhaust all logarithmic vertex corrections. In addition, one has to consider two diagrams, shown in Fig. 24, as they are of the same order $O(\lambda_\mu^2)$ and also logarithmically divergent. They may be viewed as a correction to the two-electron vertex $\Gamma^{(2)}(\mathbf{p},\epsilon,\mathbf{p}',\epsilon';\mathbf{q},\omega)$. The bare value of $\Gamma^{(2)}$ is given just by the phonon single-phonon propagator, combined to the electron-phonon vertices. Diagrams of Fig. 24 are evaluated in Appendix D, and give

$$\begin{aligned}\Gamma^{(2)}&(\mathbf{p},\epsilon,\mathbf{p}',\epsilon';\mathbf{q},\omega)\\ &= \frac{v^2}{2}[\lambda_\Gamma D_\Gamma(\omega)(\Lambda_z\Sigma_y \otimes \Lambda_z\Sigma_y + \Lambda_z\Sigma_x \otimes \Lambda_z\Sigma_x)\\ &\quad + \lambda_{E_1} D_K(\omega)(\Lambda_y\Sigma_z \otimes \Lambda_y\Sigma_z + \Lambda_x\Sigma_z \otimes \Lambda_x\Sigma_z)],\end{aligned} \tag{134a}$$

$$\begin{aligned}\delta\Gamma^{(2)}&(\mathbf{p},\epsilon,\mathbf{p}',\epsilon';\mathbf{q},\omega)\\ &= \frac{v^2}{2} \ln \frac{\xi_{max}}{\xi_{min}} \left[\frac{\lambda_K^2}{2\pi} D_{E_1'+E_1'}(\omega)(\Lambda_z\Sigma_y \otimes \Lambda_z\Sigma_y + \Lambda_z\Sigma_x \otimes \Lambda_z\Sigma_x)\right.\\ &\quad \left. + \frac{\lambda_\Gamma \lambda_{E_1}}{\pi} D_{E_2+E_1'}(\omega)(\Lambda_y\Sigma_z \otimes \Lambda_y\Sigma_z + \Lambda_x\Sigma_z \otimes \Lambda_x\Sigma_z)\right],\end{aligned} \tag{134b}$$

$$D_{\mu+\mu'}(\omega) \equiv \frac{2(\omega_\mu + \omega_{\mu'})}{\omega^2 - (\omega_\mu + \omega_{\mu'} - io)^2}. \tag{134c}$$

The following features of the expression for $\delta\Gamma^{(2)}$ are worth noting: (i) the matrix structure of $\delta\Gamma^{(2)}$ is identical to that of $\Gamma^{(2)}$; (ii) $\delta\Gamma^{(2)}$ depends on electronic energies and momenta only through ξ_{min}, i.e., logarithmically; and (iii) the ω dependence of $\delta\Gamma^{(2)}$ is analogous to that of $\Gamma^{(2)}$, but the pole is at the sum of two-phonon frequencies.

The latter fact has a simple physical meaning. Before the reduction in the ultraviolet cutoff ξ_{max} the excitations of the lattice were phonons with momenta $|\mathbf{q}| < \xi_{max}/v$, as well as their combinations. In the theory with the reduced cutoff $\xi_{max}e^{-\ell}$, besides phonons with momenta $|\mathbf{q}| < (\xi_{max}/v)e^{-\ell}$,

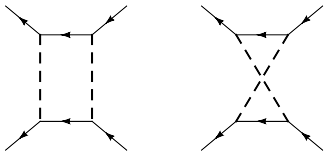

FIG. 24. Logarithmic diagrams of the order $O(\lambda^2)$ not reduced to a renormalization of the electron-phonon vertex.

one has to consider also pairs of phonons with large and almost opposite momenta $\mathbf{q}'$ and $\mathbf{q}-\mathbf{q}'$, so that the total momentum of the pair is $|\mathbf{q}| < \xi_{max}e^{-\ell}$. Each of the phonons constituting the pair has $(\xi_{max}/v)e^{-\ell} < |\mathbf{q}'|, |\mathbf{q}-\mathbf{q}'| < \xi_{max}/v$ and thus has been integrated out. The pair, however, having small total momentum, has to be included into the low-energy theory as a single excitation. Thus, $D_{\mu+\mu'}(\omega)$ has the meaning of the propagator of this excitation, and comparing expressions (134a) and (134b), one can define electron-two-phonon vertex by analogy with the electron-phonon one.

Iterations of the RG procedure will generate electron coupling to excitations with larger number of phonons, hence all these excitations with frequencies $n\omega_\Gamma + n'\omega'_{E_1}$ have to be included in the low-energy theory separately. Obviously, electron coupling to excitations of the type $n\Gamma + 2kE_1'$ will have the same matrix structure as coupling to the E_2 phonons, while coupling to excitations $n\Gamma + (2k+1)E_1'$ the same as to the E_1' phonons. Denoting the dimensionless coupling constant for the excitation $n\omega_\Gamma + n'\omega'_{E_1}$ by $\lambda_{n,n'}$, we can generalize the RG equations [Eqs. (128a)–(128c)] as follows:

$$\frac{1}{g}\frac{dg}{d\ell} = -\frac{8f(g)}{\pi^2\mathcal{N}} + \sum_{n,k=0}^{\infty} \frac{\lambda_{n,2k} + \lambda_{n,2k+1}}{2\pi}, \tag{135a}$$

$$\frac{d\lambda_{n,2k}}{d\ell} = \frac{1}{2\pi} \sum_{n'=0}^{n} \sum_{k'=1}^{k} \lambda_{n',2k'-1}\lambda_{n-n',2k-2k'+1}, \tag{135b}$$

$$\begin{aligned}\frac{d\lambda_{n,2k+1}}{d\ell} &= \left[\frac{16f(g)}{\pi^2\mathcal{N}} - \sum_{n',k'=0}^{\infty} \frac{\lambda_{n',2k'}}{\pi}\right]\lambda_{n,2k+1}\\ &\quad + \frac{1}{\pi} \sum_{n'=0}^{n} \sum_{k'=0}^{k} \lambda_{n',2k'}\lambda_{n-n',2k-2k'+1}.\end{aligned} \tag{135c}$$

These equations can be simply related to Eq. (12) of Ref. 34, where λ_Γ and λ_{A_1} denoted the total oscillator strength of all E_2-like and all E_1'-like excitations, respectively,

$$\lambda_{E_2}^{(\text{Ref. 34})} = \sum_{n,k=0}^{\infty} \lambda_{n,2k}, \quad \lambda_{A_1}^{(\text{Ref. 34})} = \sum_{n,k=0}^{\infty} \lambda_{n,2k+1}.$$

Namely, Eqs. (12b) and (12c) of Ref. 34 are obtained by summing Eqs. (135b) and (135c) over n and k.

We will not solve Eqs. (135a) and (135c), since in graphene the effect of the electron-phonon interaction turns out to be negligibly small due to the smallness of λ_Γ, λ_K, as we mentioned in the beginning of this section. In particular,

the modification of the plot in Fig. 22 would not be noticeable by the naked eye.

IX. SUMMARY

In this paper we have calculated the frequency-integrated intensities of two- and four-phonon Raman peaks in disorder-free graphene. We started by writing down the low-energy Hamiltonian of the interaction of electrons with the crystal vibrations and the electromagnetic field from pure symmetry considerations; as a result, we obtained a description of the system in terms of just a few independent coupling constants, considered to be parameters of the theory. Another parameter of the theory, introduced phenomenologically, is the electron-scattering rate 2γ.

First, we analyzed the one-phonon peak at 1580 cm^{-1} and have shown that the scattering is completely off-resonant: the intermediate electron and hole states in the whole first Brillouin zone contribute to the Raman-scattering amplitude. As a result, the intensity of the peak is expected to be insensitive to most external parameters: polarization, electron concentration, degree of disorder, etc. However, according to our results, it is proportional to the fourth power of the excitation frequency.

Then we calculated the intensities I_{2K} and $I_{2\Gamma}$ of the two-phonon peaks at 2700 and 3250 cm^{-1}, respectively. We have shown that two-phonon scattering is fully resonant, so that the intermediate electron and hole states correspond to real particles, propagating along the quasiclassical trajectories and subject to scattering processes. As a result, the intensities are determined by the electron-scattering rate. Besides, the quasiclassical character of the process imposes a severe restriction on the electron and hole trajectories which can contribute to the two-phonon Raman scattering: upon the phonon emission the electron and the hole must be scattered backward. This restriction results in a significant polarization memory: it is almost three times more probable for the scattered photon to have the same polarization as the incident photon than to have the orthogonal polarization.

We have also calculated the intensity I_{4K} of the most intense four-phonon peak at 5400 cm^{-1}. The four-phonon Raman scattering is also fully resonant. As a consequence, we have shown that measurement of the ratio I_{4K}/I_{2K} enables one to extract information about the relative contributions of different processes to the electron scattering rate.

Having compared the experimental two-phonon peak intensities, we extracted the ratio of the corresponding electron-phonon coupling constants. This ratio turned out to be significantly different from that obtained earlier from the density-functional theory calculations. We have shown that the reason for this discrepancy is the renormalization of the coupling constants due to the Coulomb interaction between electrons, missed by DFT calculations based on local or semilocal approximations for the exchange-correlation functional. In particular, we found that the constant, responsible for the peak at 3250 cm^{-1}, is enhanced, and this enhancement is in quantitative agreement with the experimental Raman data, provided that the screening of the Coulomb interaction by the substrate is weak.

ACKNOWLEDGMENTS

The author is grateful to I. L. Aleiner for numerous discussions and for collaboration in writing Secs. III and V of this paper. The author also acknowledges stimulating discussions with J. Yan, M. S. Foster, F. Guinea, S. Piscanec, A. C. Ferrari, F. Mauri, M. Calandra, and M. Lazzeri.

APPENDIX A: MATRIX ALGEBRA

The natural basis in the 16-dimensional space of all 4×4 Hermitian matrices is represented by the $\tau_i^{KK'}\times\tau_j^{AB}$, $i,j=x,y,z,0$, where $\tau_i^{KK'}$, τ_j^{AB}, $i,j=x,y,z$, are the Pauli matrices acting in the corresponding subspaces, respectively, and $\tau_0^{KK'}$, τ_0^{AB} are the 2×2 unit matrices. The square of each matrix is equal to $\mathbb{1}$—the 4×4 unit matrix.

These 16 matrices can be split into two sets: those diagonal and those off diagonal in the KK' subspace (i.e., containing $\tau_0^{KK'}$, $\tau_z^{KK'}$ and $\tau_x^{KK'}$, $\tau_y^{KK'}$, respectively). These two sets are invariant with respect to C_{6v} because any transformation from C_{6v} either (i) leaves K and K' in place (thus belonging to C_{3v}) or (ii) swaps between K and K' (belonging to C_2C_{3v}) but never mixes them. Thus, these two sets form two eight-dimensional representations. Both are reduced as $A_1+A_2+B_1+B_2+E_1+E_2$, since each set contains a matrix transforming according to A_1; for the valley-diagonal set it is $\mathbb{1}$, while for the off-diagonal one it is the matrix U_{C_2} of the C_2 rotation which commutes with all C_{6v} and is Hermitian since $C_2^{-1}=C_2$.

Let us focus on the valley-diagonal set. The two matrices which transform according to E_1 (vector) representation will be denoted by Σ_x, Σ_y. To establish their multiplication rules, we form the direct product $E_1\times E_1=A_1+A_2+E_2$. The corresponding linear combinations are

$$\Sigma_x\Sigma_x+\Sigma_y\Sigma_y\sim A_1, \tag{A1}$$

$$\Sigma_x\Sigma_y-\Sigma_y\Sigma_x\sim A_2, \tag{A2}$$

$$\{\Sigma_x\Sigma_x-\Sigma_y\Sigma_y,\Sigma_x\Sigma_y+\Sigma_y\Sigma_x\}\sim E_2. \tag{A3}$$

Since $\Sigma_x^2=\Sigma_y^2=\mathbb{1}$, the proportionality coefficient in the last line must be zero, so $\Sigma_x\Sigma_y=-\Sigma_y\Sigma_x=i\Sigma_z$. The matrix Σ_z defined in this way (i) is Hermitian, (ii) transforms according to A_2, and (iii) $\Sigma_z^2=\mathbb{1}$. Thus, it must coincide with the corresponding matrix from the basis (the sign may need to be changed). In other words, the set $\{\Sigma_x,\Sigma_y,\Sigma_z\}$ satisfies the usual Pauli-matrix algebra.

As the subgroup $C_{2v}=\{E,\sigma_v,\sigma_v',C_2\}$ is a direct product, the matrices of B_1, B_2, A_2 representations of the valley-diagonal set must commute, and the product of any two will give the third one. Let us denote by Λ_z the matrix of the B_1 representation, then that of B_2 is $\Lambda_z\Sigma_z$.

The two matrices transforming according to the E_2 (pseudovector or tensor) representation are denoted by $\{T_x,T_y\}\equiv\mathbf{T}$. Just like for $\boldsymbol{\Sigma}$, using $E_2\times E_2=A_1+A_2+E_2$, we establish the Pauli-matrix algebra for the set $\{T_x,T_y,\Sigma_z\}$. It is important that matrices of σ_a', σ_b', σ_c' reflections are expressed in terms of T_x, T_y. Indeed, (i) $\sigma_a'=(\sigma_a')^{-1}$, so its ma-

trix is Hermitian and its square is equal to $\mathbb{1}$; (ii) this matrix is diagonal in the KK' indices; (iii) $C_3^{-1}\sigma_a' C_3 = \sigma_b'$, so the matrix of σ_a' cannot belong to a one-dimensional representation; and (iv) $C_2\sigma_a' C_2 = \sigma_a'$, so it must be the E_2 representation. Since we have a rotational arbitrariness in the choice of T_x, T_y, we simply fix T_y to be the matrix of the σ_a' reflection.

The products of $\boldsymbol{\Sigma}$ and $\mathbf{T}$ can be analyzed by using $B_1 \times E_1 = B_2 \times E_1 = E_2$. The rotational arbitrariness in the choice of Σ_x, Σ_y can be removed by fixing their behavior under the σ_a' reflection: $T_y\Sigma_x T_y = \Sigma_x$, $T_y\Sigma_y T_y = -\Sigma_y$. The algebraic relations established earlier leave us with

$$T_x = -\zeta\Lambda_z\Sigma_y, \quad T_y = \zeta\Lambda_z\Sigma_x, \quad \zeta^4 = 1. \tag{A4}$$

The sign of ζ is not important as one can always redefine $\Lambda_z \to -\Lambda_z$. The difference between real and imaginary ζ is essential, as it determines the symmetry under the time reversal and will be discussed below.

The off-diagonal set can be obtained from the diagonal one by simply multiplying it by U_{C_2}, the matrix of C_2, which transforms according to the identical representation of C_{6v}, but swaps K and K'. According to the representation algebra, U_{C_2} commutes with Σ_z, T_x, T_y and anticommutes with Λ_z, $\Lambda_z\Sigma_z$, Σ_x, Σ_y. Generally, if two Hermitian operators commute, their product is Hermitian, while if they anticommute, their product is anti-Hermitian, so the proportionality coefficient in the corresponding algebraic relation must be imaginary. Hence, the matrices of the off-diagonal set can be written as U_{C_2}, $iU_{C_2}\Lambda_z$, $U_{C_2}\Sigma_z$, $iU_{C_2}\Lambda_z\Sigma_z$, $iU_{C_2}\Sigma_x$, $iU_{C_2}\Sigma_y$, $-U_{C_2}T_x$, and $-U_{C_2}T_y$. Denoting $U_{C_2}\Sigma_z = \Lambda_x$, we recover the bottom row of Table III, provided that $\zeta = 1$.

To establish the form of the matrix of the C_3 rotation, we note that (i) it must be diagonal in the valley subspace, (ii) commute with U_{C_2}, and (iii) its third power should be equal to the unit matrix. This fixes $U_{C_3} = e^{\pm(2\pi i/3)\Sigma_z}$.

Now let us establish the symmetry properties of the matrices with respect to the time reversal. The explicit form of the corresponding matrix $U_{\mathcal{T}}$ needs not be specified. We only note that time reversal must commute with any spatial transformation. Applying this condition to the matrices U_{C_2}, $\mathbf{T}$, and $e^{2\pi i\Sigma_z/3}$, we obtain $U_{C_2} \mapsto U_{C_2}$, $\mathbf{T} \mapsto \mathbf{T}$, and $\Sigma_z \mapsto -\Sigma_z$. Next, the time reversal swaps K and K', so $\Lambda_z \mapsto -\Lambda_z$. Applying the algebraic relations established above, we obtain

$$\Lambda_z \underset{\mathcal{T}}{\mapsto} -\Lambda_z, \quad \boldsymbol{\Lambda} \underset{\mathcal{T}}{\mapsto} -\boldsymbol{\Lambda}, \quad \Sigma_z \underset{\mathcal{T}}{\mapsto} -\Sigma_z, \quad \boldsymbol{\Sigma} \underset{\mathcal{T}}{\mapsto} -\zeta^2\boldsymbol{\Sigma}. \tag{A5}$$

Next, since the matrices of σ_a, σ_b, σ_c reflections are expressed in terms of $U_{C_2}\mathbf{T}$, we must have $\Lambda_y\boldsymbol{\Sigma} \mapsto \Lambda_y\boldsymbol{\Sigma}$, which fixes $\zeta = \pm 1$.

To help those readers who prefer to work with a particular representation, rather than basis-independent algebraic relations, we give specific expressions for the matrices defined above. In Ref. 59 the representation is introduced by defining the column state vector as

$$\psi = \begin{bmatrix} \psi_{AK} \\ \psi_{BK} \\ \psi_{BK'} \\ \psi_{AK'} \end{bmatrix}, \tag{A6}$$

and the Σ_i, Σ_j' matrices have the form

$$\Sigma_x = \tau_z^{KK'}\tau_x^{AB}, \quad \Lambda_x = \tau_x^{KK'}\tau_z^{AB},$$

$$\Sigma_y = \tau_z^{KK'}\tau_y^{AB}, \quad \Lambda_y = \tau_y^{KK'}\tau_z^{AB},$$

$$\Sigma_z = \tau_0^{KK'}\tau_z^{AB}, \quad \Lambda_z = \tau_z^{KK'}\tau_0^{AB}, \tag{A7}$$

where $\tau_i^{KK'}$, τ_j^{AB}, $i,j = x,y,z$, are the Pauli matrices acting in the corresponding subspaces, respectively, and $\tau_0^{KK'}$, τ_0^{AB} are the 2×2 unit matrices.

In Ref. 58 the column state vector is defined as

$$\psi = \begin{bmatrix} \psi_{AK} \\ \psi_{BK} \\ \psi_{BK'} \\ -\psi_{AK'} \end{bmatrix}, \tag{A8}$$

and it is assumed that $\mathcal{U}_{\mathbf{K}',A(B)}(\mathbf{r}) = \mathcal{U}^*_{\mathbf{K},A(B)}(\mathbf{r})$. In this representation the electronic matrices acquire an especially simple form $\Sigma_i = \tau_0^{KK'}\tau_i^{AB}$, $\Lambda_i = \tau_i^{KK'}\tau_0^{AB}$ and the time-reversal matrix $U_{\mathcal{T}} = \tau_y^{KK'}\tau_y^{AB}$.

APPENDIX B: EFFECTIVE HAMILTONIAN IN AN EXTERNAL FIELD

The theory of electrons in a crystal lattice subject to a magnetic field was developed long ago.[60] Here we consider the specific case of the two-dimensional graphene crystal.

Let us start from the simpler case of the scalar potential $\varphi(\mathbf{r},z)$, assumed to be smooth on the scale of the lattice constant. Definition (9) of the effective Hamiltonian can be written as

$$\int \psi_\alpha^*(\mathbf{r}) H^{\varphi}_{\alpha\beta}\psi_\beta(\mathbf{r})d^2\mathbf{r} = \int \psi_\alpha^*(\mathbf{r}) e\varphi(\mathbf{r},z)\psi_\beta(\mathbf{r}) \times [e^{i(\mathbf{K}_\beta - \mathbf{K}_\alpha)\mathbf{r}}\mathcal{U}^*_\alpha(\mathbf{r},z)\mathcal{U}_\beta(\mathbf{r},z)]d^2\mathbf{r}dz. \tag{B1}$$

Here $\alpha,\beta = 1,2,3,4$ label the four states with zero energy, $\mathbf{K}_{\alpha,\beta}$ are $\mathbf{K}$ or $\mathbf{K}'$, correspondingly, and summation over repeating indices is assumed hereafter, unless stated explicitly otherwise.

The integration over z in Eq. (B1) is straightforward due to confinement provided by the Bloch functions. As for the integration over x, y, we note that the combination of functions in the square brackets can be represented as $\delta_{\alpha\beta}\chi_\alpha(z) + \tilde{\chi}_{\alpha\beta}(\mathbf{r},z)$, where the second function (i) has zero spatial average and (ii) is periodic in x, y with the period corresponding to the tripled unit cell. The first term is written using normalization (7) of the Bloch functions (no summation over α is assumed). The rest of the integrand,

$\psi^*_\alpha(\mathbf{r})\varphi(\mathbf{r},z)\psi_\beta(\mathbf{r})$, is a smooth function of x, y, i.e., its spatial harmonics have wave vectors much smaller than the inverse lattice constant.

To study the integral of an arbitrary smooth function $f(\mathbf{r})$ with the periodic function $\tilde{\chi}_{\alpha\beta}(\mathbf{r},z)$, we expand the latter in the Fourier sum over the reciprocal-lattice vectors $\mathbf{G}$,

$$\tilde{\chi}_{\alpha\beta}(\mathbf{r},z)=\sum_{\mathbf{G}}\sum_{j=0,\pm1}C^j_{\alpha\beta}(\mathbf{G},z)e^{i(\mathbf{G}+j\mathbf{K})\mathbf{r}}. \tag{B2}$$

Then the integral can be rewritten in the Fourier space,

$$\int f(\mathbf{r})\tilde{\chi}_{\alpha\beta}(\mathbf{r},z)d^2\mathbf{r}=\sum_{\mathbf{G}}\sum_{j=0,\pm1}\tilde{f}^*(\mathbf{G}+j\mathbf{K})C^j_{\alpha\beta}(\mathbf{G},z). \tag{B3}$$

The sum does not contain the term with $\mathbf{G}=0$, $j=0$, which has been excluded from $\tilde{\chi}_{\alpha\beta}(\mathbf{r},z)$ by construction. The Fourier transform of $f(\mathbf{r})$,

$$\tilde{f}(\mathbf{p})=\int e^{-i\mathbf{p}\mathbf{r}}f(\mathbf{r})d^2\mathbf{r}, \tag{B4}$$

is rapidly decaying away from $\mathbf{p}=0$. If all spatial derivatives of $f(\mathbf{r})$ are continuous, this decay is exponential. This leads to the following expression for the effective Hamiltonian:

$$H^\varphi_{\alpha\beta}=e\varphi(\mathbf{r},z=0)\delta_{\alpha\beta}-d_z\mathcal{E}_z(\mathbf{r},z=0)\delta_{\alpha\beta}, \tag{B5a}$$

$$d_z=\int ez|\mathcal{U}_\alpha(\mathbf{r},z)|^2\frac{d^2\mathbf{r}dz}{L_xL_y}, \tag{B5b}$$

where $\mathcal{E}_z=-\partial_z\varphi$. The fact that d_z does not depend on α follows from the transformation properties of the Bloch functions under the σ_v, σ_v' reflections. The matrix element between states with $\mathbf{K}_\alpha\neq\mathbf{K}_\beta$ is small as $e^{-1/(pa)}$ and thus cannot be included in the regular expansion of the effective Hamiltonian in the parameter $pa\ll1$.

To describe the effect of an external magnetic field, we introduce the vector potential $\mathbf{A}(\mathbf{r},z)$ in the gauge $A_z=0$. The microscopic Hamiltonian is given by

$$\mathcal{H}^A=-\frac{e}{2c}[A_i(\mathbf{r},z)\hat{v}_i+\hat{v}_iA_i(\mathbf{r},z)]+\frac{e^2}{2mc^2}\mathbf{A}^2(\mathbf{r},z),$$

$$\hat{\mathbf{v}}\equiv\frac{-i\nabla}{m}. \tag{B6}$$

In the first order of the $\mathbf{k}\cdot\mathbf{p}$ perturbation theory we obtain

$$\begin{aligned}-\frac{e}{2c}\int\psi^*_\alpha(\mathbf{r})\mathcal{U}^*_\alpha(\mathbf{r},z)e^{-i\mathbf{K}_\alpha\mathbf{r}}[A_i(\mathbf{r},z)\hat{v}_i+\hat{v}_iA_i(\mathbf{r},z)]\\ \times e^{i\mathbf{K}_\beta\mathbf{r}}\mathcal{U}_\beta(\mathbf{r},z)\psi_\beta(\mathbf{r})d^2\mathbf{r}dz\\ =-\frac{e}{c}\langle\alpha|\hat{v}_i|\beta\rangle\int d^2\mathbf{r}\psi^*_\alpha(\mathbf{r})A_i(\mathbf{r},0)\psi_\beta(\mathbf{r})\\ -\frac{e}{2c}\delta_{\alpha\beta}\int d^2\mathbf{r}\psi^*_\alpha(\mathbf{r})[A_i(\mathbf{r},0)\hat{v}_i+\hat{v}_iA_i(\mathbf{r},0)]\psi_\beta(\mathbf{r})\\ -\frac{e}{c}\langle\alpha|z\hat{v}_i|\beta\rangle\int d^2\mathbf{r}\psi^*_\alpha(\mathbf{r})\frac{\partial A_i(\mathbf{r},0)}{\partial z}\psi_\beta(\mathbf{r}),\end{aligned} \tag{B7}$$

where we introduced the following notation for the matrix elements of an arbitrary operator $\mathcal{O}$ between the Bloch functions:

$$\langle\alpha|\mathcal{O}|\beta\rangle=\int e^{-i\mathbf{K}_\alpha\mathbf{r}}\mathcal{U}^*_\alpha(\mathbf{r},z)\mathcal{O}e^{i\mathbf{K}_\beta\mathbf{r}}\mathcal{U}_\beta(\mathbf{r},z)\frac{d^2\mathbf{r}dz}{L_xL_y}. \tag{B8}$$

We again encounter integrals of smooth functions with periodic ones, such as $\mathcal{U}^*_\alpha e^{-i\mathbf{K}_\alpha\mathbf{r}}\hat{v}_ie^{i\mathbf{K}_\beta\mathbf{r}}\mathcal{U}_\beta$, so the matrix elements are different from zero only if $\mathbf{K}_\alpha=\mathbf{K}_\beta$. Recalling that in the first order of the $\mathbf{k}\cdot\mathbf{p}$ perturbation theory the Dirac Hamiltonian is obtained as

$$[H_1(\mathbf{p})]_{\alpha\beta}=\langle\alpha|\hat{\mathbf{v}}|\beta\rangle\cdot\mathbf{p}=v\boldsymbol{\Sigma}_{\alpha\beta}\cdot\mathbf{p}, \tag{B9}$$

the first term on the right-hand side of Eq. (B7) can be identified with the gauge elongation $\mathbf{p}\to-i\nabla-(e/c)\mathbf{A}$ in the Dirac Hamiltonian [Eq. (28)].

In the second order of the $\mathbf{k}\cdot\mathbf{p}$ perturbation theory one has to include the contribution of remote bands $b\neq\alpha\ \forall\ \alpha=1,2,3,4$ with energies E_b taken at the points $\mathbf{K},\mathbf{K}'$. The correction to the Dirac Hamiltonian is then given by

$$[H_2(\mathbf{p})]_{\alpha\beta}=\frac{p^2}{2m}\delta_{\alpha\beta}+p_ip_j{\sum_b}'\frac{\langle\alpha|\hat{v}_i|b\rangle\langle b|\hat{v}_j|\beta\rangle+(i\leftrightarrow j)}{2E_b}. \tag{B10}$$

The gauge elongation $\mathbf{p}\to-i\nabla-(e/c)\mathbf{A}$ of the first term on the right-hand side corresponds to the second term on the right-hand side of Eq. (B7) and the $\mathbf{A}^2$ term of $\mathcal{H}^A$. The effective-mass tensor originating from remote bands in Eq. (B10) is symmetrized with respect to i, j in order to ensure the Hermiticity of the effective Hamiltonian upon the gauge elongation. Taking $\mathcal{H}^A$ in the first order (the contribution of the div $\mathbf{A}$ vanishes, as it is a smooth function) and $\mathbf{p}_i\hat{v}_i$ in the first order, we obtain the following contribution of the remote bands to the effective Hamiltonian:

$$-\frac{e}{c}{\sum_b}'\frac{\langle\alpha|\hat{v}_i|b\rangle\langle b|\hat{v}_j|\beta\rangle}{E_b}[A_i(\mathbf{r},0)m\hat{v}_j+m\hat{v}_iA_j(\mathbf{r},0)]. \tag{B11}$$

The ij-symmetric part of this expression corresponds to the gauge elongation of the last term in Eq. (B10), while the antisymmetric part can be rewritten as

$$\begin{aligned}-\frac{em}{2c}{\sum_b}'\frac{\langle\alpha|\hat{v}_i|b\rangle\langle b|\hat{v}_j|\beta\rangle-(i\leftrightarrow j)}{E_b}[A_i(\mathbf{r},0)\hat{v}_j+\hat{v}_iA_j(\mathbf{r},0)]\\ =\frac{ie}{4c}{\sum_b}'\frac{\langle\alpha|\hat{v}_i|b\rangle\langle b|\hat{v}_j|\beta\rangle-(i\leftrightarrow j)}{E_b}\left[\frac{\partial A_i(\mathbf{r},0)}{\partial x_j}-\frac{\partial A_j(\mathbf{r},0)}{\partial x_i}\right].\end{aligned} \tag{B12}$$

The expression in the square brackets is an antisymmetric tensor whose xy and yx components are equal to $\mathcal{B}_z$ and $-\mathcal{B}_z$, respectively. Thus, this term corresponds to $-\mu_z\mathcal{B}_z\tilde{\Sigma}_z$ term in Eq. (29).

Since $\mathcal{B}_x=-\partial A_y/\partial z$, $\mathcal{B}_y=\partial A_x/\partial z$, the last term in Eq. (B7) corresponds to the $\mu_{xy}(\mathcal{B}_x\Sigma_y-\mathcal{B}_y\Sigma_x)$ term in Eq. (29). Using the facts that (i) $\langle\alpha|z|\beta\rangle=(d_z/e)\delta_{\alpha\beta}$, (ii) $z\hat{v}_i=\hat{v}_iz$, and (iii) $\langle\alpha|z|b\rangle=(i/2E_b)\langle\alpha|\hat{v}_z|b\rangle$ (the latter follows from the com-

mutation relation $[\mathcal{H},z]=-(i/2)\hat{v}_z$, valid in the absence of the field), we can write

$$\langle\alpha|z\hat{v}_i|\beta\rangle = \frac{d_z}{e}\langle\alpha|\hat{v}_i|\beta\rangle + \frac{i}{2}\sum_b{}' \frac{\langle\alpha|\hat{v}_z|b\rangle\langle b|\hat{v}_i|\beta\rangle}{E_b}$$

$$= \frac{d_z}{e}\langle\alpha|\hat{v}_i|\beta\rangle - \frac{i}{2}\sum_b{}' \frac{\langle\alpha|\hat{v}_i|b\rangle\langle b|\hat{v}_z|\beta\rangle}{E_b}. \quad \text{(B13)}$$

The contribution of the $(d_z/e)\langle\alpha|\hat{v}_i|\beta\rangle$ term to the effective Hamiltonian has the form $-d_z(v\Sigma_x\mathcal{B}_y - v\Sigma_y\mathcal{B}_x)$ and may be viewed as the Lorentz force contribution to the $-d_z\mathcal{E}_z$ term.

APPENDIX C: KINETIC EQUATION

Kinetic equation is the most natural way to describe the dynamics when real quasiparticles (electrons and holes) move along quasiclassical trajectories, and interference between different trajectories is suppressed. Since electrons and holes are created in pairs, the kinetic equation should be written for the joint distribution function $f_{\mathbf{p}_e,\mathbf{p}_h}(\mathbf{r}_e,\mathbf{r}_h;t)$—the joint probability for the electron to be in the elementary volume of phase space $d^2\mathbf{r}_e d^2\mathbf{p}_e/(2\pi)^2$ around $\mathbf{r}_e,\mathbf{p}_e$ and for the hole in the elementary volume $d^2\mathbf{r}_h d^2\mathbf{p}_h/(2\pi)^2$ around $\mathbf{r}_h,\mathbf{p}_h$. We write the kinetic equation as

$$\frac{\partial f}{\partial t} + \frac{\partial\,\mathrm{Re}\,\xi_{\mathbf{p}_e}}{\partial\mathbf{p}_e}\frac{\partial f}{\partial\mathbf{r}_e} + \frac{\partial\,\mathrm{Re}\,\bar{\xi}_{-\mathbf{p}_h}}{\partial\mathbf{p}_h}\frac{\partial f}{\partial\mathbf{r}_h} = \mathrm{St}^{e,out}_{\mathbf{p}_e,\mathbf{p}_h} f + \mathrm{St}^{e,in}_{\mathbf{p}_e,\mathbf{p}_h} f + \mathrm{St}^{h,out}_{\mathbf{p}_e,\mathbf{p}_h} f + \mathrm{St}^{h,in}_{\mathbf{p}_e,\mathbf{p}_h} f, \quad \text{(C1a)}$$

$$\mathrm{St}^{e,out}_{\mathbf{p}_e,\mathbf{p}_h} f = -2\pi\int\frac{d^2\mathbf{q}}{(2\pi)^2}\frac{F_K^2}{M\omega_\mathbf{q}}\frac{\sqrt{27a^2}}{4}\sin^2\frac{\varphi_{\mathbf{p}_e}-\varphi_{\mathbf{p}_e-\mathbf{q}}}{2} \times\delta(\mathrm{Re}\,\xi_{\mathbf{p}_e}-\mathrm{Re}\,\xi_{\mathbf{p}_e-\mathbf{q}}-\omega_\mathbf{q})f_{\mathbf{p}_e,\mathbf{p}_h}, \quad \text{(C1b)}$$

$$\mathrm{St}^{e,in}_{\mathbf{p}_e,\mathbf{p}_h} f = 2\pi\int\frac{d^2\mathbf{q}}{(2\pi)^2}\frac{F_K^2}{M\omega_\mathbf{q}}\frac{\sqrt{27a^2}}{4}\sin^2\frac{\varphi_{\mathbf{p}_e+\mathbf{q}}-\varphi_{\mathbf{p}_e}}{2} \times\delta(\mathrm{Re}\,\xi_{\mathbf{p}_e+\mathbf{q}}-\mathrm{Re}\,\xi_{\mathbf{p}_e}-\omega_\mathbf{q})f_{\mathbf{p}_e+\mathbf{q},\mathbf{p}_h}, \quad \text{(C1c)}$$

$$\mathrm{St}^{h,out}_{\mathbf{p}_e,\mathbf{p}_h} f = -2\pi\int\frac{d^2\mathbf{q}}{(2\pi)^2}\frac{F_K^2}{M\omega_\mathbf{q}}\frac{\sqrt{27a^2}}{4}\sin^2\frac{\varphi_{-\mathbf{p}_h}-\varphi_{-\mathbf{p}_h+\mathbf{q}}}{2} \times\delta(\mathrm{Re}\,\bar{\xi}_{-\mathbf{p}_h}-\mathrm{Re}\,\bar{\xi}_{-\mathbf{p}_h+\mathbf{q}}-\omega_\mathbf{q})f_{\mathbf{p}_e,\mathbf{p}_h}, \quad \text{(C1d)}$$

$$\mathrm{St}^{h,in}_{\mathbf{p}_e,\mathbf{p}_h} f = 2\pi\int\frac{d^2\mathbf{q}}{(2\pi)^2}\frac{F_K^2}{M\omega_\mathbf{q}}\frac{\sqrt{27a^2}}{4}\sin^2\frac{\varphi_{-\mathbf{p}_h-\mathbf{q}}-\varphi_{-\mathbf{p}_h}}{2} \times\delta(\mathrm{Re}\,\bar{\xi}_{-\mathbf{p}_h-\mathbf{q}}-\mathrm{Re}\,\bar{\xi}_{-\mathbf{p}_h}-\omega_\mathbf{q})f_{\mathbf{p}_e,\mathbf{p}_h+\mathbf{q}}. \quad \text{(C1e)}$$

The left-hand side of the kinetic equation (Liouville operator acting on the distribution function) represents the free propagation of the electron and the hole with the corresponding (group) velocities $\mathbf{v}_e=\partial\,\mathrm{Re}\,\xi_{\mathbf{p}_e}/\partial\mathbf{p}_e$ and $\mathbf{v}_h=\partial\,\mathrm{Re}\,\bar{\xi}_{-\mathbf{p}_h}/\partial\mathbf{p}_h$. The right-hand side (collision integral) describes emission of phonons; assuming to be in the linear regime, we have neglected the Fermi statistics of electrons and holes. In what follows, we will write the out-scattering part of the collision integral as $-2(\gamma_{\mathbf{p}_e}+\bar{\gamma}_{-\mathbf{p}_h})f_{\mathbf{p}_e,\mathbf{p}_h}$ and include it in the Liouville operator. In the scattering rates $2\gamma_{\mathbf{p}_e}, 2\bar{\gamma}_{-\mathbf{p}_h}$ we also include those for emission of electron-hole pairs or other excitations with broad spectrum; the contribution of such processes to the in-scattering part of the collision integral is neglected (see discussion in Sec. I A).

The Raman signal is treated as a weak probe not affecting the electron and hole population and thus is not included into the kinetic equation. It is determined by the radiative recombination rate and can be calculated from the Fermi's golden rule. The probability of emission of a photon with a given polarization $\mathbf{e}_{out}$ per unit solid angle, per unit frequency interval, and *per unit time* is expressed in terms of the joint distribution function as

$$\frac{4\pi dI}{do_{out}d\omega_{out}dt} = 2\pi\left(\frac{ev}{c}\right)^2\frac{2\pi c^2}{\omega_{out}}\frac{\omega_{out}^2}{2\pi^2c^3}\int d^2\mathbf{r}\frac{d^2\mathbf{p}}{(2\pi)^2} \times\delta(\omega_{out}-\mathrm{Re}\,\xi_\mathbf{p}-\mathrm{Re}\,\bar{\xi}_\mathbf{p}) \times|[\mathbf{e}_{out}\times\mathbf{e}_\mathbf{p}]_z|^2 f_{\mathbf{p},-\mathbf{p}}(\mathbf{r},\mathbf{r}). \quad \text{(C2)}$$

The easiest way to arrive at this expression is to calculate the electronic radiative self-energy,

$$\Sigma^{\mathrm{rad}}(\mathbf{p},\epsilon) = i\left(\frac{ev}{c}\right)^2\int\frac{d^3\mathbf{Q}}{(2\pi)^3}\frac{d\Omega}{2\pi}\frac{2\pi c^2}{cQ}\frac{2cQ}{\Omega^2-(cQ-io)^2} \times(\mathbf{e}_{out}\cdot\boldsymbol{\Sigma})\frac{\epsilon-\Omega+v\mathbf{p}\cdot\boldsymbol{\Sigma}}{(\epsilon-\Omega+io)^2-(vp)^2}(\mathbf{e}_{out}^*\cdot\boldsymbol{\Sigma}). \quad \text{(C3)}$$

Note that the imaginary shift of the poles in the electron Green's function is different from prescription (31). Indeed, the latter corresponds to the full valence band and empty conduction band, while radiative recombination requires the valence band to be empty, hence the shift of both poles to the lower half-plane of ϵ in Eq. (C3).

The kinetic equation [Eqs. (C1a)–(C1e)] contains no term corresponding to the generation of electron-hole pairs by incoming photons. Instead, we prefer to choose the initial condition at $t=0$, which would correspond to the electron-hole population upon arrival of a short pulse of the electromagnetic field of the total energy ω_{in}, i.e., containing a single photon,

$$f_{\mathbf{p}_e,\mathbf{p}_h}(\mathbf{r}_e,\mathbf{r}_h;t=0) = \frac{\pi e^2}{c}2|[\mathbf{e}_{in}\times\mathbf{e}_{\mathbf{p}_e}]_z|^2\frac{\delta(\mathbf{r}_e-\mathbf{r}_h)}{L_xL_y}\frac{8\pi v^2}{\omega_{in}} \times\delta(\mathrm{Re}\,\xi_{\mathbf{p}_e}+\mathrm{Re}\,\bar{\xi}_{-\mathbf{p}_h}-\omega_{in})(2\pi)^2\delta(\mathbf{p}_e+\mathbf{p}_h). \quad \text{(C4)}$$

The last δ function takes care of momentum conservation during photon absorption; since the photon momentum is very small, the electron and the hole must have opposite momenta. The energy δ function ensures that the total energy of the electron-hole pair is equal to the energy of the

absorbed photon; the coefficient in front of it is just the inverse density of states of electron-hole pairs with zero total momentum, necessary to preserve the normalization of $f_{\mathbf{p}_e,\mathbf{p}_h}(\mathbf{r}_e,\mathbf{r}_h)$. The factor $\delta(\mathbf{r}_e-\mathbf{r}_h)/(L_xL_y)$ reflects the fact that the electron and the hole are born at the same spatial point, which can be located anywhere in the sample. The angular factor $2|[\mathbf{e}_{in}\times\mathbf{e}_\mathbf{p}]_z|^2$ shows that the transition dipole is perpendicular to the electron momentum, and the factor of 2 fixes the average to unity. As a result, the integral of $f_{\mathbf{p}_e,\mathbf{p}_h}(\mathbf{r}_e,\mathbf{r}_h)$ over the whole phase space equals $\pi e^2/c$, which is nothing else but the total probability for the incident photon to be absorbed; all subsequent factors, discussed above, represent the partitioning of this probability over different states of the electron-hole pairs. The total probability can be found directly from the Fermi's golden rule, and is given by

$$\frac{L_z}{c}4\sum_{\mathbf{p}}\left|\frac{ev}{c}\sqrt{\frac{2\pi c^2}{V\omega_{in}}}\right|^2 2\pi\delta(\mathrm{Re}\,\xi_\mathbf{p}+\mathrm{Re}\,\bar{\xi}_\mathbf{p}-\omega_{in}),$$

where the factor of 4 keeps track of the valley and spin degeneracy and L_z/c is the attempt period.

Solution of the kinetic equations [Eqs. (C1a)–(C1e)], corresponding to emission of n phonons, is obtained by n iterations of the collision integral. First of all, we find the inverse of the Liouville operator, acting on a source $J_{\mathbf{p}_e,\mathbf{p}_h}(\mathbf{r}_e,\mathbf{r}_h;t)$,

$$\left[\frac{\partial}{\partial t}+2(\gamma_e+\gamma_h)+\mathbf{v}_e\frac{\partial}{\partial\mathbf{r}_e}+\mathbf{v}_h\frac{\partial}{\partial\mathbf{r}_h}\right]^{-1}J_{\mathbf{p}_e,\mathbf{p}_h}(\mathbf{r}_e,\mathbf{r}_h;t)$$
$$=\int_{-\infty}^{t}dt'J_{\mathbf{p}_e,\mathbf{p}_h}[\mathbf{r}_e-\mathbf{v}_e(t-t'),\mathbf{r}_h-\mathbf{v}_h(t-t');t']e^{-2(\gamma_e+\gamma_h)(t-t')}. \quad \text{(C5)}$$

Let us follow evolution of a single electron-hole pair, created at $t=0$ at the point $\mathbf{r}=0$ [evolution of initial condition (C4) can be obtained by a simple convolution]. The zero-approximation distribution function is given by

$$f^{(0)}_{\mathbf{p}_e,\mathbf{p}_h}(\mathbf{r}_e,\mathbf{r}_h;t)=(2\pi)^2\delta(\mathbf{p}_e-\mathbf{p}_0)(2\pi)^2\delta(\mathbf{p}_h+\mathbf{p}_0)\times\delta(\mathbf{r}_e-\mathbf{v}_et)\delta(\mathbf{r}_h-\mathbf{v}_ht)e^{-2\gamma_{\mathbf{p}_0}t-2\bar{\gamma}_{\mathbf{p}_0}t}. \quad \text{(C6)}$$

After one iteration of the in-scattering part of the collision integral we obtain the first-approximation correction—the contribution from electrons and holes which have emitted one phonon,

$$f^{(1)}_{\mathbf{p}_e,\mathbf{p}_h}(\mathbf{r}_e,\mathbf{r}_h;t)=f^{(e)}_{\mathbf{p}_e,\mathbf{p}_h}(\mathbf{r}_e,\mathbf{r}_h;t)+f^{(h)}_{\mathbf{p}_e,\mathbf{p}_h}(\mathbf{r}_e,\mathbf{r}_h;t), \quad \text{(C7a)}$$

$$f^{(e)}_{\mathbf{p}_e,\mathbf{p}_h}(\mathbf{r}_e,\mathbf{r}_h;t)=(2\pi)^d\delta(\mathbf{p}_h+\mathbf{p}_0)\delta(\mathbf{r}_h+\bar{\mathbf{v}}_0t)e^{-2\bar{\gamma}_{\mathbf{p}_0}t}\times\frac{2\pi F_K^2}{M\omega_{\mathbf{p}_0-\mathbf{p}_e}}\frac{\sqrt{27a^2}}{4}\sin^2\frac{\varphi_{\mathbf{p}_0}-\varphi_{\mathbf{p}_e}}{2}\times\delta(\mathrm{Re}\,\xi_{\mathbf{p}_0}-\mathrm{Re}\,\xi_{\mathbf{p}_e}-\omega_{\mathbf{p}_0-\mathbf{p}_e})\times\int_0^t dt_0\delta[\mathbf{r}_e-\mathbf{v}_e(t-t_0)-\mathbf{v}_0t_0]\times e^{-2\gamma_{\mathbf{p}_e}(t-t_0)-2\gamma_{\mathbf{p}_0}t_0}, \quad \text{(C7b)}$$

$$f^{(h)}_{\mathbf{p}_e,\mathbf{p}_h}(\mathbf{r}_e,\mathbf{r}_h;t)=(2\pi)^d\delta(\mathbf{p}_e-\mathbf{p}_0)\delta(\mathbf{r}_e-\mathbf{v}_0t)e^{-2\gamma_{\mathbf{p}_0}t}\times\frac{2\pi F_K^2}{M\omega_{\mathbf{p}_0-\mathbf{p}_e}}\frac{\sqrt{27a^2}}{4}\sin^2\frac{\varphi_{\mathbf{p}_0}-\varphi_{-\mathbf{p}_h}}{2}\times\delta(\mathrm{Re}\,\bar{\xi}_{\mathbf{p}_0}-\mathrm{Re}\,\bar{\xi}_{-\mathbf{p}_h}-\omega_{-\mathbf{p}_0-\mathbf{p}_h})\times\int_0^t d\bar{t}_0\delta[\mathbf{r}_h-\mathbf{v}_h(t-\bar{t}_0)+\bar{\mathbf{v}}_0\bar{t}_0]\times e^{-2\bar{\gamma}_{-\mathbf{p}_h}(t-\bar{t}_0)-2\bar{\gamma}_{\mathbf{p}_0}\bar{t}_0}. \quad \text{(C7c)}$$

After the second iteration we have[61]

$$f^{(2)}_{\mathbf{p}_e,\mathbf{p}_h}(\mathbf{r}_e,\mathbf{r}_h;t)=f^{(ee)}_{\mathbf{p}_e,\mathbf{p}_h}(\mathbf{r}_e,\mathbf{r}_h;t)+f^{(eh)}_{\mathbf{p}_e,\mathbf{p}_h}(\mathbf{r}_e,\mathbf{r}_h;t)+f^{(hh)}_{\mathbf{p}_e,\mathbf{p}_h}(\mathbf{r}_e,\mathbf{r}_h;t), \quad \text{(C8a)}$$

$$f^{(ee)}_{\mathbf{p}_e,\mathbf{p}_h}(\mathbf{r}_e,\mathbf{r}_h;t)=(2\pi)^d\delta(\mathbf{p}_h+\mathbf{p}_0)\delta(\mathbf{r}_h+\bar{\mathbf{v}}_0t)e^{-2\bar{\gamma}_{\mathbf{p}_0}t}\int\frac{d^2\mathbf{p}_1}{(2\pi)^2}\frac{2\pi F_K^2}{M\omega_{\mathbf{p}_0-\mathbf{p}_1}}\frac{\sqrt{27a^2}}{4}\sin^2\frac{\varphi_{\mathbf{p}_0}-\varphi_{\mathbf{p}_1}}{2}\delta(\mathrm{Re}\,\xi_{\mathbf{p}_0}-\mathrm{Re}\,\xi_{\mathbf{p}_1}-\omega_{\mathbf{p}_0-\mathbf{p}_1})\times\frac{2\pi F_K^2}{M\omega_{\mathbf{p}_1-\mathbf{p}_e}}\frac{\sqrt{27a^2}}{4}\sin^2\frac{\varphi_{\mathbf{p}_1}-\varphi_{\mathbf{p}_e}}{2}\delta(\mathrm{Re}\,\xi_{\mathbf{p}_1}-\mathrm{Re}\,\xi_{\mathbf{p}_e}-\omega_{\mathbf{p}_1-\mathbf{p}_e})\times\int_0^t dt_1\int_0^{t_1}dt_0\delta[\mathbf{r}_e-\mathbf{v}_e(t-t_1)-\mathbf{v}_1(t_1-t_0)-\mathbf{v}_0t_0]e^{-2\gamma_{\mathbf{p}_e}(t-t_1)-2\gamma_{\mathbf{p}_1}(t_1-t_0)-2\gamma_{\mathbf{p}_0}t_0}, \quad \text{(C8b)}$$

$$f^{(eh)}_{\mathbf{p}_e,\mathbf{p}_h}(\mathbf{r}_e,\mathbf{r}_h;t)=\frac{2\pi F_K^2}{M\omega_{\mathbf{p}_0-\mathbf{p}_e}}\frac{\sqrt{27a^2}}{4}\sin^2\frac{\varphi_{\mathbf{p}_0}-\varphi_{\mathbf{p}_e}}{2}\delta(\mathrm{Re}\,\xi_{\mathbf{p}_0}-\mathrm{Re}\,\xi_{\mathbf{p}_e}-\omega_{\mathbf{p}_0-\mathbf{p}_e})\int_0^t dt_0\delta[\mathbf{r}_e-\mathbf{v}_e(t-t_0)-\mathbf{v}_0t_0]$$
$$\times e^{-2\gamma_{\mathbf{p}_e}(t-t_0)-2\gamma_{\mathbf{p}_0}t_0}\frac{2\pi F_K^2}{M\omega_{\mathbf{p}_0-\mathbf{p}_e}}\frac{\sqrt{27a^2}}{4}\sin^2\frac{\varphi_{\mathbf{p}_0}-\varphi_{-\mathbf{p}_h}}{2}\delta(\mathrm{Re}\,\bar{\xi}_{\mathbf{p}_0}-\mathrm{Re}\,\bar{\xi}_{-\mathbf{p}_h}-\omega_{-\mathbf{p}_0-\mathbf{p}_h})$$
$$\times\int_0^t d\bar{t}_0\delta[\mathbf{r}_h-\mathbf{v}_h(t-\bar{t}_0)+\bar{\mathbf{v}}_0\bar{t}_0]e^{-2\bar{\gamma}_{-\mathbf{p}_h}(t-\bar{t}_0)-2\bar{\gamma}_{\mathbf{p}_0}\bar{t}_0}, \tag{C8c}$$

$$f^{(hh)}_{\mathbf{p}_e,\mathbf{p}_h}(\mathbf{r}_e,\mathbf{r}_h;t)=(2\pi)^d\delta(\mathbf{p}_e-\mathbf{p}_0)\delta(\mathbf{r}_e-\mathbf{v}_0t)e^{-2\gamma_{\mathbf{p}_0}t}\int\frac{d^2\bar{\mathbf{p}}_1}{(2\pi)^2}\frac{2\pi F_K^2}{M\omega_{\mathbf{p}_0-\mathbf{p}_1}}\frac{\sqrt{27a^2}}{4}\sin^2\frac{\varphi_{\mathbf{p}_0}-\varphi_{\bar{\mathbf{p}}_1}}{2}\delta(\mathrm{Re}\,\bar{\xi}_{\mathbf{p}_0}-\mathrm{Re}\,\bar{\xi}_{\bar{\mathbf{p}}_1}-\omega_{-\mathbf{p}_0+\bar{\mathbf{p}}_1})$$
$$\times\frac{2\pi F_K^2}{M\omega_{-\bar{\mathbf{p}}_1-\mathbf{p}_h}}\frac{\sqrt{27a^2}}{4}\sin^2\frac{\varphi_{\bar{\mathbf{p}}_1}-\varphi_{-\mathbf{p}_h}}{2}\delta(\mathrm{Re}\,\bar{\xi}_{\bar{\mathbf{p}}_1}-\mathrm{Re}\,\bar{\xi}_{-\mathbf{p}_h}-\omega_{-\bar{\mathbf{p}}_1-\mathbf{p}_h})\int_0^t d\bar{t}_1\int_0^{\bar{t}_1}d\bar{t}_0$$
$$\times\delta[\mathbf{r}_h-\mathbf{v}_h(t-\bar{t}_1)+\bar{\mathbf{v}}_1(\bar{t}_1-\bar{t}_0)+\bar{\mathbf{v}}_0\bar{t}_0]e^{-2\bar{\gamma}_{-\mathbf{p}_h}(t-\bar{t}_1)-2\bar{\gamma}_{\bar{\mathbf{p}}_1}(\bar{t}_1-\bar{t}_0)-2\bar{\gamma}_{\mathbf{p}_0}\bar{t}_0}. \tag{C8d}$$

After four iterations we have $f^{(4)}=f^{(eeee)}+f^{(eeeh)}+f^{(eehh)}+f^{(ehhh)}+f^{(hhhh)}$. The term contributing to the four-phonon Raman signal is given by

$$f^{(eehh)}_{\mathbf{p}_e,\mathbf{p}_h}(\mathbf{r}_e,\mathbf{r}_h;t)=\int\frac{d^2\mathbf{p}_1}{(2\pi)^2}\frac{2\pi F_K^2}{M\omega_{\mathbf{p}_0-\mathbf{p}_1}}\frac{\sqrt{27a^2}}{4}\sin^2\frac{\varphi_{\mathbf{p}_0}-\varphi_{\mathbf{p}_1}}{2}\delta(\mathrm{Re}\,\xi_{\mathbf{p}_0}-\mathrm{Re}\,\xi_{\mathbf{p}_1}-\omega_{\mathbf{p}_0-\mathbf{p}_1})\frac{2\pi F_K^2}{M\omega_{\mathbf{p}_1-\mathbf{p}_e}}\frac{\sqrt{27a^2}}{4}\sin^2\frac{\varphi_{\mathbf{p}_1}-\varphi_{\mathbf{p}_e}}{2}$$
$$\times\delta(\mathrm{Re}\,\xi_{\mathbf{p}_1}-\mathrm{Re}\,\xi_{\mathbf{p}_e}-\omega_{\mathbf{p}_1-\mathbf{p}_e})\int_0^t dt_1\int_0^{t_1}dt_0\delta[\mathbf{r}_e-\mathbf{v}_e(t-t_1)-\mathbf{v}_1(t_1-t_0)-\mathbf{v}_0t_0]e^{-2\gamma_{\mathbf{p}_e}(t-t_1)-2\gamma_{\mathbf{p}_1}(t_1-t_0)-2\gamma_{\mathbf{p}_0}t_0}$$
$$\times\int\frac{d^2\bar{\mathbf{p}}_1}{(2\pi)^2}\frac{2\pi F_K^2}{M\omega_{\mathbf{p}_0-\mathbf{p}_1}}\frac{\sqrt{27a^2}}{4}\sin^2\frac{\varphi_{\mathbf{p}_0}-\varphi_{\bar{\mathbf{p}}_1}}{2}\delta(\mathrm{Re}\,\bar{\xi}_{\mathbf{p}_0}-\mathrm{Re}\,\bar{\xi}_{\bar{\mathbf{p}}_1}-\omega_{-\mathbf{p}_0+\bar{\mathbf{p}}_1})$$
$$\times\frac{2\pi F_K^2}{M\omega_{-\bar{\mathbf{p}}_1-\mathbf{p}_h}}\frac{\sqrt{27a^2}}{4}\sin^2\frac{\varphi_{\bar{\mathbf{p}}_1}-\varphi_{-\mathbf{p}_h}}{2}\delta(\mathrm{Re}\,\bar{\xi}_{\bar{\mathbf{p}}_1}-\mathrm{Re}\,\bar{\xi}_{-\mathbf{p}_h}-\omega_{-\bar{\mathbf{p}}_1-\mathbf{p}_h})$$
$$\times\int_0^t d\bar{t}_1\int_0^{\bar{t}_1}d\bar{t}_0\delta[\mathbf{r}_h-\mathbf{v}_h(t-\bar{t}_1)+\bar{\mathbf{v}}_1(\bar{t}_1-\bar{t}_0)+\bar{\mathbf{v}}_0\bar{t}_0]e^{-2\bar{\gamma}_{-\mathbf{p}_h}(t-\bar{t}_1)-2\bar{\gamma}_{\bar{\mathbf{p}}_1}(\bar{t}_1-\bar{t}_0)-2\bar{\gamma}_{\mathbf{p}_0}\bar{t}_0}. \tag{C9}$$

In terms of this correction, the Raman-scattering probability can be expressed as

$$4\pi\frac{dI_{4K}}{do_{out}}=2\pi\left(\frac{ev}{c}\right)^2\frac{2\pi c^2}{\omega_{out}}\frac{\omega_{out}^2}{2\pi^2c^3}\frac{2\pi e^2}{c}\frac{8\pi v^2}{\omega_{in}}$$
$$\times\int d^2\mathbf{r}\frac{d^2\mathbf{p}_0}{(2\pi)^2}\frac{d^2\mathbf{p}_2}{(2\pi)^2}|[\mathbf{e}_{in}\times\mathbf{e}_{\mathbf{p}_0}]_z|^2|[\mathbf{e}_{out}\times\mathbf{e}_{\mathbf{p}_2}]_z|^2\delta(\mathrm{Re}\,\xi_{\mathbf{p}_0}+\mathrm{Re}\,\bar{\xi}_{\mathbf{p}_0}-\omega_{in})f^{(eehh)}_{\mathbf{p}_2,-\mathbf{p}_2}(\mathbf{r},\mathbf{r}). \tag{C10}$$

Let us change time integration variables according to

$$\int_0^\infty dt\left[\int_0^t dt_1\int_0^{t_1}dt_0\mathcal{F}(t-t_1,t_1-t_0,t_0)\right]\left[\int_0^t d\bar{t}_1\int_0^{\bar{t}_1}d\bar{t}_0\bar{\mathcal{F}}(t-\bar{t}_1,\bar{t}_1-\bar{t}_0,\bar{t}_0)\right]$$
$$=\int_0^\infty dt_0dt_1dt_2d\bar{t}_0d\bar{t}_1d\bar{t}_2\delta(t_0+t_1+t_2-\bar{t}_0-\bar{t}_1-\bar{t}_2)\mathcal{F}(t_2,t_1,t_0)\bar{\mathcal{F}}(\bar{t}_2,\bar{t}_1,\bar{t}_0) \tag{C11}$$

and evaluate the time integral, following Sec. VII C. We obtain

$$\frac{1}{2|[\mathbf{v}_0\times\mathbf{v}_2]_z|}\int_0^\infty dt_1d\bar{t}_1e^{-2\gamma_xt_1-2\gamma_y\bar{t}_1}\int_{\mathcal{O}}dt_0=\frac{1}{|[\mathbf{v}_0\times\mathbf{v}_2]_z|}\int_0^{\pi/2}d\phi\frac{\zeta_{max}(\phi)-\zeta_{min}(\phi)}{8[\gamma_x\cos\phi+\gamma_y\sin\phi]^3}. \tag{C12}$$

Rearranging the energy δ functions and we arrive at

$$4\pi\frac{dI_{4K}}{do_{out}} = 16\pi^2\left(\frac{e}{c}\right)^4\left(\frac{\lambda_K}{2\pi}\right)^4 v^8 \int d^2\mathbf{p}_0 d^2\mathbf{p}_1 d^2\bar{\mathbf{p}}_1 d^2\mathbf{p}_2 |[\mathbf{v}_0\times\mathbf{e}_{in}]_z|^2 |[\mathbf{v}_2\times\mathbf{e}_{out}]_z|^2 \sin^2\frac{\varphi_0-\varphi_1}{2}\sin^2\frac{\varphi_1-\varphi_2}{2}\sin^2\frac{\varphi_0-\bar{\varphi}_1}{2}$$
$$\times\sin^2\frac{\bar{\varphi}_1-\varphi_2}{2} 2\delta(\mathrm{Re}\,\xi_{\mathbf{p}_0}+\mathrm{Re}\,\bar{\xi}_{\mathbf{p}_0}-\omega_{in})\delta(\mathrm{Re}\,\xi_{\mathbf{p}_1}-\mathrm{Re}\,\xi_{\mathbf{p}_0}+\omega_{\mathbf{p}_0-\mathbf{p}_1})\delta(\mathrm{Re}\,\bar{\xi}_{\bar{\mathbf{p}}_1}-\mathrm{Re}\,\bar{\xi}_{\mathbf{p}_0}+\omega_{-\mathbf{p}_0+\bar{\mathbf{p}}_1})$$
$$\times 2\delta(\mathrm{Re}\,\xi_{\mathbf{p}_2}+\mathrm{Re}\,\bar{\xi}_{\mathbf{p}_2}-\omega_{in}+\omega_{\mathbf{p}_0-\mathbf{p}_1}+\omega_{\mathbf{p}_1-\mathbf{p}_2}+\omega_{-\mathbf{p}_0+\bar{\mathbf{p}}_1}+\omega_{-\bar{\mathbf{p}}_1+\mathbf{p}_2})\delta(\mathrm{Re}\,\xi_{\mathbf{p}_2}-\mathrm{Re}\,\bar{\xi}_{\mathbf{p}_2}-\mathrm{Re}\,\xi_{\mathbf{p}_0}+\mathrm{Re}\,\bar{\xi}_{\mathbf{p}_0}+\omega_{\mathbf{p}_0-\mathbf{p}_1}$$
$$+\omega_{\mathbf{p}_1-\mathbf{p}_2}-\omega_{-\mathbf{p}_0+\bar{\mathbf{p}}_1}-\omega_{-\bar{\mathbf{p}}_1+\mathbf{p}_2})\frac{1}{|[\mathbf{v}_0\times\mathbf{v}_2]_z|}\int_0^{\pi/2} d\phi\frac{\zeta_{max}(\phi)-\zeta_{min}(\phi)}{8[\gamma_x\cos\phi+\gamma_y\sin\phi]^3}. \tag{C13}$$

The first four δ functions constrain the electronic momenta to lie on the resonant manifold (Fig. 16). The argument of the fifth δ function is nothing but Δ, defined in Eq. (86b). For $\omega_{\mathbf{q}}=\omega_0$ this δ function equals either ∞ in electron-hole symmetric case or 0 in the electron-hole asymmetric case. Thus, Eq. (C13) makes sense only for dispersive phonons. In this case it gives the probability four times smaller than that given by Eqs. (93) and (105). One factor of 2 is due to the constructive interference of the amplitudes for the two spin projections: the spin degeneracy multiplies the *matrix element* obtained by tracing in the electron loop. The other factor of 2 is due to the constructive interference of two-time-reversed processes, described in the end of Sec. VII A, which may also be viewed as the interference of the processes in the two valleys.

APPENDIX D: LOGARITHMIC TERMS IN SELF-ENERGY AND VERTEX CORRECTIONS

The RPA-dressed Coulomb propagator (122) determines the electron self-energy,

$$\Sigma^{ee}(\mathbf{p},\epsilon) = i\int\frac{d\omega}{2\pi}\frac{d^2\mathbf{q}}{(2\pi)^2}V(\mathbf{q},\omega)G(\mathbf{p}-\mathbf{q},\epsilon-\omega) = -\int\frac{d\varpi}{2\pi}\frac{d^2\mathbf{q}}{(2\pi)^2}V(\mathbf{q},i\varpi)G(\mathbf{p}-\mathbf{q},\epsilon-i\varpi)$$
$$\approx\frac{16g}{\mathcal{N}}\int\frac{d\varpi}{2\pi}\frac{d^2(v\mathbf{q})}{(2\pi)^2}\frac{1}{vq}\frac{\sqrt{(vq)^2+\varpi^2}}{gvq+\sqrt{(vq)^2+\varpi^2}}\left[-\frac{i\varpi+v\mathbf{q}\boldsymbol{\Sigma}}{\varpi^2+(vq)^2}+\frac{\epsilon+v\mathbf{p}\boldsymbol{\Sigma}}{\varpi^2+(vq)^2}+\frac{2(i\epsilon\varpi-v\mathbf{pq})(i\varpi+v\mathbf{q}\boldsymbol{\Sigma})}{[\varpi^2+(vq)^2]^2}\right]$$
$$=\frac{4g}{\pi^2\mathcal{N}}\int_{\xi_{min}}^{\xi_{max}}d\xi\int_{-\infty}^{\infty}d\varpi\frac{\sqrt{\xi^2+\varpi^2}}{g\xi+\sqrt{\xi^2+\varpi^2}}\left[\frac{\xi^2-\varpi^2}{(\varpi^2+\xi^2)^2}\epsilon+\frac{\varpi^2}{(\varpi^2+\xi^2)^2}v\mathbf{p}\boldsymbol{\Sigma}\right]$$
$$\approx\frac{8}{\pi^2\mathcal{N}}\left(\ln\frac{\xi_{max}}{\xi_{min}}\right)\int_0^{\pi}d\varphi\left[(-\epsilon+v\mathbf{p}\boldsymbol{\Sigma})\frac{g}{2(1+g\sin\varphi)}+(2\epsilon-v\mathbf{p}\boldsymbol{\Sigma})\frac{g\sin^2\varphi}{2(1+g\sin\varphi)}\right]$$
$$=\frac{8}{\pi^2\mathcal{N}}\left(\ln\frac{\xi_{max}}{\xi_{min}}\right)\left[(-\epsilon+v\mathbf{p}\boldsymbol{\Sigma})\frac{g\arccos g}{\sqrt{1-g^2}}+(2\epsilon-v\mathbf{p}\boldsymbol{\Sigma})\left(1-\frac{\pi}{2g}+\frac{\arccos g}{g\sqrt{1-g^2}}\right)\right]. \tag{D1}$$

In the first line we have performed the Wick rotation $\omega=i\varpi$ (corresponding to the Matsubara representation for zero temperature). In the second line we have expanded $G(\mathbf{p}-\mathbf{q},\epsilon-i\varpi)$ to the first order in ϵ and $v\mathbf{p}$, since the integral is dominated by $\varpi\sim vq\gg\epsilon, vp$. In the third line we have integrated over the directions of $\mathbf{q}$. In the fourth line we have replaced the integration region with the momentum cutoff $\xi_{min}<vq<\xi_{max}$, $-\infty<\varpi<\infty$ by the region $\xi_{min}<\sqrt{(vq)^2+\varpi^2}<\xi_{max}$, which does not change the leading logarithmic asymptotics. The lower cutoff $\xi_{min}\sim\max\{vp,\epsilon\}$, while the upper cutoff $\xi_{max}\sim v/a$ is of the order of the electronic bandwidth.

Let us now calculate the Coulomb correction to an arbitrary matrix vertex $-i\Gamma(\mathbf{p},\epsilon;\mathbf{q},\omega)$, corresponding to the process, shown in Fig. 25,

$$\delta\Gamma(\mathbf{p},\epsilon;\mathbf{q},\omega) = i\int \frac{d\omega'}{2\pi}\frac{d^2\mathbf{q}'}{(2\pi)^2}V(\mathbf{q}',\omega')G(\mathbf{p}+\mathbf{q}',\epsilon-\omega')\Gamma(\mathbf{p}+\mathbf{q}',\epsilon+\omega';\mathbf{q},\omega)G(\mathbf{p}+\mathbf{q}+\mathbf{q}',\epsilon+\omega+\omega')$$

$$= -\int \frac{d\varpi}{2\pi}\frac{d^2\mathbf{q}'}{(2\pi)^2}\frac{2\pi e^2}{q'}\frac{\sqrt{(vq')^2+\varpi^2}}{gvq'+\sqrt{(vq')^2+\varpi^2}}\frac{\epsilon - i\varpi + v(\mathbf{p}+\mathbf{q}')\cdot\mathbf{\Sigma}}{(-i\epsilon+\varpi)^2+v^2|\mathbf{p}+\mathbf{q}'|^2}$$

$$\times\Gamma(\mathbf{p}+\mathbf{q}',\epsilon+\omega';\mathbf{q},\omega)\frac{\epsilon-\omega-i\varpi+v(\mathbf{p}+\mathbf{q}+\mathbf{q}')\cdot\mathbf{\Sigma}}{(-i\epsilon+i\omega+\varpi)^2+v^2|\mathbf{p}+\mathbf{q}+\mathbf{q}'|^2}$$

$$\approx \frac{e^2}{2\pi v}\int_{\xi_{min}}^{\xi_{max}} d\xi\int_{-\infty}^{\infty} d\varpi\frac{\sqrt{\xi^2+\varpi^2}}{g\xi+\sqrt{\xi^2+\varpi^2}}\frac{\varpi^2\Gamma-\xi^2\mathbf{\Sigma}\Gamma\mathbf{\Sigma}/2}{(\varpi^2+\xi^2)^2}$$

$$= \frac{4g}{\pi^2\mathcal{N}}\ln\frac{\xi_{max}}{\xi_{min}}\int_0^{\pi} d\varphi\frac{(1-\sin^2\varphi)\Gamma-\sin^2\varphi\mathbf{\Sigma}\Gamma\mathbf{\Sigma}/2}{1+g\sin\varphi} = \frac{8}{\pi^2\mathcal{N}}\ln\frac{\xi_{max}}{\xi_{min}}[\tilde{f}(g)\Gamma - f(g)(\Gamma+\mathbf{\Sigma}\Gamma\mathbf{\Sigma}/2)]. \tag{D2}$$

Here we have assumed that the dependence of $\Gamma(\mathbf{p},\epsilon;\mathbf{q},\omega)$ on $\mathbf{p}$ and ϵ is weak. If this dependence comes entirely from the renormalization, which is true in our case, its weakness is due to the smallness of the parameter $1/\mathcal{N}$.

Let us repeat the calculation of self-energy (50) due to electron-phonon interaction,

$$\Sigma^{ph}(\mathbf{p},\epsilon) = -\int \frac{d\varpi}{2\pi}\frac{d^2\mathbf{q}}{(2\pi)^2}\sum_{\mu}\frac{F_\mu^2}{2M\omega_\mu}\frac{\sqrt{27}a^2}{4}D_\mu(\mathbf{q},i\varpi)$$

$$\times(\Lambda\Sigma)_\mu G(\mathbf{p}-\mathbf{q},\epsilon-i\varpi)(\Lambda\Sigma)_\mu$$

$$\approx (\lambda_\Gamma+\lambda_K)\int\frac{d^2(v\mathbf{q})}{(2\pi)^2}\frac{\epsilon}{(vq)^2}$$

$$= (\lambda_\Gamma+\lambda_K)\left(\ln\frac{\xi_{max}}{\xi_{min}}\right)\frac{\epsilon}{2\pi}, \tag{D3}$$

where the phonon mode index μ runs over the two modes belonging to the E_2 representation and the two modes belonging to the E_1' representation, the corresponding matrices $(\Lambda\Sigma)_\mu$ being $-\Lambda_z\Sigma_y$, $\Lambda_z\Sigma_x$, $\Lambda_x\Sigma_z$, $\Lambda_y\Sigma_z$. Note that the here the integral is dominated by $\varpi\sim\max\{\epsilon,\omega_\mu\}$, in contrast with the Coulomb self-energy where we had $\varpi\sim vq$. Thus, to calculate the integral in Eq. (D3) we simply approximated

$$D_\mu(\mathbf{q},i\varpi)\to\frac{2\omega_\mu}{-\varpi^2-\omega_\mu^2}\approx -2\pi\delta(\varpi),\quad |\varpi|\gg\omega_\mu. \tag{D4}$$

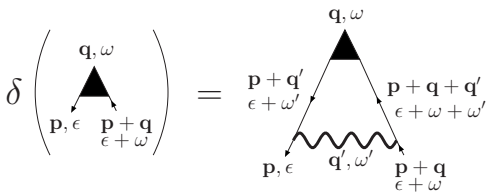

FIG. 25. Coulomb correction to a generic vertex $-i\Gamma(\mathbf{p},\epsilon;\mathbf{q},\omega)$ shown by the triangle.

The sum of the two diagrams in Fig. 24 gives the following expression for the effective two-electron vertex [we denoted $\underline{p}\equiv(\mathbf{p},\epsilon)$, $\underline{q}\equiv(\mathbf{q},\omega)$ for compactness]:

$$\delta\Gamma^{(2)}(\underline{p},\underline{p}';\underline{q}) = i\int\frac{d^3q'}{(2\pi)^3}\sum_{\mu,\mu'}\frac{F_\mu^2}{2M\omega_\mu}\frac{\sqrt{27}a^2}{4}\frac{F_{\mu'}^2}{2M\omega_{\mu'}}\frac{\sqrt{27}a^2}{4}$$

$$\times D_\mu(\underline{q}-\underline{q}')D_{\mu'}(\underline{q}')(\Lambda\Sigma)_\mu G(\underline{p}+\underline{q}')$$

$$\times(\Lambda\Sigma)_{\mu'}\otimes[(\Lambda\Sigma)_\mu G(\underline{p}'-\underline{q}')(\Lambda\Sigma)_{\mu'}$$

$$+(\Lambda\Sigma)_{\mu'}G(\underline{p}'-\underline{q}+\underline{q}')(\Lambda\Sigma)_\mu]. \tag{D5}$$

Due to condition (D4), we can approximate

$$G(\underline{p}+\underline{q}')\approx -G(\underline{p}'-\underline{q}')\approx G(\underline{p}'-\underline{q}+\underline{q}')\approx -\frac{v\mathbf{q}\cdot\mathbf{\Sigma}}{(vq)^2}. \tag{D6}$$

Then the frequency integral is simply

$$i\int\frac{d\omega'}{2\pi}D_\mu(\omega-\omega')D_{\mu'}(\omega') = \frac{2(\omega_\mu+\omega_{\mu'})}{\omega^2-(\omega_\mu+\omega_{\mu'}-io)^2}$$

$$\equiv D_{\mu+\mu'}(\omega). \tag{D7}$$

Taking the $\mathbf{q}'$ integral, we obtain

$$\delta\Gamma^{(2)}(\underline{p},\underline{p}';\underline{q}) = \frac{v^2}{4}\ln\frac{\xi_{max}}{\xi_{min}}\sum_{\mu,\mu'}\frac{\lambda_\mu\lambda_{\mu'}}{2\pi}\left\{\frac{1}{2}(\Lambda\Sigma)_\mu\Sigma_i(\Lambda\Sigma)_{\mu'}\right.$$

$$\left.\otimes[-(\Lambda\Sigma)_\mu\Sigma_i(\Lambda\Sigma)_{\mu'}+(\Lambda\Sigma)_{\mu'}\Sigma_i(\Lambda\Sigma)_\mu]\right\}. \tag{D8}$$

The matrix expression appearing in the braces is evaluated for each of the 16 combinations of the indices μ, μ' in Table IV. Adding up the contributions, we obtain Eq. (134b).

TABLE IV. The matrix expression in the braces in Eq. (D8) evaluated for all 16 combinations of the phonon indices μ,μ'.

μ,μ'	$-\Lambda_z\Sigma_y$	$\Lambda_z\Sigma_x$	$\Lambda_x\Sigma_z$	$\Lambda_y\Sigma_z$
$-\Lambda_z\Sigma_y$	0	0	$\Lambda_y\Sigma_z\otimes\Lambda_y\Sigma_z$	$\Lambda_x\Sigma_z\otimes\Lambda_x\Sigma_z$
$\Lambda_z\Sigma_x$	0	0	$\Lambda_y\Sigma_z\otimes\Lambda_y\Sigma_z$	$\Lambda_x\Sigma_z\otimes\Lambda_x\Sigma_z$
$\Lambda_x\Sigma_z$	$\Lambda_y\Sigma_z\otimes\Lambda_y\Sigma_z$	$\Lambda_y\Sigma_z\otimes\Lambda_y\Sigma_z$	0	$\Lambda_z\Sigma_y\otimes\Lambda_z\Sigma_y+\Lambda_z\Sigma_x\otimes\Lambda_z\Sigma_x$
$\Lambda_y\Sigma_z$	$\Lambda_x\Sigma_z\otimes\Lambda_x\Sigma_z$	$\Lambda_x\Sigma_z\otimes\Lambda_x\Sigma_z$	$\Lambda_z\Sigma_y\otimes\Lambda_z\Sigma_y+\Lambda_z\Sigma_x\otimes\Lambda_z\Sigma_x$	0

APPENDIX E: POLARIZATION OPERATOR

Polarization operator with arbitrary matrix vertices Σ_i, Σ_j, $i,j=x,y,z,0$ (we denoted $\Sigma_0\equiv\mathbb{1}$), can be conveniently calculated in the coordinate representation,[62]

$$-i\Pi_{ij}(\mathbf{r}-\mathbf{r}',t-t') = \frac{\mathcal{N}}{2}\operatorname*{Tr}_{4\times4}\{\Sigma_i G(\mathbf{r}-\mathbf{r}',t-t')\Sigma_j G(\mathbf{r}'-\mathbf{r},t'-t)\}, \quad \text{(E1)}$$

$$(i\partial_t + iv\boldsymbol{\Sigma}\cdot\nabla)G(\mathbf{r},t) = \mathbb{1}\delta(\mathbf{r})\delta(t). \quad \text{(E2)}$$

If Λ matrices are also present in the vertices, tracing of them is trivial; the matrices in the two vertices must coincide for the trace not to vanish, then their product is equal to the unit matrix.

It is convenient to switch to the imaginary time $\tau=it$, $i\partial_t\to-\partial_\tau$. Then Green's function in the coordinate representation can be found by using the analogy with the 3D Coulomb problem. Namely, we introduce the third dimension $z=v\tau$ and note that

$$(-\partial_\tau + iv\boldsymbol{\Sigma}\cdot\nabla)(-\partial_\tau - iv\boldsymbol{\Sigma}\cdot\nabla) = v^2\nabla_{3\mathrm{D}}^2. \quad \text{(E3)}$$

Since the inverse of the 3D Laplacian is the Coulomb potential, we obtain

$$G(\mathbf{r},\tau) = (\partial_\tau + iv\boldsymbol{\Sigma}\cdot\nabla)\frac{1}{4\pi v\sqrt{v^2\tau^2+r^2}} = -\frac{v\tau + i\boldsymbol{\Sigma}\cdot\mathbf{r}}{4\pi(v^2\tau^2+r^2)^{3/2}}. \quad \text{(E4)}$$

Using auxiliary relations (here $i,j=x,y,z$),

$$\operatorname*{Tr}_{4\times4}\{\Sigma_i\Sigma_k\Sigma_j\Sigma_l\} = 4\delta_{ik}\delta_{jl} + 4\delta_{il}\delta_{jk} - 4\delta_{ij}\delta_{kl}, \quad \text{(E5a)}$$

$$\partial_i\partial_j\frac{1}{R^2} = \frac{8x_ix_j - 2\delta_{ij}R^2}{R^6}, \quad R^2 = x^2+y^2+z^2, \quad \text{(E5b)}$$

we calculate the polarization operator (here $i,j=x,y$),

$$\Pi_{00}(\mathbf{r},\tau) = -\mathcal{N}\frac{v^2\tau^2 - r^2}{8\pi^2(v^2\tau^2+r^2)^3} = \frac{\mathcal{N}}{32\pi^2}(\partial_x^2+\partial_y^2)\frac{1}{v^2\tau^2+r^2}, \quad \text{(E6a)}$$

$$\Pi_{zz}(\mathbf{r},\tau) = -\mathcal{N}\frac{v^2\tau^2 + r^2}{8\pi^2(v^2\tau^2+r^2)^3} = -\frac{2\mathcal{N}}{32\pi^2}\nabla_{3\mathrm{D}}^2\frac{1}{v^2\tau^2+r^2}, \quad \text{(E6b)}$$

$$\Pi_{ij}(\mathbf{r},\tau) = \mathcal{N}\frac{4x_ix_j - 2\delta_{ij}(v^2\tau^2+r^2)}{16\pi^2(v^2\tau^2+r^2)^3} = \frac{\mathcal{N}}{32\pi^2}\partial_i\partial_j\frac{1}{v^2\tau^2+r^2} + \frac{\delta_{ij}}{2}\Pi_{zz}, \quad \text{(E6c)}$$

$$\Pi_{0i}(\mathbf{r},\tau) = -\mathcal{N}\frac{izx_i}{8\pi^2(v^2\tau^2+r^2)^3} = -\frac{\mathcal{N}}{32\pi^2}\frac{i}{v}\partial_\tau\partial_i\frac{1}{v^2\tau^2+r^2}. \quad \text{(E6d)}$$

Using the 3D Fourier transform

$$\int d^3\mathbf{R}\frac{e^{i\mathbf{QR}}}{32\pi^2R^2} = \int\frac{d^3\mathbf{R}}{(2\pi)^3}\frac{\pi}{4R^2}e^{i\mathbf{QR}} = \frac{1}{16}\frac{1}{Q}, \quad \text{(E7)}$$

we obtain $\Pi(\mathbf{q},\omega)$ (up to a $\mathbf{q},\omega$-independent constant coming from $r,\tau\to0$),

$$\Pi_{00}(\mathbf{q},\omega) = -\frac{\mathcal{N}}{16v^2}\frac{v^2q^2}{\sqrt{v^2q^2-\omega^2}}, \quad \text{(E8a)}$$

$$\Pi_{0i}(\mathbf{q},\omega) = -\frac{\mathcal{N}}{16v^2}\frac{\omega v q_i}{\sqrt{v^2q^2-\omega^2}}, \quad \text{(E8b)}$$

$$\Pi_{ij}(\mathbf{q},\omega) = -\frac{q_iq_j}{q^2}\frac{\mathcal{N}}{16v^2}\frac{\omega^2}{\sqrt{v^2q^2-\omega^2}} + \left(\delta_{ij}-\frac{q_iq_j}{q^2}\right)\frac{\mathcal{N}}{16v^2}\sqrt{v^2q^2-\omega^2}, \quad \text{(E8c)}$$

$$\Pi_{zz}(\mathbf{q},\omega) = \frac{2\mathcal{N}}{16v^2}\sqrt{v^2q^2-\omega^2}, \quad \text{(E8d)}$$

$$\Pi_{0z}(\mathbf{q},\omega) = 0, \quad \text{(E8e)}$$

$$\Pi_{iz}(\mathbf{q},\omega) = 0. \quad \text{(E8f)}$$

Given the polarization operator, one can find corrections to

the optical phonon frequencies due the electron-phonon interaction,

$$D_K^{-1}(\mathbf{q},\omega) - \frac{\lambda_K}{2} v^2 \Pi_{zz}(\mathbf{q},\omega) = 0 \Rightarrow \delta\omega_K(\mathbf{q}) \approx \frac{\lambda_K}{4}\sqrt{v^2q^2 - \omega_K^2}, \tag{E9a}$$

$$D_{\Gamma,L}^{-1}(\mathbf{q},\omega) - \frac{\lambda_\Gamma}{2} v^2 \Pi_T(\mathbf{q},\omega) = 0 \Rightarrow \delta\omega_{\Gamma,L}(\mathbf{q}) \approx \frac{\lambda_\Gamma}{8}\sqrt{v^2q^2 - \omega_\Gamma^2}, \tag{E9b}$$

$$D_{\Gamma,T}^{-1}(\mathbf{q},\omega) - \frac{\lambda_\Gamma}{2} v^2 \Pi_L(\mathbf{q},\omega) = 0$$

$$\Rightarrow \delta\omega_{\Gamma,T}(\mathbf{q}) \approx -\frac{\lambda_\Gamma}{8}\frac{\omega_\Gamma^2}{\sqrt{v^2q^2 - \omega_\Gamma^2}}. \tag{E9c}$$

At $vq < \omega_\mu$ the square roots are imaginary which corresponds to the decay of phonons into the continuum of electron-hole pairs.

*basko@sissa.it

[1] L. I. Mandelshtam and G. S. Landsberg, Z. Phys. **50**, 169 (1928); C. V. Raman and K. S. Krishnan, Nature (London) **121**, 501 (1928); **121**, 619 (1928).

[2] S. Reich and C. Thomsen, Philos. Trans. R. Soc. London, Ser. A **362**, 2271 (2004).

[3] J. Kastner, T. Pichler, H. Kuzmany, S. Curran, W. Blau, D. N. Weldon, M. Dlamesiere, S. Draper, and H. Zandbergen, Chem. Phys. Lett. **221**, 53 (1994).

[4] A. M. Rao, E. Richter, S. Bandow, B. Chase, P. C. Eklund, K. W. Williams, M. Menon, K. R. Subbaswamy, A. Thess, R. E. Smalley, G. Dresselhaus, and M. S. Dresselhaus, Science **275**, 187 (1997).

[5] K. S. Novoselov, A. K. Geim, S. V. Morozov, D. Jiang, Y. Zhang, S. V. Dubonos, I. V. Grigorieva, and A. A. Firsov, Science **306**, 666 (2004).

[6] A. C. Ferrari, J. C. Meyer, V. Scardaci, C. Casiraghi, M. Lazzeri, F. Mauri, S. Piscanec, D. Jiang, K. S. Novoselov, S. Roth, and A. K. Geim, Phys. Rev. Lett. **97**, 187401 (2006).

[7] A. Gupta, G. Chen, P. Joshi, S. Tadigadapa, and P. C. Eklund, Nano Lett. **6**, 2667 (2006).

[8] D. Graf, F. Molitor, K. Ensslin, C. Stampfer, A. Jungen, C. Hierold, and L. Wirtz, Nano Lett. **7**, 238 (2007).

[9] J. Yan, Y. Zhang, P. Kim, and A. Pinczuk, Phys. Rev. Lett. **98**, 166802 (2007).

[10] S. Pisana, M. Lazzeri, C. Casiraghi, K. S. Novoselov, A. K. Geim, A. C. Ferrari, and F. Mauri, Nat. Mater. **6**, 198 (2007).

[11] C. Casiraghi, S. Pisana, K. S. Novoselov, A. K. Geim, and A. C. Ferrari, Appl. Phys. Lett. **91**, 233108 (2007).

[12] A. Das, S. Pisana, S. Piscanec, B. Chakraborty, S. K. Saha, U. V. Waghmare, R. Yiang, H. R. Krishnamurhthy, A. K. Geim, A. C. Ferrari, and A. K. Sood, Nat. Nanotechnol. **3**, 210 (2008).

[13] C. Thomsen and S. Reich, Phys. Rev. Lett. **85**, 5214 (2000).

[14] L. G. Cançado, R. Beams, and L. Novotny, arXiv:0802.3709 (unpublished).

[15] L. G. Cançado, A. Jorio, and M. A. Pimenta, Phys. Rev. B **76**, 064304 (2007).

[16] R. P. Vidano, D. B. Fischbach, L. J. Willis, and T. M. Loehr, Solid State Commun. **39**, 341 (1981).

[17] Y. Wang, D. C. Alsmeyer, and R. L. McCreery, Chem. Mater. **2**, 557 (1990).

[18] I. Pócsik, M. Hundhausen, M. Koos, and L. Ley, J. Non-Cryst. Solids **227-230**, 1083 (1998).

[19] M. J. Matthews, M. A. Pimenta, G. Dresselhaus, M. S. Dresselhaus, and M. Endo, Phys. Rev. B **59**, R6585 (1999).

[20] R. Saito, G. Dresselhaus, and M. S. Dresselhaus, *Physical Properties of Carbon Nanotubes* (Imperial College, London, 1998).

[21] S. Xu, J. Cao, C. C. Miller, D. A. Mantell, R. J. D. Miller, and Y. Gao, Phys. Rev. Lett. **76**, 483 (1996).

[22] G. Moos, C. Gahl, R. Fasel, M. Wolf, and T. Hertel, Phys. Rev. Lett. **87**, 267402 (2001).

[23] A. Bostwick, T. Ohta, T. Seyller, K. Horn, and E. Rotenberg, Nat. Mater. **3**, 36 (2007).

[24] J. González, F. Guinea, and M. A. H. Vozmediano, Phys. Rev. Lett. **77**, 3589 (1996).

[25] R. C. C. Leite, J. F. Scott, and T. C. Damen, Phys. Rev. Lett. **22**, 780 (1969).

[26] M. V. Klein and S. P. S. Porto, Phys. Rev. Lett. **22**, 782 (1969).

[27] R. M. Martin and C. M. Varma, Phys. Rev. Lett. **26**, 1241 (1971).

[28] R. Zeyher, Solid State Commun. **16**, 49 (1975).

[29] D. M. Basko, Phys. Rev. B **76**, 081405(R) (2007).

[30] There is an overall factor of 2π missing in Eq. (6) of Ref. 29, which affects all I_{2K}, $I_{2\Gamma}$, and I_{4K} but not their ratios. Besides, there is a factor of $\pi/4$ missing in Eq. (9) of Ref. 29, which affects the central result [Eq. (1) of Ref. 29]. Fortunately, $\pi/4 \approx 0.79$ is not very much different from unity.

[31] S. Piscanec, M. Lazzeri, F. Mauri, A. C. Ferrari, and J. Robertson, Phys. Rev. Lett. **93**, 185503 (2004).

[32] M. Calandra and F. Mauri, Phys. Rev. B **76**, 205411 (2007).

[33] J. Maultzsch, S. Reich, C. Thomsen, H. Requardt, and P. Ordejón, Phys. Rev. Lett. **92**, 075501 (2004).

[34] D. M. Basko and I. L. Aleiner, Phys. Rev. B **77**, 041409(R) (2008).

[35] A. A. Abrikosov and S. D. Beneslavskii, Zh. Eksp. Teor. Fiz. **59**, 1280 (1970) [Sov. Phys. JETP **32**, 699 (1971)].

[36] J. González, F. Guinea, and M. A. H. Vozmediano, Mod. Phys. Lett. B **7**, 1593 (1994); Nucl. Phys. B **424**, 595 (1994); J. Low Temp. Phys. **99**, 287 (1994).

[37] J. González, F. Guinea, and M. A. H. Vozmediano, Phys. Rev. B **59**, R2474 (1999).

[38] I. L. Aleiner, D. E. Kharzeev, and A. M. Tsvelik, Phys. Rev. B **76**, 195415 (2007).

[39] J. Ye, Phys. Rev. B **60**, 8290 (1999).

[40] T. Stauber, F. Guinea, and M. A. H. Vozmediano, Phys. Rev. B **71**, 041406(R) (2005).

[41] M. S. Foster and I. L. Aleiner, Phys. Rev. B **77**, 195413 (2008).

[42] Sections III and V of the present paper were written in coauthorship with I. L. Aleiner.

[43] M. Lax, *Symmetry Principles in Solid State and Molecular Physics* (Dover, New York, 2001).
[44] P. R. Wallace, Phys. Rev. **71**, 622 (1947).
[45] H. Suzuura and T. Ando, Phys. Rev. Lett. **89**, 266603 (2002).
[46] L. D. Landau and E. M. Lifshits, *Theory of Elasticity* (Pergamon, New York, 1970), Sec. 25.
[47] Note that in this case the symmetry C_{6v} becomes distinguishable from D_6.
[48] I. A. Luk'yanchuk and A. M. Bratkovsky, Phys. Rev. Lett. **100**, 176404 (2008).
[49] Σ^{ph} in graphite was considered long ago [F. Guinea, J. Phys. C **14**, 3345 (1981)], but the logarithmic divergence was not noted in that work.
[50] M. Lazzeri, S. Piscanec, F. Mauri, A. C. Ferrari, and J. Robertson, Phys. Rev. B **73**, 155426 (2006).
[51] M. Lazzeri and F. Mauri, Phys. Rev. Lett. **97**, 266407 (2006).
[52] A. H. Castro Neto and F. Guinea, Phys. Rev. B **75**, 045404 (2007).
[53] A. Grüneis, R. Saito, T. Kimura, L. G. Cançado, M. A. Pimenta, A. Jorio, A. G. Souza Filho, G. Dresselhaus, and M. S. Dresselhaus, Phys. Rev. B **65**, 155405 (2002).
[54] V. B. Berestetskii, E. M. Lifshits, and L. P. Pitaevskii, *Quantum Electrodynamics* (Pergamon, New York, 1982), Sec. 79.
[55] In principle, momentum conservation allows emission of just three K phonons, as $\mathbf{K}+\mathbf{K}+\mathbf{K}$ is equivalent to 0. However, this process cannot be resonant.
[56] J. Maultzsch, S. Reich, and C. Thomsen, Phys. Rev. B **70**, 155403 (2004).
[57] At small q the phonon dispersion is determined by the electron-phonon interaction and can be calculated from the polarization operator $\Pi_{zz}(\mathbf{q},\omega)$. The latter was calculated for the case $\omega=0$ in Ref. 31; for abitrary $\mathbf{q}$ and ω at zero doping it is given by Eq. (E8d).
[58] I. L. Aleiner and K. B. Efetov, Phys. Rev. Lett. **97**, 236801 (2006).
[59] E. McCann, K. Kechedzhi, V. I. Fal'ko, H. Suzuura, T. Ando, and B. L. Altshuler, Phys. Rev. Lett. **97**, 146805 (2006).
[60] E. I. Blount, Phys. Rev. **126**, 1636 (1962).
[61] Upon applying the operator $\mathrm{St}^{e,in}+\mathrm{St}^{h,in}$ twice one would expect a binomial-type expression: $f^{(2)}=f^{(ee)}+f^{(eh)}+f^{(he)}+f^{(hh)}$. However, in these form $f^{(eh)}$ and $f^{(he)}$ correspond to different ordering of t_0 and $\bar{t}_0$. We prefer to join the terms without assuming any relation between emission events for the electron and the hole.
[62] The idea of this calculation was suggested to the author by M. S. Foster.